EXPERIMENTAL AND NUMERICAL INVESTIGATION OF ENERGY RECOVERY TECHNOLOGIES IN AIR HANDLING UNITS

By

Laith Faisal Abdelrazzaq Alhyari

Supervisor
Dr. Kassai Miklos PhD.

This Thesis was Submitted in Partial Fulfillment of the Requirements for the PhD Degree in Mechanical Engineering

Department of Building Service and Process Engineering

Faculty of Mechanical Engineering

Budapest University of Technology and Economics

6th April 2021

Acknowledgement

I would like to express the deepest appreciation to my committee chair **Dr. Kassai Miklos** for his guidance, patience during his supervision of this research, and to all the people who supported me to finish this work. The support of my department in executing this research is highly appreciated.

Table of Contents:

List of Figures:

List of Tables:

Nomenclature:

Notation	Description	Units
ASHRAE	American Society of Heating, Refrigeration and Air conditioning Engineers	-
HVAC	Heating, ventilation, and air-conditioning	
EPBD	Energy Performance of Building Directive	
NZEB	Nearly zero-energy buildings	
PEE	Polyethylene–polyether copolymer material-based counter-flow air-to-air energy exchanger	
PHE	Polystyrene material-based counter-flow air-to-air heat exchanger	
VRV	Variable Refrigerant Volume	
VRF	Variable Refrigerant Flow	
AHU	Air Handling Unit	
NMBE	Normalized Mean Bias Error	
CVRMSE	Coefficient of Variation of the Root Mean Square Error	
U	Overall heat transfer coefficient	W/m^2 °C
h	Specific Enthalpy	kJ/kg
C_p	Specific heat Capacity	kJ/kg °C
T	Dry Bulb Temperature	^oC
x	Absolute Humidity	$kg/kg_{dry\ air}$
R	Function of a desired result	-
x_R	independent variables in the R function	-
ω_R	Uncertainty for R function	-
ω_x	Uncertainty for the independent	-
p_w	Partial Pressure of water vapor	Pa
h_g	Specific enthalpy of saturated gas	kj/kg
$\dot{m}$	Mass flow rate	kg/h
$\dot{V}$	Volume flow rate	m^3/h
p	Partial pressure	Pa
RH	Relative Humidity	(%)
EER	Energy Efficiency Ratio for cooling load	-
PI	Power input	W
m	Hot water demand	kg
Q	Heat Capacity	kW
E_t	Power Consumption	kW
ERV	Energy Recovery Ventilation	-
v_{1o}	specific volume for the outside condition	m^3/kg
h_{1i}	inlet convection heat transfer coefficient from supply fresh air	W/m^2 °C
h_{1o}	Outlet convection heat transfer coefficient from supply fresh air	W/m^2 °C
Q_{max}	maximum ventilation load	W
$T_{1,i}$	inlet temperature from supply fresh air	°C
$T_{1,o}$	outlet temperature from supply fresh air	°C
$T_{2,i}$	inlet temperature from exhaust air	°C

$T_{2,o}$	Outlet temperature from exhaust air	°C
Greek Notations		
ρ	Density	kg/m^3
τ	Time	h
ε	Effectiveness	-
ω	Wheel rotation speed	rpm
Subscript		
a	Moist air	-
o	Outdoor	-
ei	Exhaust Inlet	-
eo	Exhaust Outlet	-
si	Supply Inlet	-
so	Supply Outlet	-
L	Latent	-
S	Sensible	-
t	total	-

Abstract

In this work, investigation of the maximum effectiveness values of the energy wheel by experimental tests conducted under extreme difference ambient air conditions parameters, different air volume flow rates and energy wheel rotation speeds. Air temperature and humidity experimental tests were performed using a test facility that was developed and installed into the Indoor Air Quality and Thermal Comfort Laboratory of Budapest University of Technology and Economics. The objective was to get the effectiveness values of sorption coated air-to-air energy recovery wheel for steady state conditions under different ambient air (as supply air inlet) conditions. It was found that the sensible effectiveness increases by decreasing the volumetric flow rate through the wheel, and the optimum values of the effectiveness were given at the maximum wheel rotation speed based on the tests. As for the latent and total effectivenesses, their characteristics show an increasing trend by decreasing the air volume flow rate, ambient air temperature and relative humidity and increasing the wheel rotation speed.

Moreover, the performance of two counter-flow heat/enthalpy energy exchangers are experimentally tested under different operating conditions, and the values of the sensible, latent, and total effectiveness are presented. The results show that the energy recovery of ventilation air with a polymer membrane material-based counter-flow energy exchanger performs better than using a polystyrene sensible heat recovery unit.

The results show reductions in heating load up to 10%, achieved by using thermal insulation and 61.3 % by using exhaust air heat recovery system.

On the other hand, the energy performance of a heat recovery wheel system equipped in an air handling unit was tested year-round, and the results compared with the simulation output for the system using TRNSYS software. The selected conditioned space was the staff

offices of an H&M fashion shop, located in Eger, Hungary. Temperature, relative humidity, and air velocity sensors were placed at the wheel inlet and outlet sections to record data and determine the annual energy saving. The results revealed a good agreement between the measured and simulated results.

Afterwards, a TRNSYS model was introduced in order to build a simulation model to calculate the energy performance of an existing variable refrigerant flow system located in the university to build a model that can be used as a reference when a VRF system is proposed to a certain situation. The TRNSYS model was compared with the actual energy consumption to see the data agreement between the two models. Temperature, Relative Humidity, and energy consumption were metered using proper instruments, and it was compared with the obtained simulation results. The validation of the simulation model showed close values to the actual system.

Besides, an Energy Recovery Ventilation was proposed to be simulated with the existing TRNSYS model to compare it with the same system without ventilation to see if it is feasible to add an Energy Recovery Ventilation unit to the existing system. It shows a worthy reason to be used, as it saves 18.8% annually of the energy consumption of the system

The economical analysis based on the applied experiments indicated that the novel heat recovery/desiccant cooling system could save energy which has a significant influence on the environment as it decreases the CO_2 emission per year compared to the traditional HVAC system. Although, the capital and maintenance cost of the energy recovery system is higher than the traditional one, but its running cost compensate the capital cost in a short period comparing to traditional HVAC system. Hence, the energy recovery systems can be considered as an environmentally friendly and a cost-effective technology HVAC system.

Chapter 1

Introduction

Background

The necessity for green energy usage on building energy consumption is becoming more demanding these days. The reason why every building constructed or renovated to become a so-called "green building" is to reduces the detrimental impact for these buildings on natural energy sources and to achieve sustainable development, which is one of the leading goals of the organization of the united nations [1]. The impact of the HVAC (Heating, Ventilation and Air Conditioning) systems on buildings has a strong effect on building energy consumption. Implementing an efficient HVAC system has a key role in saving energy toward a green building by minimizing the thermal load of the building.

The concerns about building thermal load are getting more attentions these days as the buildings are the most energy consumers in overall in the countries. Heat recovery is an approach for HVAC towards, which protects the environment and by lowering the energy usage in buildings. In addition, it improves the energy efficiency and reduces the energy consumption as the energy losses from ventilation reaches up to 50% of the total energy losses in buildings as well as, it make a positive impact on public health and the environment; and to help creating a sustainable building and lowering the building consumption [2].

The climate significantly influences the building energy consumption [3]. The usage of energy was investigated by several researchers under different climate conditions [4]. Different weather conditions, such as dry-bulb temperature, wet-bulb temperature, wind speed, and global solar radiation, were studied and described in terms of how those parameters affected the necessary heating and cooling energy performances [5]. Based on some studies, from the mentioned ambient condition parameters, the variation of the ambient air temperature most influences the energy requirements.

According to the nearly zero-energy building (NZEB) definition in the directive, the buildings should have a very high energy performance [6]. To achieve the high energy requirements, the thermal insulation of the building envelopes needs to be developed.

One of the techniques, which considered a proper reach the nearly zero-energy building, is Energy Recovery. It minimizes the input of energy to an overall system by the exchange of energy from one sub-system of the overall system with another. The energy can be in any form in either subsystem, but most energy recovery systems exchange thermal energy in either sensible or latent form. It can be used as an energy recovery unit to handle the outdoor ventilation air by preheating or precool the outgoing air [7]. The ERV system in general consists of a supply fan, exhaust fan, and an air-to-air heat exchanger.

The use of energy recovery units in commercial buildings increased significantly in the last recent years. Rapid enhancement of energy efficiency is essential for a reduction in energy use and promotion of sustainable environment. Accordingly, improving energy performance of the building will significantly reduce the energy consumption. Investments in these units are feasible, as it reduces the operating costs and improve more the energy efficiency [8]. Energy recovery units, like the energy wheel, can be implemented in the design to transfer the indoor temperature and humidity (energy) to the incoming outdoor air. Therefore, more outdoor air can be used at a lower energy cost. The exchange of indoor air for outdoor air represents a considerable wastage of energy, especially places, which need a higher rate of the air change per hour. Total energy recovery wheels transfer both sensible heat and moisture. In cooling mode the outdoor air is precooled and dehumidified. In heating mode the transfer of heat and moisture is reversed, as the outdoor air is preheated and pre-humidified [9]. There are many advantages for applying the energy wheel as an energy recovery that includes simultaneous heat and mass transfer, low pressure drop, and available to all ventilation system platforms. The disadvantages of the energy wheel application are further cooling/heating required for

supply air, there is possibility of cross contamination, and it increases maintenance requirements especially under cold climates [10].

Another efficient HVAC system to be used in buildings is the Variable Refrigerant Flow (VRF) technology. It has been spreading more and more on the air-conditioning market for the past decade. More manufacturing HVAC companies began to manufacture and improve the VRF system. The main concept of the VRF system is by using one outdoor unit to control multiple indoor units [11]. A variable refrigerant flow is used in the system to control the amount of refrigerant entering to the indoor unit depending on the amount of cooling or heating demand. Therefore, a VRF (Variable Refrigerant flow) is considered an efficient HVAC system to make the building more sustainable. A schematic diagram of the VRF system is shown in **Figure 1.1**

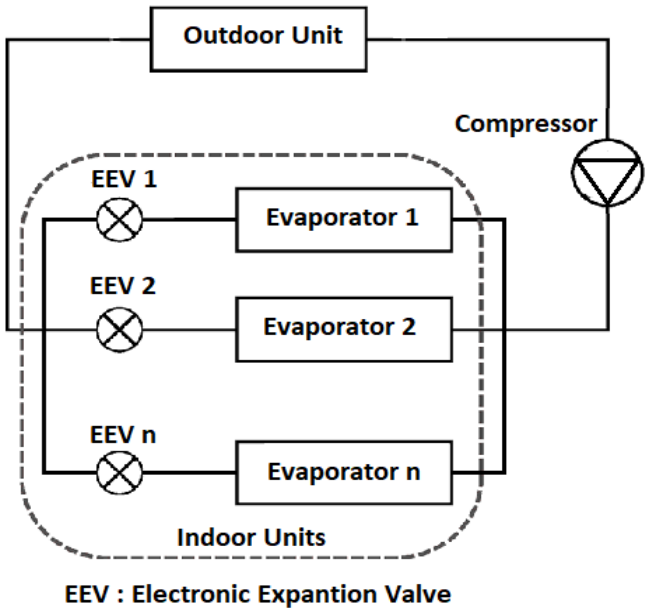

Figure 1.1. Schematic Diagram for VRF system

Chapter 2

Literature Review

2.1 Introduction:

An energy recovery is a process uses HVAC exhaust air to precondition the supply air, which enters the building at outdoor temperature and humidity. This process recovers some of the heating or cooling output that would otherwise be lost. During summer, the ERV system can pre-cool and dehumidify the outdoor air supply, by exchanging energy with the cooler and drier exhaust air. During Winter, the ERV system preheats the air supply, extracting heat from the warmer exhaust air.

It reduces the electricity consumption of HVAC systems, while improving indoor air quality. It is based on air-to-air heat exchange, using a spinning wheel or a stationary core where airstreams can exchange energy without mixing [12]. The experimental setup for ERV is shown in **Figure 2.1**

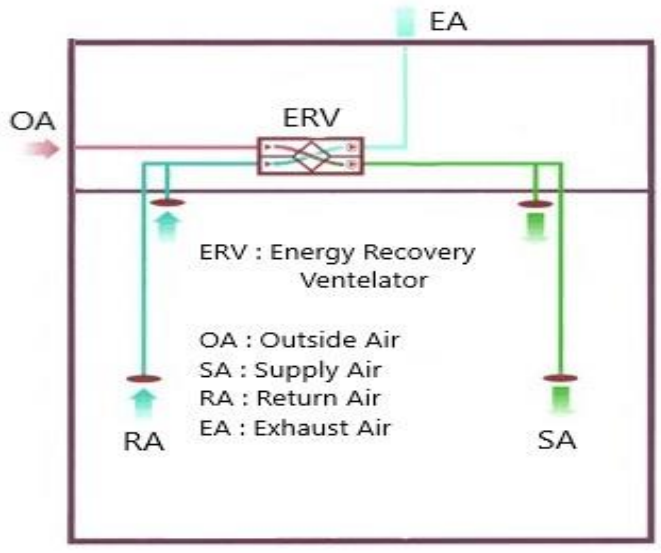

Figure 2.1 Schematic of the ERV system

2.2 Previous Studies:

2.2.1 Energy Recovery Wheels

Simonson and Besant [13] developed a numerical sample in rotating energy wheels and were calculated using the experimental data acquired. The performance of energy wheel was presented for a desiccant coating with a sorption isotherm (molecular sieve) and a linear sorption isotherm (silica gel). The numerical algorithm is changed from sorption to saturation when the air relative humidity exceeds 100 percent and when the wheel speed reduced the uncontrolled condensation and frosting.

Experimental investigation had been executed by Sparrow et al. [14] to determine the operating conditions of an energy wheel. The sensible and moisture transfer effectiveness of a wheel device had been measured in a particular experimental facility. They found that the sensible effectiveness decreases by increasing the air volume flow rate and when the flow rates were matchless, higher values of effectiveness were came across. As for the moisture transfer effectiveness, the characteristic trend decreased by increasing flow rate.

Jeong and Mumma [15] developed practical effectiveness correlations for desiccant wheel. During their research linear equations were developed to calculate the desiccant wheel total effectiveness at nominal operating wheel speeds. The silica gel and molecular sieve coated wheel were investigated depending on different factors; outside air and temperature of exhaust air, relative humidity, air velocity, and air volume flow rate. It was found that the air velocity and air volume flow rate contribute highly to sensible and latent effectiveness. The entering outside air and exhaust air showed a small contribution to sensible effectiveness, and higher contribution to latent effectiveness.

Harmati et al. [16] analyzed the annual energy performance of office building located in the center of Belgrade to evaluate the energy recovery units in order to perform the most suitable heating and cooling solution.

Experimental investigations on desiccant wheel material was performed by Angrisani et al. [17] The results obtained by the authors were used to calculate the performance parameters as a function of the regenerated temperature, the inlet humidity ratio and the ratio between the regeneration and process air-flow rates. The obtained results indicated that the dehumidification process has a high influences on desiccant wheel material due to the regeneration temperature rather than the regeneration air volume flow rate. The difference between the data was lower than 17%.

Chung et al. [18] optimized the design parameters of plastic rotary wheels. A numerical model was built and established to predict the performance of a plastic regeneration wheel taking into account the leakage and adsorption impacts. The effects of the rotational speed, and purge section angle and aspect ratio on the sensible and latent effectiveness were investigated using the numerical model. The optimum values for wheel speed, purge section angle and aspect ratio in the plastic regeneration wheel were specified. The maximized sensible effectiveness was 0.85 and the minimized moisture or latent effectiveness with using the optimal values was 0.042, which yielded to an almost 40% improvement in the moisture effectiveness comparing to the use of the basic design parameters.

Smith and Svendsen [19] built and simulated equations for room ventilation with moisture absorbance energy wheel. The study assumed that all moisture condensed in the exhaust air stream evaporated into the supply. Simulations evaluated the prospect for moisture and compared the results with sensible recovery ventilation systems. The study also focused on the influenced parameters, such as, relative humidity, and indoor temperature. The rotary heat wheel was appropriate just for single-room ventilation of dry rooms. However, it minimized the relative humidity in each room which is good for health breathing

The performance of solid desiccant wheel was studied by Goodarzia et al. [20] air humidity ratio, mass flow rates, wheel rotational speed and air process temperatures, were the

factors investigated in this study. Simulation program was used to calculate output conditions. The performance of a rotary desiccant wheel was investigated based on effectiveness parameters that includes moisture removal capacity, sensible and latent coefficient of performance and afterwards calculating the total coefficient of performance (COP). In conclusion, all the factors influenced on the COP and the MRCs with a positive relation expect inlet temperature.

Goldanlou et al. [21] proposed a novel design of the air handling unit (AHU) equipped with the primary and secondary heat recovery units to diminishing energy demand through the energetic analysis. In the primary heat recovery unit, the incoming fresh air is pre-cooled to decrease energy usage in cooling coil whereas, in the second one, the cooling coil outlet air is preheated to diminish the heating coil load. Due to the installing energy recovery units, the cooling and heating coils load decreased by 21.65% and 81.17%, respectively, which improved the energy efficiency by 43.75%

Calautit et al. [22] Studied the energy costs for space-heating consumption to recover the thermal energy in ventilation exhaust air and transfer the energy to the incoming air, to be redistributed using natural ventilation windcatcher. A rotary heat recovery device suitable to be incorporated with a roof mounted multi directional windcatcher system was developed. The results showed that the addition of the heat recovery wheel rotating at 15 rpm reduced the indoor airflow speed between 14 and 30%, depending on the outdoor wind conditions, and the heat recovery system had a positive impact on the indoor air temperature, raising the temperature up to 3.7 °C depending on the indoor/outdoor conditions

2.2.2 Ambient Condition Parameters

Lam et al. [23] Studied different weather conditions, such as dry-bulb temperature, wet-bulb temperature, wind speed, and global solar radiation in terms of how those parameters affected the necessary heating and cooling energy performances

Based on Giannakopoulos et al. [24] studies, the variation of the ambient air temperature most influences the energy requirements. Consequently, the degree day method is one of the most useful calculation procedures to estimate the energy demand, which considers the difference between indoor air temperature (in the conditioned space) and ambient air temperature.

Karlsson et al. [25] studied the assumption of a constant indoor air temperature that can result in considerable errors. It could happen due to the transient dynamic effects of the other weather parameters, as well as the heat losses, heat gains, thermal storage, and thermal inertia of building components, on the energy consumption, are not considered

Calise et al. [26] investigated the degree day-based estimation that can result in many errors during the cooling period since solar radiation and internal heat gains have a higher impact on the cooling energy needed than the set indoor air temperature.

2.2.3 Energy Performance of Buildings

Giuseppe et al. [27] developed a solution to decrease the energy losses, which involves reducing the heat losses due to the infiltration of the air in the building and using heat and energy recovery ventilation units instead of natural ventilation

Al-Zubaydi et al. [28] point out that almost 20–40% of the overall energy consumption of whole-building service systems is consumed for ventilation in most commercial buildings. In buildings that require 100% outdoor air to meet ventilation standards (e.g., hospitals), this percentage can be even higher (e.g.,50–60%)

Guillén et al. [29] emphasized that without energy recovery, ventilation air increases the energy consumption of buildings since outdoor air must be cooled or heated to bring it close to the indoor thermal comfort conditions. Hence, Mechanical ventilation was used for many years in a limited number of commercial buildings and is now becoming increasingly common in residences, particularly those that must meet the energy requirements of nearly zero-energy buildings in EU countries.

Davidsson et al. [30] discussed the consequences on a system level of using hybrid ventilation with heat recovery. The simulation program TRNSYS was used in order to investigate a ventilation system with heat recovery. The system also includes a ground source storage and waste water heat recovery system. The result of the analysis shows that the annual energy gain from ground source storage is limited. However, this is partly a consequence of the fact that the well functioning hybrid ventilation system leaves little room for improvements. The analysis shows that the hybrid ventilation system has the potential to be an attractive solution for low energy buildings with a very low need for electrical energy

Jani et al. [31] developed a TRNSYS (Transient System Simulation Tool) model to simulate a desiccant dehumidifier. Experimental measurements were obtained and compared to the simulation results. The simulated results showed that the system coefficient of performance (COP) had a critical influence when the regeneration temperature and relative humidity varied.

Improvement of the energy performance of a building using a heat pump was investigated by Wallin et al. [32]. The heat pump system was simulated using TRNSYS. They found that there is the potential to increase the heat exchange rate of the air-handling unit by coupling a heat pump to the system.

Zendehboudi et al. [33] determined the performance of a simple desiccant evaporative cooling cycle in four cities in Iran. The coefficient of performance (COP) was calculated in

each case and the results were compared. They found that the city with the highest humidity levels had the best potential for the cooling system with the use of a desiccant wheel

Rasouli et al. [34] performed a study on a run-around membrane energy exchanger (RAMEE) using simulation computed programs for various climates to estimate the reduced annual energy consumption and greenhouse gas emissions

Jokisalo et al. [35] simulated the performance of various mechanical supply and exhaust ventilation systems, incorporating heat recovery, in a typical Finnish residential apartment building. Dynamic thermal simulations were undertaken, representing a period of a year. Results show that a traditional exhaust ventilation system can use up to 67% more energy than a heat recovery system having 80% efficiency and 41% more energy than a heat recovery system having 60% energy recovery efficiency.

A numerical model was developed in TRNSYS by Bogatu et al. [36] for a low-energy residential building in Romania. The developed model was simulated in two phases, with the aim to use the construction standard to be implemented without changing its energy performances.

Fan et al. [37] executed field studies to examine the thermal performance of package air-conditioners and an energy recovery ventilator (ERV). CO_2 concentration, temperature, and Relative Humidity (RH) were considered throughout the test. The results showed that the energy consumption of the proposed system could be reduced by almost 30% compared to a standard ventilation system.

2.2.4 Variable Refrigerant Flow (VRF) System

The actual energy consumption of a building equipped with a VRF system simulated with EnergyPlus simulation results was compared with the experimental result by Park et al. [38] by analyzing the performance of VRF system with energy recovery ventilation (ERV). The difference between simulation and measured data was minimal and was found to be higher

than the VRF system without ventilation. The indoor air condition was found 16.2% and 17.2% in summer and Winter, respectively, for the VRF system without ERV. On the other hand, the indoor air condition data provided by the VRF system with ERV was found 65.7% and 76.8%, respectively, for the summer and winter seasons.

Jaime et al. [39] developed a VRF system model in order to give more accurate results than the actual model in EnergyPlus program. The new model was validated and compared with the running system, which represents an office building located in different locations. The improvement of the EnergyPlus model was better in importing the information provided by the manufacturer as it has a major role in the estimation of the building energy consumption.

Zhu et al. [40] proposed a VRF with an outdoor air processing unit to be combined as an air conditioning system to solve the ventilation problems in VRF systems were studied, and it was found that the new system could maintain the specific set-points temperature within small relative errors

Sanchez & Richman [41] analyzed the energy consumption of an / building located in Canada by utilizing the VRF System with heat recovery for the reason to optimize the design of VRF system with heat recovery through case study data using EnergyPlus simulation program.

Li & Wu [42] built a new simulation model using EnergyPlus for a heat recovery variable refrigerant flow (HR-VRF). The model was tested for a commercial building. It was found that heat recovery has an impact on the relative ratio of energy saving. The HR-VRF system reaches around 17% energy saving comparing to a heat pump VRF system.

Zhai and Revas [43] modeled a VRF system using a simulation program. The developed model predicts the energy consumption of a VRF system and shows how this system had a prospect to save energy compared to the conventional system.

Yau and Amer [44] studied and investigated the energy consumption for an existing multi-split system in a building and compared it with a VRF system using TRNSYS simulation program. The simulation results showed that a VRF system could save energy compared to the existing multi-split system. In addition, the VRF System has a PBP (payback period) of around 6.6 years, which is considered promising as the capital cost for the VRF system covered its cost before the lifespan of this system, which is 15 years

Zhang et al. [45] developed a novel model to simulate the energy performance of VRF-HR systems. The validation study shows good agreements between the simulated energy use from the new VRF-HR model and the laboratory measurement data across all operational modes at sub-hourly time steps. Results show that the new model can present a satisfactory match with the measured data across all the operation modes at sub-hourly levels.

Kalaimani et al. [46] focused on a detailed study on VRF system regarding the simulation of the system. They concentrate their simulation work in EnergyPlus to analyse the performance of an existing VRF system to see how it can reduce the energy consumption comparing to conventional HVAC system.

2.3 The Scope of this Work:

This work tackles analyze the situation of an energy recovery system as a case study. Studies will be applied for different types of energy recovery moving towards Low Energy buildings.

This research work will study the effect of different wheel rotation speeds on effectiveness of the investigated sorption wheel under difference ambient air conditions and air volume flow rates.

On the other hand, the values of sensible, latent, and total effectiveness of a polystyrene material-based counter-flow heat exchanger (PHE) and a polymer membrane (polyethylene–polyether copolymer) material-based counter-flow energy exchanger (PEE) integrated in a Zehnder ComfoAir 350 were investigated with experimental tests in the Indoor Air Quality and Thermal Comfort Laboratory of the Budapest University of Technology and Economics, which enables the researchers to test different types of full-size air-to-air heat and energy exchangers under different supply inlet and exhaust inlet air conditions.

Apart from this, a complete system of an existing air-handling unit (AHU) with an air-to-air rotary heat wheel was modeled for simulation using TRNSYS 18. The investigated running ventilation system was designed by the HVAC design engineer to supply fresh air and to provide the proper indoor air quality in the conditioned space, located in Eger, Hungary. The heating and cooling demands are covered by an independent system, the investigated ventilation system, which includes indoor air units connected to additional outdoor units and does not affect the ventilation energy consumption and was not investigated by our research work and investigations.

Finally, a complete, existing operated VRF system has been modeled using the simulation studio module of TRNSYS to study the energy performance of VRF system during the year. Experimental measurement has been conducted using metering instruments for

temperature, relative humidity, and energy consumption to evaluate the difference with the simulation model and assess the agreement between the measured and simulated data. In the second stage, this work proposed an ERV (Energy Recovery Ventilation) to be simulated with the new VRF TRNSYS model to compare it with VRF system without ventilation to see if it is feasible to add an ERV unit to the existing VRF system.

In general, the estimation of energy consumption of ventilation systems is a very complex design problem requiring many pieces of information, such as ambient weather condition, indoor set point temperature and relative humidity, mass flow rate of ventilation air, effectiveness of the exchanger, and technique to add auxiliary heating and cooling. The calculations needed to evaluate the operating energy consumption involve functions of these parameters integrated over time are quite complex procedures. This is further complicated when the unit recovers both heat and moisture.

This work generally concentrates on studying different energy recovery systems under wide range of ambient and operating parameters. It extended the measurement ranges to see more realistic and practical results as the producers in most cases make investigations based only on the minimum requirements.

The extension of the study range is significantly important to know to reach the highest energy savings during different seasons. The obtained results can be useful not only for researchers, developers, but also for building service and energy engineers in practice.

The main objective of this research work is

1- To investigate the maximum effectiveness values of the energy wheel by experimental tests conducted under extreme difference ambient air conditions parameters (T: -15 ^{o}C ~ 40^{o}C, RH: 30% ~ 100%), different air volume flow rates (400, 600, 800, 1000 and 1200 m^3/h) and energy wheel rotation speeds (2, 6, 10, 15 and 20 rpm) which was not investigated previously with the above boundary conditions.

2- To get much more data for effectiveness under extended ambient temperature and humidity ranges for a polystyrene material-based counter-flow heat exchanger (PHE) and a polymer membrane (polyethylene–polyether copolymer) material-based counter-flow energy exchanger (PEE) with the same boundary conditions in the previous object.
3- Development of a simulation model that can be suitable for determining the energy consumption of ventilation systems.
4- To investigate the annual energy performance of the heat wheel with high accuracy.
5- To build a TRNSYS model in order to build a model to calculate the energy performance of an existing variable refrigerant flow system and to build a model that can be used as a reference when a VRF system is proposed to a certain situation.
6- To investigate the feasibility to add an Energy Recovery Ventilation unit to an existing VRF system.
7- Performing a feasibility and economical study built as a function of thermal and estimated economic parameters using suitable optimization technique in order to achieve an optimum combination of the systems.
8- The obtained results can be useful for researchers as well as for building service and energy engineers in practice.

Chapter 3

Desiccant Coated Total Energy Recovery Wheel

3.1 Background

In literature review, no work was found to investigate the effectiveness of air-to-air energy recovery wheel coated with 3Å molecular sorption sieve under extreme difference ambient air conditions. No research results were found how the different air volume flow rates and different wheel rotation speeds as significant operation parameters influences the value of the sensible, latent and total effectivenesses. In this research work scientific experimental investigation was performed on the effect of different wheel rotation speeds on effectivenesses of sorption wheel under difference ambient air conditions and air volume flow rates. Optimal operating conditions are significantly important to know to reach the highest energy savings during different seasons.

At first in this chapter, the experimental methods used to test the performance of energy recovery wheel is discussed. The experimental test facilities will be described. In addition, the test equipment used in this work, the experimental procedures and the test plan will be introduced. Finally, the results and discussion will be presented

3.2 Description of the Test Facility

The experimental test facility was installed into the Indoor Air Quality and Thermal Comfort Laboratory of Budapest University of Technology and Economics. The size of the laboratory, where the test facility is placed, is 15 m long, 14,3 m wide and the size of the inner height is 5 m. The schematic diagram of the test facility is shown on **Figure 3.1.** A heat plate direct evaporation type exchanger used to generate the desired ambient air by a connected heat pump. Supply inlet air was produced from the exhaust air flowing through the direct evaporator which cooled or heated up the air due to a refrigerator. Therefore, more extreme supply input air condition range with less energy demand can be established considering also the available cooling/heating capacity. Humidification of the supply and exhaust air was ensured by mist generators placed inside the air duct for the exhaust air and for the AHU sections for the supply air. Capacity of evaporation unit was 1.8 [l/h] water for each one which increase the humidity of the air to reach the indoor standard conditions. Mist generators were placed into plastic trays. The generated mist adjusted and placed on a floating base while floating on top of the water inside the tray. However, due to their low capacities, the mist humidifiers were incorporated with ceramic water atomizer nozzles spraying water with rates of 12-20 [l/h]. This was fed by regulating tap water network pressure placed in points (9) as shown on **Figure 3.1.** to reach the desired and extreme relative humidity values. **Table 3.1** represents the path of air depending on to **Figure 3.1.** with the variable values measured at each point.

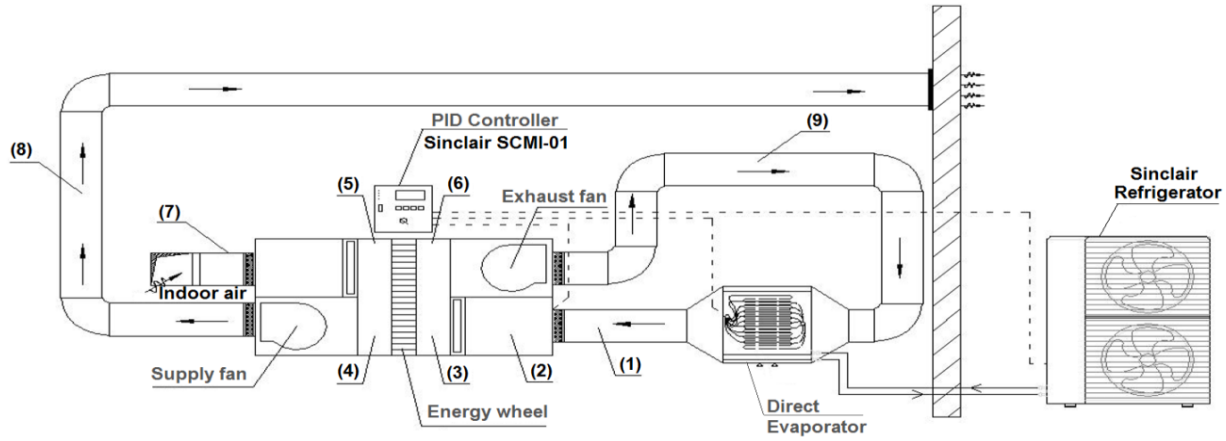

Figure 3.1. Schematic of the experimental test facility

Table 3.1. Variables measured on the experimental test facility

	Path of the air	**Variables measured**
1	Fresh Air Duct	$\dot{V}_{si}$[m^3/h]
2	AHU supply section	-
3	Sorption wheel (supply input)	T_{si} [°C]
		RH_{si} [%]
4	Sorption wheel (supply output)	T_{so} [°C]
		RH_{so} [%]
5	Sorption wheel (exhaust input)	T_{ei} [°C]
		RH_{ei} [%]
6	Sorption wheel (exhaust output)	T_{eo} [°C]
		RH_{eo} [%]
7	Indoor air duct	$\dot{V}_{ei}$[m^3/h]
8	Supply air duct	$\dot{V}_{so}$[m^3/h]
9	Exhaust air duct	$\dot{V}_{eo}$ [m^3/h]

A high-efficiency Enventus [47] energy wheel was installed into the test facility, which transfers sensible energy (temperature) and latent energy (humidity) between the two air streams to recover the heat energy and provides proper air quality. The following specifications are given by the wheel producer in **Table 3.2.**

Table3.2. Specifications of the investigated sorption wheel

Material of sorption wheel	Aluminium
Coating of sorption wheel	Molecular sieve 3A^o
Coefficient of thermal conduction of the wheel	230 W/m K
Geometrical diameter of the wheel	540 mm
Geometrical width of the wheel	200 mm
Height of corrugated plates in the wheel	1.5 mm
Width of corrugated plates in the wheel	3 mm
Size of surfaces capable of heat-, and moisture transfer	170 m^2

Temperature (T_{si}, $T_{so,}$ T_{ei}, T_{eo} [°C]) and relative humidity, (RH_{si}, RH_{so}, $RH_{ei,}$ RH_{eo} [%]) values were measured with the help of TESTO type humidity and temperature metering instruments one of the world leader in the manufacture of portable test and measurement instrumentation and solutions [48], these instruments were placed in as indicated on **Figure 3.1.** The calibration of these instruments was executed by the producer. These temperature and

relative humidity measurements in points which were in the mid-plane of air ducts in the mixing chamber before and after the energy wheel to control of the actual air flow data with the set point value. But to get the steady-state conditions, the velocity-profile was measured in the duct according to standard EN 12599 before each measurement. The measurements were taken at the same time range to avoid fluctuation of supply side entering air temperature and exhaust side entering air temperature.

A TESTO480 data recorder recorded the data measured by the metering devices. Intervals of 2 seconds were used. The TESTO480 data was implemented to the pc through the producer application software. The volumetric flow rate of supply air was measured by another TESTO instrument with type hot-wire anemometer was placed in the center of the air duct, at point (8), in order to measure the volumetric flowrate of the supply air.

3.3 Experimental Procedure

Experimental tests were conducted under different operating conditions to investigate the sensible, latent and total effectiveness of the sorption rotary wheel. The goal was to maintain the parameters measured constant as much as possible. Based on test measurements, the exhaust air inlet temperatures range during the test periods was set between Tei = (14-26) [°C] and relative humidity range of RHei = (25-55) [%].

3.2.1 Regulation of temperature and humidity of fresh air supplied

The supply air temperature (Tsi) was set with the use of *Sinclair SCMI-01* type PID controller as indicated in **Figure 3.1** to regulate the power input in DC inverter refrigerator unit, installed to the test facility. The measurements were performed within the widest temperature and relative humidity possible range that the test facility can provide. As it could be regulated between the 10 to 100%, with 10 %, intervals, the compressor begins to operate instead of the DC-Inverter compressor. The suitable selection of the P (proportional), I (integral) and D (derivative) parameters of the PID controller provided the minimization of the instability of the system. Therefore, the proper PID parameter values were determined under different air conditions to obtain the desired temperatures with minimum fluctuations in the PID signals.

Relative humidity of supply input air (RHsi [%]) was regulated with the help of ultrasound humidifiers placed into sections (2) as indicated in **Figure 3.1**. It was incorporated with two ceramic water atomizer nozzles spraying water that was placed into section (9) to be able to obtain higher relative humidity range especially for higher volumetric flow rates. The ceramic insert spray nozzles were connected to the tap water network by pipes. The two water nozzles were separately connected to two water outlets. By this way there was no change on the water pressure that would influence the water spray rate.

The uncertainty in calculations of the temperature and humidity instruments is discussed in Chapter 7.

3.2.2 Regulation of temperature and humidity of exhaust air

The temperature of exhaust air (Tei [°C]) was controlled with the use of a portable electrical air heater that was placed in point (7) in **Figure 3.1.** The exhaust air (Tei [°C]) could only increase the temperature to the desired range. The humidity of exhaust air (RHei [%]) was regulated with the help of two of the mentioned ultrasound humidifiers placed in point (7) in **Figure 3.1**, that helped to increase the humidity to be (RHei = 2-8 [%]) by the turning on every ultrasound humidifier in separate.

3.2.3 Setting the speed of rotation of the wheel

The speed of rotation of the wheel (ω [rpm]) was controlled with a potentiometer connected to the control panel. The speed of the wheel deducted from the voltage screen shown on the control panel. The speed-values were obtained through measurement, using a *Voltcraft DT30LK* type laser tachometer. Based on the results shown in **Table 3.3** wheel speed could be collected indirectly.

Table 3.3 Average wheel rotation speed ω [rpm] – voltage U [V] relation measurement

Average rotation speed [rpm]	**Voltage [V]**	**Measurement duration [min]**	**Average fluctuation of rotation speed [±rpm]**
1.998	0.83	10	0.002
6.059	2.87	10	0.002
10.030	4.80	10	0.002
15.088	7.28	10	0.002
20.011	9.69	10	0.002

3.4 Test Plan

The measurement plan was compiled based on the following aspects:

- The measurement plan was divided into two conditions (Summer and Winter).
- Summer condition represent the period between (April-September) while the winter condition represent the period between (October-March)
- The indoor ambient conditions have been selected as per recommended inside design values in ASHRAE HVAC Application As shown in **Table 3.4.** [49]

Table 3.4. Recommended inside design conditions for summer and winter operations

Application	Summer				Winter		
	Extra		Commercial		With Humidification		Without Humd
	T_{DB} (ºC)	RH (%)	T_{DB} (ºC)	RH (%)	T_{DB} (ºC)	RH (%)	T_{DB} (ºC)
Comfort House Apartments	23 - 24	50 - 45	25 - 26	50 - 54	23 - 24	35 - 30	24 - 25
Retail Shops	24 - 26	50 - 45	26 - 27	50 - 45	22 - 23	35 - 30	23 - 24
High latent load app.	24 - 26	60 - 55	26 - 27	60 - 50	22 - 23	40 - 35	23 - 24
Factories	25 - 27	55 - 45	27 - 29	60 - 50	20 - 22	35 - 30	21 - 23

- From the **Table 3.4** the winter indoor conditions was selected to be as follows:

  Tei = 22 [°C]

  RHei = 35 [%]

  While the summer indoor conditions was selected to be as follows:

  Tei = 24 [°C]

  RHei = 45 [%]

- The target values of fresh air temperature were conducted by a step of Tsi = 5 °C in the range of Tsi = (-15 to 0) [°C] measured in winter conditions and Tsi = (5 to 40) [°C] measured in summer conditions.
- The target values of supply air inlet relative humidity were conducted by a step of RHsi = 10 % in the range of RHsi = (30 to 100) [%] measured in Winter and summer. But the relative humidity of supply inlet air was 100 [%] from Tsi = (-15 to 20) [°C].

- All target value pairs Tsi [°C] – RHsi [%] were measured under different five rotational speeds.
- The input variable parameters for wheel speed was 2,6,10,15 and 20 rpm.
- The input variable parameters for volume flow rate was 400,600,800,1000 and 1200 m^3/h. which represents the set volume flow rate interval for the direct evaporator.
- All measurements were taken under continuous monitoring of the Tei [°C], RHei [%], $\dot{}$ [m^3/h] variables, and maintenance these values within the desired range.
- The order of setting wheel speed and fresh air variables shall be the follows:

$$\omega \text{ [rpm]} \rightarrow \dot{} \text{ [m}^3\text{/h]} \rightarrow \text{Tsi [°C]} \rightarrow \text{RHei [\%]}.$$

- The duration of measurements was at least 300 seconds at intervals of 2 seconds which were enough to get the steady-state conditions
- The sequence of measurements was determined so that the difference between desired temperature and humidity values was minimal. This helped reaching the stationary state of operation faster.

3.5 Calculation of the Energy Wheel Effectiveness

The effectiveness **Equations (3.1-3.3)** proposed by ASHRAE Standard 2008 [50] that is used in this work is defined in the equations below as the effectiveness is given as sensible effectiveness (heat transfer process), latent effectiveness (moisture transfer process), and total effectiveness (total energy transfer including heat and moisture transfer).

The methodology is based on air temperature and air humidity measurements on the inlet and outlet parts of the energy wheel under steady state conditions.

$$\varepsilon_S = \frac{m_{si}\times(T_{si}-T_{so})}{Min\,\lfloor m_{si},m_{ei}\rfloor\times(T_{si}-T_{ei})} \quad (3.1)$$

$$\varepsilon_L = \frac{m_{si}\times(X_{si}-X_{so})}{Min\,\lfloor m_{si},m_{ei}\rfloor\times(X_{si}-X_{ei})} \quad (3.2)$$

$$\varepsilon_T = \frac{m_{si}\times(h_{si}-h_{so})}{Min\,\lfloor m_{si},m_{ei}\rfloor\times(h_{si}-h_{ei})} \quad (3.3)$$

The supply and exhaust mass flow rate are calculated from **Equation (3.4).**

$$\dot{m} = \rho_a \times \dot{V} \quad (3.4)$$

The sensible effectiveness can be calculated directly as the dry bulb temperature can be substituted in the equation with no need to convert. In contrast, the latent and total effectivenesses were calculated after obtaining the values for absolute humidity and specific enthalpy from the **Equation (3.5-3.6).**

$$x = 0.622 \times \left[\frac{p_w}{p_a-p_w}\right] \quad (3.5)$$

$$h = Cp_a \times T + x \times \left[Cp_v \times T + h_g\right] \quad (3.6)$$

3.6 Results and Discussion

Using the measured data, the calculated sensible, latent, and total effectiveness values of the tested energy wheel at different operation and ambient parameters and correlation between the wheel and different parameters will be presented in this section.

All results were obtained under Tei = 22 [°C] and RHei = 35 [%] constant exhaust air parameters and in the range of supply air temperature (Tsi) between -15 °C to 0 °C and at supply relative humidity (RHsi) 100 [%]. In summer conditions, the results obtained for Tei = 24 [°C] and RHei = 45 [%] constant exhaust air parameters and in the range of supply air temperature 5 °C to 40 °C and supply air relative humidity varied depending on the experimental process.

3.6.1 Sensible Effectiveness vs. Dry-Bulb Temperature

Figure 3.2 presents the sensible effectiveness vs. dry bulb temperature under different volume flow rates at the maximum wheel speed (ω = 20 [rpm]). It seems, from trending data, the maximum sensible effectiveness occurs at the lowest air volume flow rate. However, the trend for every volume flow rate shows almost the same values at different temperatures

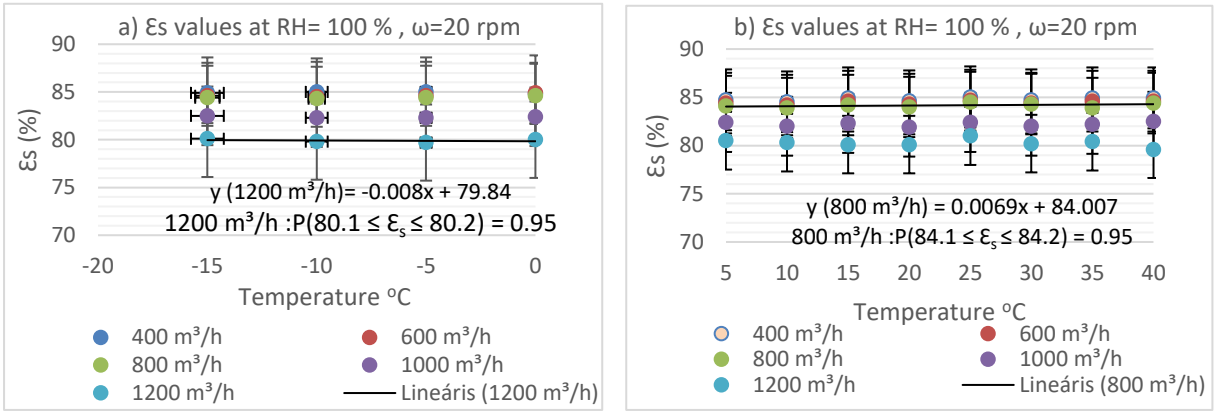

Figure 3.2. Sensible effectiveness (%) vs. Dry Bulb Temperature (°C) at different air volume flow rate and at ω = 20 rpm; (a) Winter Condition, (b) Summer Condition

3.6.2 Latent Effectiveness vs. Wheel Speed

Latent effectiveness was more sensitive for wheel rotation speed step changing under the same air volume flow rate and different supply inlet temperature conditions **Figure 3.3.** It can be realized, from trending data, the maximum Latent effectiveness occurs at the highest wheel speed. However, the temperatures show almost the same trend at different wheel speeds

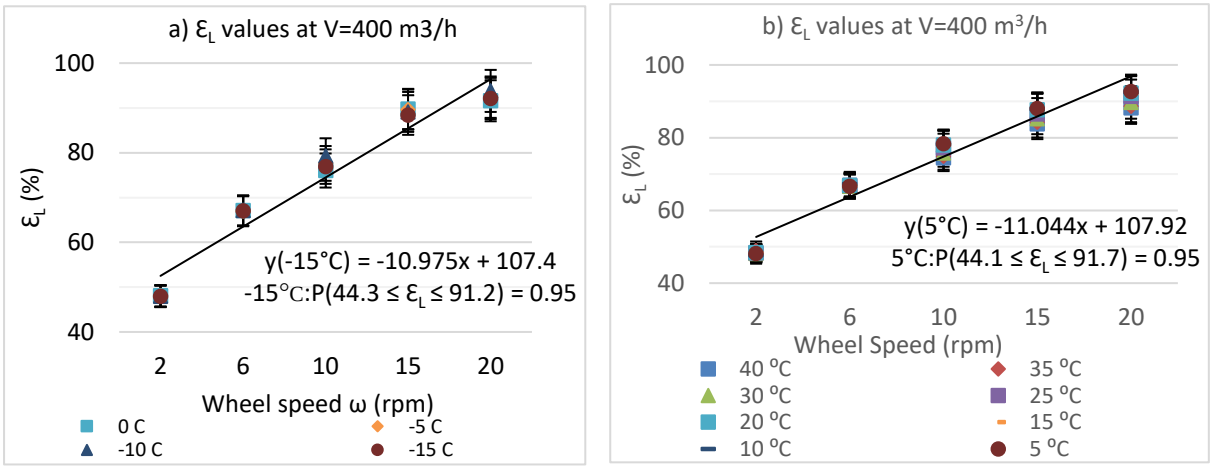

Figure 3.3 Latent effectiveness (%) vs. wheel speed (rpm) at different dry bulb temperature (°C) and at $\dot{V}$ = 400 m^3/h; (a) Winter Condition, (b) Summer Condition

3.6.3 Total Effectiveness vs. Wheel Speed

Figure 3.4 below presents the Total effectiveness vs. wheel speed for different dry bulb temperature at $\dot{V}$ = 400 m^3/h, it can be realized, from trending data, the maximum Total effectiveness occurs at the highest wheel speed. However, the temperatures show almost the same trend at different wheel speeds.

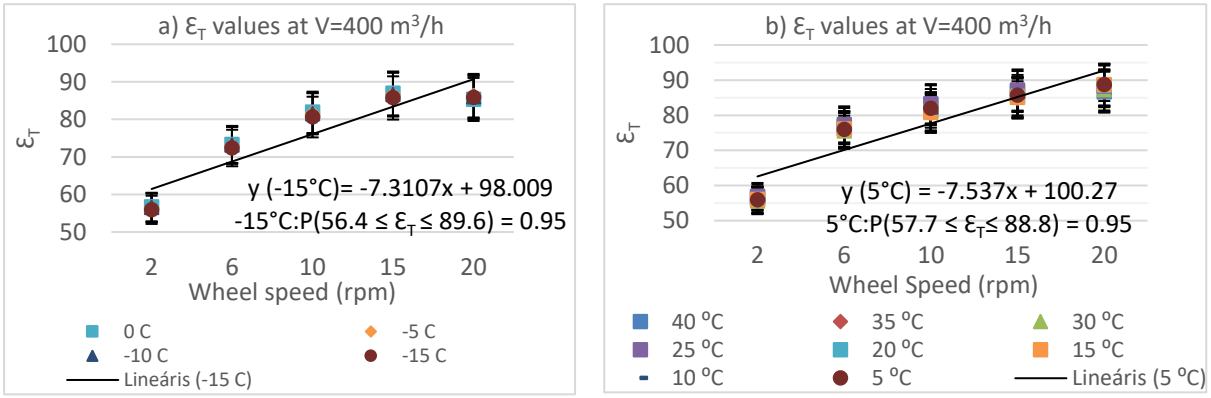

Figure 3.4. Total effectiveness (%) vs. wheel speed (rpm) at different dry bulb temperature (°C) and at $\dot{V}$ = 400 m^3/h; (a) Winter Condition, (b) Summer Condition

3.6.4 Maximum Effectiveness vs. Dry-Bulb Temperature

Figure 3.5. shows that all the effectiveness's values in the function of dry bulb temperature levels at lowest volume flow rate ($\dot{V}$ = 400 m^3/h) and maximum wheel speed (ω = 20 rpm) to obtain the highest effectiveness. It can be obtained, from trending data that the maximum effectiveness is the latent effectiveness overall at the same operating parameters which reaches almost 94 %. The same conclusion could be obtained from the other investigated volume flow rate

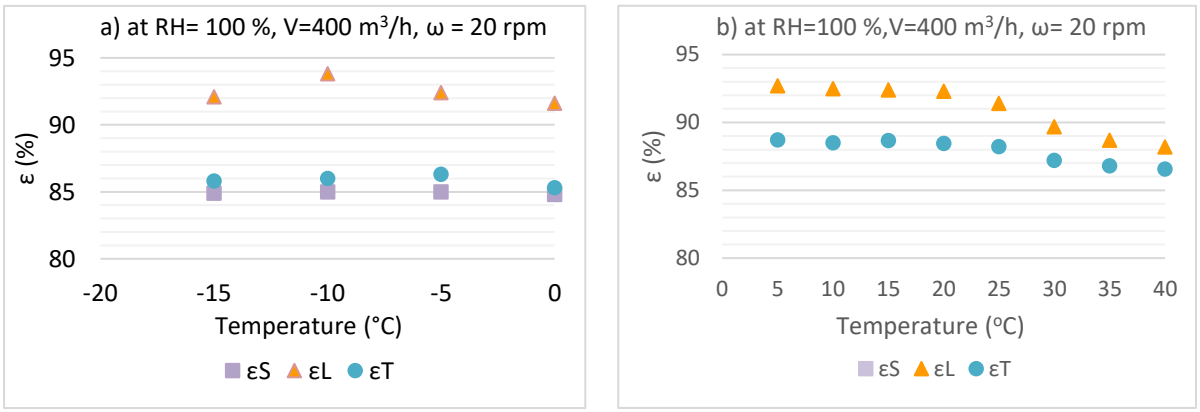

Figure 3.5. Maximum effectiveness (%) vs. Dry Bulb Temperature (°C) for effectiveness at ω = 20 rpm and at $\dot{V}$ = 400 m3/h; (a) Winter Condition, (b) Summer Condition

3.6.5 Latent and Total Effectiveness vs. Relative Humidity

Figure 3.6. below presents the latent and total effectiveness in the function of relative humidity for different dry bulb temperature (°C) at $\dot{V}$ = 400 m^3/s air volume flow rate.

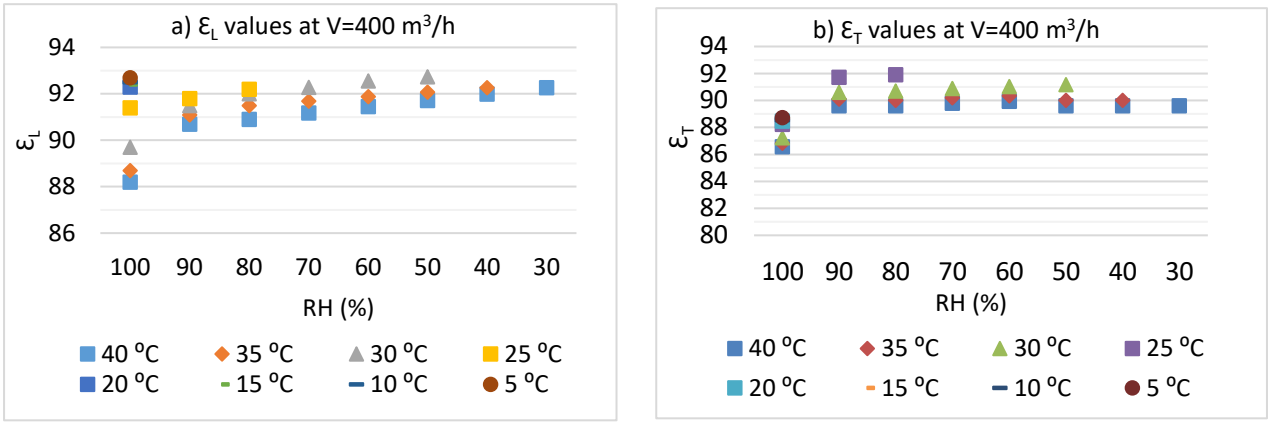

Figure 3.6. Latent (a) and Total (b) effectiveness (%) vs. Relative Humidity (%) at different dry bulb temperature (°C) and at $\dot{V}$ = 400 m^3/h

It can be realized, from trending data that the maximum latent and total effectiveness occurs at the lowest temperature values; as it can be noticed in summer condition figure. However, the effectiveness increased when the relative humidity decreased for different temperatures.

In the next chapter, the effectiveness of different energy recovery system will be studied based on an experiment to see the how is the value effectiveness is changing when using a different energy recovery system.

Chapter 4

Energy Recovery with Polymer Membrane Material-Based Counter-Flow Energy Exchanger

In this chapter, the performance of two counter-flow heat/enthalpy energy exchangers are experimentally tested under different operating conditions, and the values of the sensible, latent, and total effectiveness are presented. The EN-1314-7 [51] is used as standard in this experiment. The experimental process will be described. Furthermore, the test plan, the results and discussion will be presented.

4.1 EN 1314-7 International Standard

The international standard EN 13141-7 specifies the laboratory test methods and test requirements for testing of thermal, aerodynamic, acoustic, and electrical performance of mechanical supply and exhaust ventilation units in a single dwelling [51]. This standard covers units that contain at least within one or more casings, supply and exhaust air fans, air filters, an air-to-air heat exchanger, and a control system. It gives the most relevant instructions for performance testing of a mechanical supply and exhaust ventilation units (including heat recovery) for mechanical ventilation systems. Such a unit can be provided in more than one assembly, the separate assemblies of which are designed to be used together without dealing with non-ducted units or reciprocating heat exchangers and or with units that supply several dwellings. This standard does not cover ventilation systems that may also provide water space heating and hot water, or units including combustion engine-driven compression heat pumps and absorption heat pumps [51]. Based on the standard, the heating performance test should be conducted under 7 ^{o}C, 2 ^{o}C, and -7 ^{o}C outdoor air inlet (supply air inlet) and 20 ^{o}C exhaust air inlet dry-bulb temperature conditions. For cooling performance tests, the outdoor air temperature should be set at 35 ^{o}C and 27 ^{o}C under 27 ^{o}C exhaust air inlet dry-bulb temperature conditions [51].

4.2 Description of the Test Facility

The Energy Recovery Test Facility (ERTF) was developed in the Indoor Air Quality and Thermal Comfort Laboratory of the Budapest University of Technology and Economics. The developed (ERTF) enables the test to be conducted in a much wider range from the aspect of ambient outdoor air (as the supply air inlet) temperature and humidity values.

The effectiveness of a polystyrene material-based counter-flow heat exchanger (PHE) and a polymer membrane (polyethylene–polyether copolymer) material-based counter-flow energy exchanger (PEE) integrated in a Zehnder ComfoAir 350 ventilation device was investigated experimentally **Figure 4.1** under steady-state conditions which was reached by monitoring the measured parameters continuously till the output data has not changed. These exchangers are basically counter-flow types, but their inlet sections are from cross-flow zones as thermally and energy wasteful corners. The remaining cross-flow zones do not play as crucial a role if the counter-flow zone has sufficient surface area. For the cross-flow zones, the plates are employed; otherwise, the stream-joining problem would once again arise. For the counter-flow zones, it is possible, so as to increase efficiency, to subdivide the plates and make use of ducts **Table 4.1.** This results in more surface area being available for heat and moisture exchange.

Figure 4.1. Photo from the energy recovery test facility (ERTF) experimental test facility

The height of the duct is very small (2.5 to 4 mm), allowing a very large exchange area to be packed into a small volume [52]. An additional objective was to be able to carry out the measurements within the widest possible range.

Table 4.1. Geometrical specifications of the exchanger [52].

Parameter	Value	Unit
Length of plates	4	mm
Length of ducts	8	mm
Heat/moisture exchange area	30	m^2
Height of plate	370	mm

Setting of Air Temperature of Fresh Air (Supply Air Inlet)

The target value of supply inlet air temperature (tsi (°C)) was set by an *SCMI-01* proportional–integral–derivative (PID) controller unit as shown in **Figure 4.2.** Considering the set supply air inlet temperature and based on the measured actual supply air inlet temperature and surface temperature of the direct evaporator, the PID controls the necessary performance of the compressor through the continuous modification of the direct current (DC) inverter RPM regulation

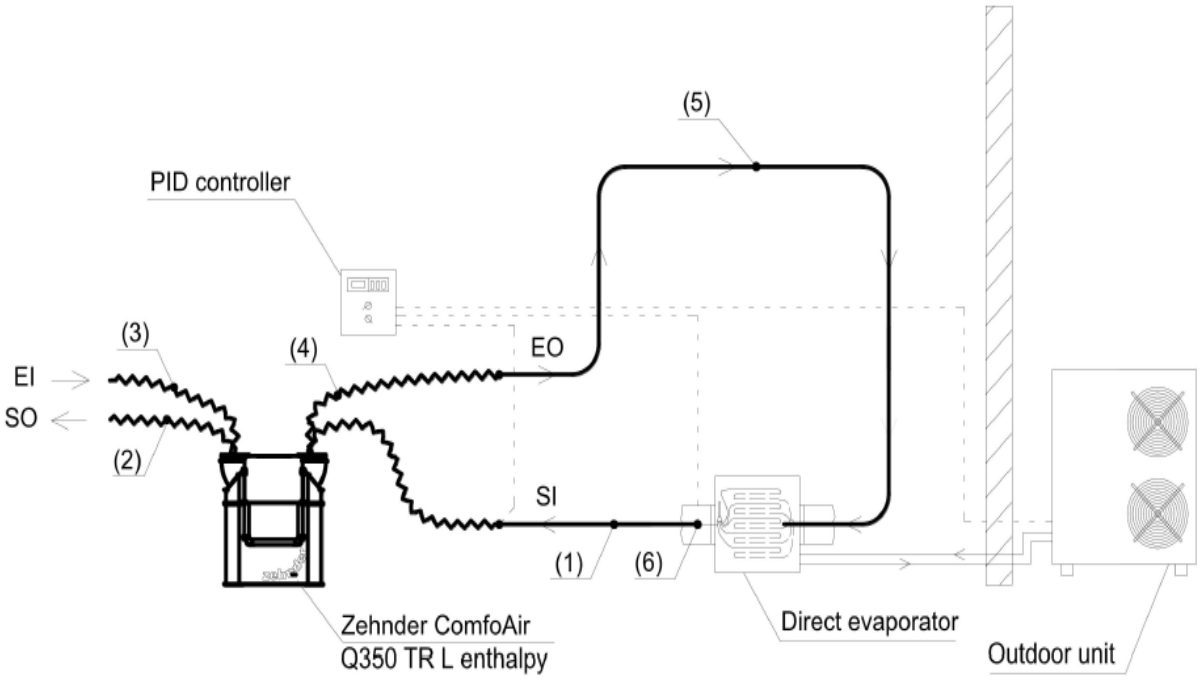

Figure 4.2. Schematic of ERTF experimental test facility.

Setting of Air Humidity of Fresh Air (Supply Air Inlet Section)

The relative humidity of the supply air inlet section (RHsi (%)) was set by water atomizers placed at point (5) in **Figure 4.2**. The material of these atomizers was ceramic, supplied from the tap water. The required mass flow of the water medium was regulated by Herz radiator valves.

Air Temperature and Humidity Settings on Exhaust Air Inlet Section

To provide a constant exhaust air inlet temperature (Tei (°C)), a *HOME FK 30* electrical heater and, to keep constant relative humidity (RHei (%)), ultrasonic humidifiers were placed close to the incoming exhaust air into the test facility

4.3 Experimental Data Recording and Evaluation

Temperature and relative humidity data were recorded using a TESTO480 data recorder with TESTO sensors, placed into the middle of the air ducts at measurement points (1), (2), and (3) indicated in Figure 2. The calibration of these instruments and the uncertainties is shown in Chapter 7.The set air volumetric flow rates were controlled by a TESTO Smart probes 405i hot-wire anemometer. The values of the effectiveness were determined from the conducted measured values using **Equations (3.1-3.3)** used in the previous chapter.

The test conditions were significantly extended for the supply air inlet condition parameters (ambient temperature, humidity, enthalpy) compared with the existing standard (EN 13141-7) used in this research work.

4.4 Description of the Test Plan

The measurement plan was compiled on the basis of the following aspects:

- The test plan was basically divided into two ambient air conditions (winter outdoor air conditions for heating performance tests and summer outdoor air conditions for cooling performance tests).
- The extract air inlet conditions were set during the experiments based on the instructions by European Standard EN 13141-7, as summarized in **Table 4.2** [51].

Table 4.2. Air temperature conditions for the heating and cooling performance tests [51].

Extract Air Inlet Dry-Bulb (Wet-Bulb) Temperature	**Outdoor Air Inlet Dry-Bulb (Wet-Bulb) Temperature**
Heating performance test	
20 (12) °C	7 (6) °C
20 (12) °C	2 (−1) °C
20 (12) °C	−7 (−8) °C
Cooling performance test	
Extract Air Inlet Dry-Bulb (Wet-Bulb) Temperature	**Outdoor Air Inlet Dry-Bulb (Wet-Bulb) Temperature**
27 (19) °C (mandatory)	35 (24) °C (mandatory)
27 (19) °C (optional)	27 (19) °C (optional)

- Based on **Table 4.2**, the extract air inlet relative humidity was set as 38% for heating performance tests and 47% for cooling performance tests during the experiments.
- A further objective was to perform tests in much wider outdoor air conditions than the EN 13141-7 standard instructs, extending also the values of effectiveness given by the producer. In this way, a 5 °C outdoor air temperature step change was managed in the range between −15 and 10 °C, and the outdoor air relative humidity was step-changed by 10% in the range between 70% and 100% for heating performance tests. For cooling performance tests, the outdoor air conditions were set between 27 and 40 °C with a 5 °C step change and between 40% and 90% with a 10% step change.

- The achievable humidity was in a ratio applicable to all states of operation, with equal distribution of achievable relative humidity.
- All tests were conducted under four different air volume flow rates (100, 200, 300, and 350 m^3/h).
- The pressure difference between supply and exhaust fan was zero during the tests.
- The order of setting the steady-state test variables was the following before data recording: air volume flow rate, supply air inlet temperature, and finally the supply air inlet relative humidity.
- All tests were conducted under continuous monitoring of the supply air inlet relative humidity variables using the data collector instrument.
- The duration of each experimental test for every sequence order was at least 3000 s with a measurement rate of one per second to get the steady-state values. The sequence of measurements for all input parameters was conducted until the system reached the steady-state conditions.

4.5 Results and Discussion

The sensible, latent, and total effectiveness values of the polystyrene material-based counter-flow heat exchanger (PHE) and the polymer membrane (polyethylene–polyether copolymer) material-based counter-flow energy exchanger (PEE) are presented in this section, as calculated from the experimentally measured data for winter and summer tests. In addition, the sensible effectiveness of the PHE and PEE exchangers are compared under the same conditions.

4.5.1. Effectiveness of Air-to-Air PEE Energy Exchanger

Sensible Effectiveness vs. Dry-Bulb Temperature of PEE

Figure 4.3 shows the sensible effectiveness vs. dry-bulb temperature at different volume flow rates for winter conditions (RH = 90%) and summer conditions (RH = 40%) which was selected based on EN-13141-7 standards. It is noticeable that a slight increase in effectiveness occurs as the dry-bulb temperature increases. However, the trend for different volume flow rates shows that the highest effectiveness occurred at the lowest volume flow rate.

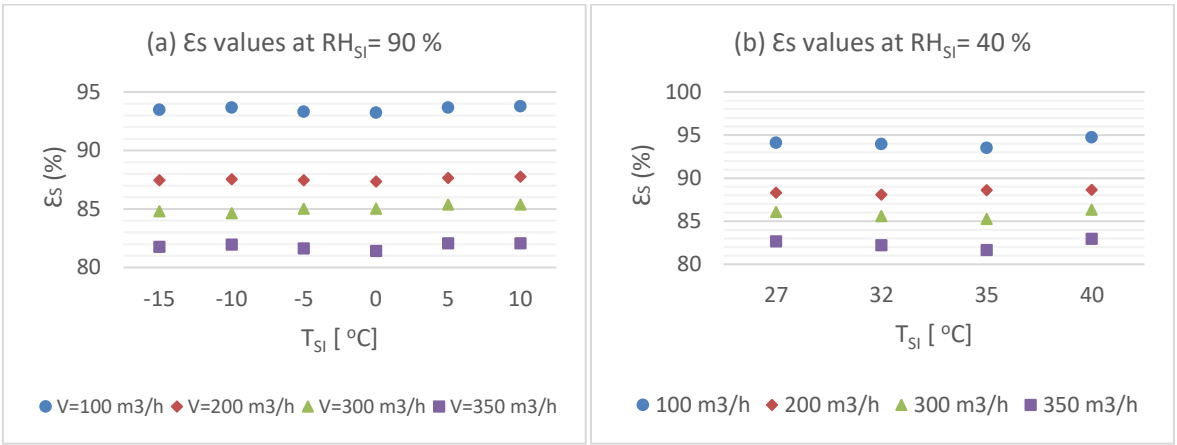

Figure 4.3 Sensible effectiveness (%) vs. dry-bulb temperature (°C) for different volume flow rates in (a) winter conditions and (b) summer conditions.

Latent Effectiveness vs. Dry-Bulb Temperature of PEE

Figure 4.4 shows the ε_L vs. T_{si} temperature at different volume flow rates for winter conditions (RH = 90%) and summer conditions (RH = 40%). A decrease in effectiveness happened as the outdoor temperature increased in Winter, and the trend shows a decreasing in effectiveness when the volume flow rate increases. On the other hand, the trend for different volume flow rates for effectiveness in summer conditions shows that the highest effectiveness occurred at the lowest temperature, and the trend shows a major difference between the effectiveness at 27 °C and that at other temperatures.

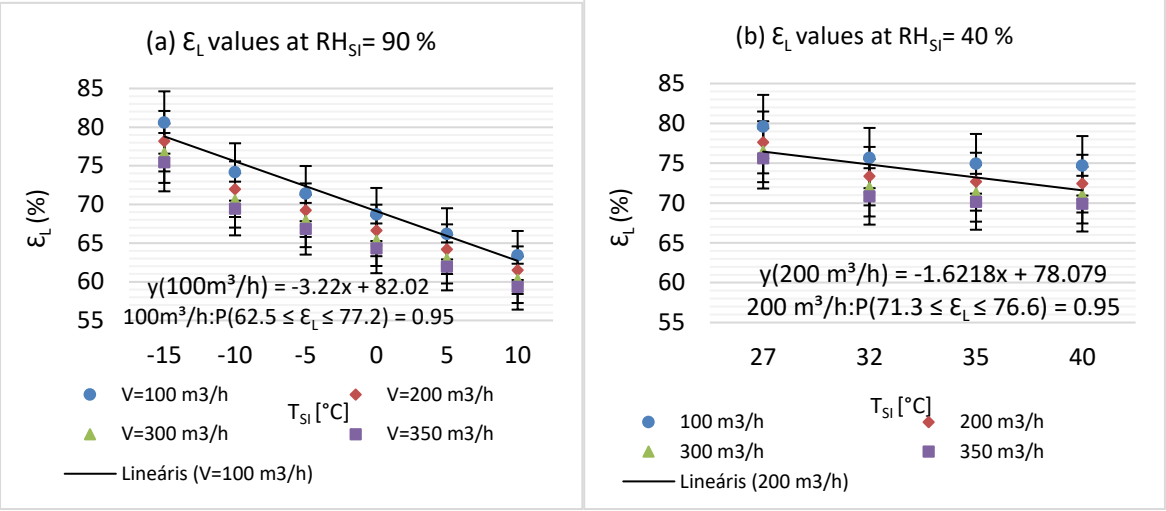

Figure 4.4. Latent effectiveness (%) vs. dry-bulb temperature (°C) for different volume flow rates in (a) winter conditions and (b) summer conditions.

Based on the results, the average values of latent effectiveness for the PEE were 69% in the winter and summer period.

Total Effectiveness vs. Dry-Bulb Temperature of PEE

Figure 4.5 shows the total effectiveness vs. dry-bulb temperature at different volume flow rates for winter conditions (RH = 90%) and summer conditions (RH = 40%). It is obvious that there is a decrease in effectiveness while the outdoor temperature increases in winter conditions, and a decrease in effectiveness when the volume flow rate increases. On the other hand, the highest effectiveness occurred at the lowest temperature in summer conditions.

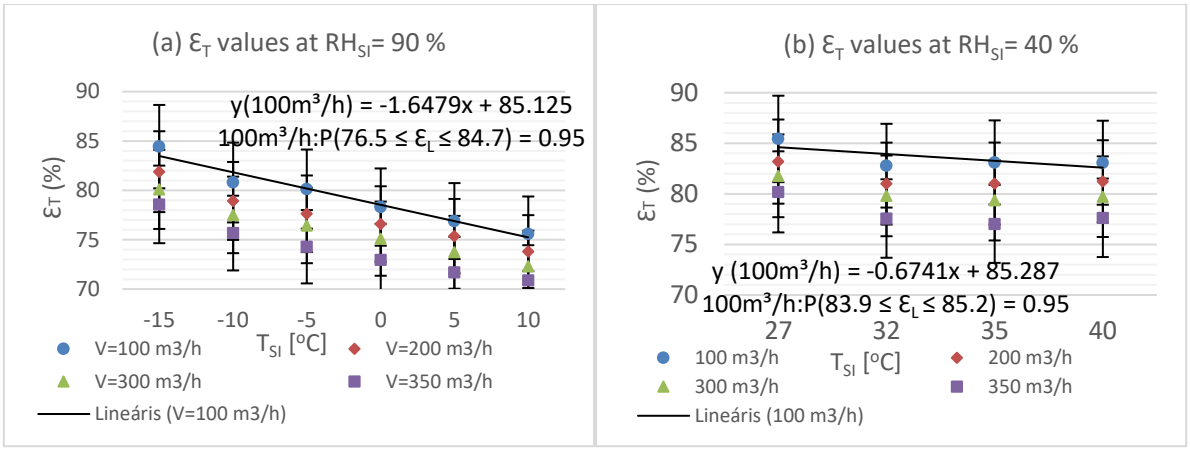

Figure 4.5. Total effectiveness (%) vs. dry-bulb temperature (°C) for different volume flow rates on (a) winter conditions and (b) summer conditions.

Based on the results, the average values of total effectiveness of the PEE were 77% in the Winter and 78% in the summer.

Latent Effectiveness vs. Relative Humidity of PEE

The correlation of latent effectiveness and relative humidity at a volume flow rate = 100 m^3/h for winter conditions and for summer conditions is presented in **Figure 4.6.** It can be seen that there is a slight decrease in effectiveness when the relative humidity increases in winter conditions, while, in summer conditions, the decrease in effectiveness is more obvious. On the other hand, the trend for different temperatures in terms of the effectiveness shows that the effectiveness decreases when the dry-bulb temperature decreases.

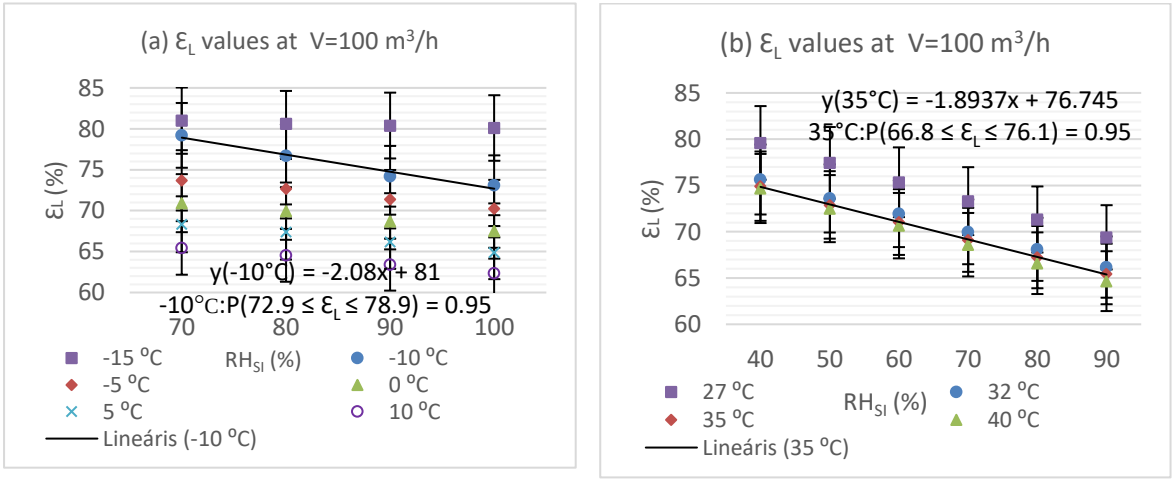

Figure 4.6. Latent effectiveness (%) vs. relative humidity (%) at a volume flow rate of 100 m^3/h in (a) winter conditions and (b) summer conditions.

Total Effectiveness vs. Relative Humidity of PEE

The correlation of total effectiveness and relative humidity at a volume flow rate = 100 m^3/h for winter conditions and for summer conditions is presented in **Figure 4.7.** Here, it can be seen that effectiveness decreases when the relative humidity increases. In addition, the effectiveness trend for different dry-bulb temperatures decreases when the temperature increases.

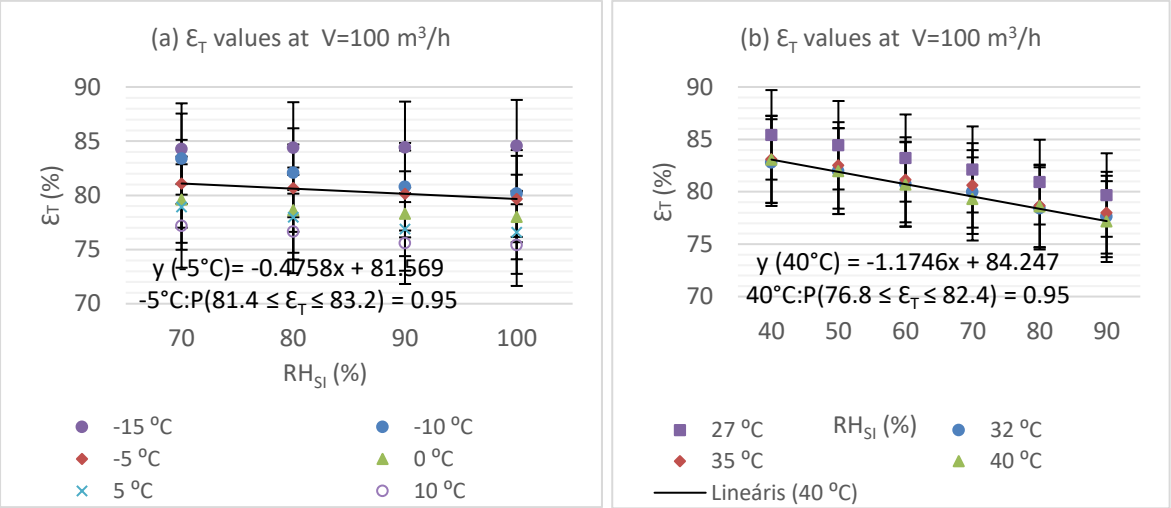

Figure 4.7. Total effectiveness (%) vs. relative humidity (%) at a volume flow rate of 100 m^3/h in (a) winter conditions and (b) summer conditions.

Effectiveness vs. Outdoor Air Inlet Dry Temperature for EN Standards

The experimental test of heating performance (winter conditions) was taken in accordance with outdoor temperature conditions defined in EN standards. It was measured separately for winter conditions, unlike the cooling performance (summer conditions), which was included in the summer conditions test plan. **Figure 4.8** below illustrates all the effectiveness values vs. dry-bulb (wet-bulb) temperatures as defined in EN standards.

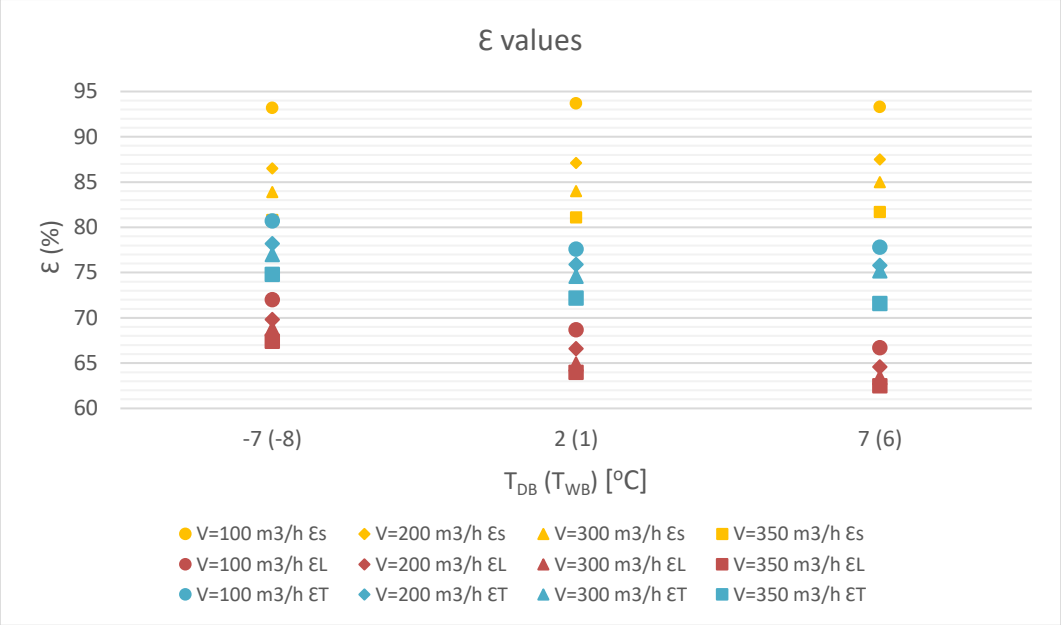

Figure 4.8. Effectiveness (%) vs. dry-bulb (wet-bulb) temperature (°C) at different volume flow rates.

4.5.2. Effectiveness of Air-to-Air PHE Heat Exchanger

Sensible Effectiveness vs. Dry-Bulb Temperature of PHE

Figure 4.9 shows the sensible effectiveness vs. dry-bulb temperature at different volume flow rates for winter conditions (RH = 90%) and summer conditions (RH = 40%). It is clearly visible that a slight increase in effectiveness occurs when the dry-bulb temperature increases. However, the highest effectiveness occurred at the lowest volume flow rate.

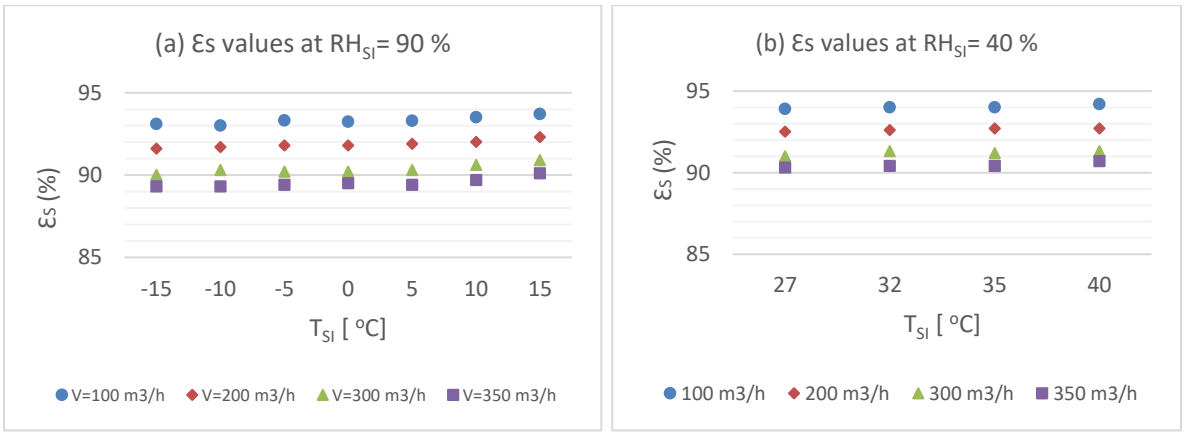

Figure 4.9. Sensible effectiveness (%) vs. dry-bulb temperature (°C) for different volume flow rates in (a) winter conditions and (b) summer conditions.

Sensible Effectiveness vs. Outdoor Air Inlet Dry Temperature for EN Standards

Figure 4.10. shows the correlation of sensible effectiveness and outdoor air inlet temperature as defined in EN standards under different volume flow rates. It can be seen that a slight increase in effectiveness occurs as the dry-bulb temperature increases.

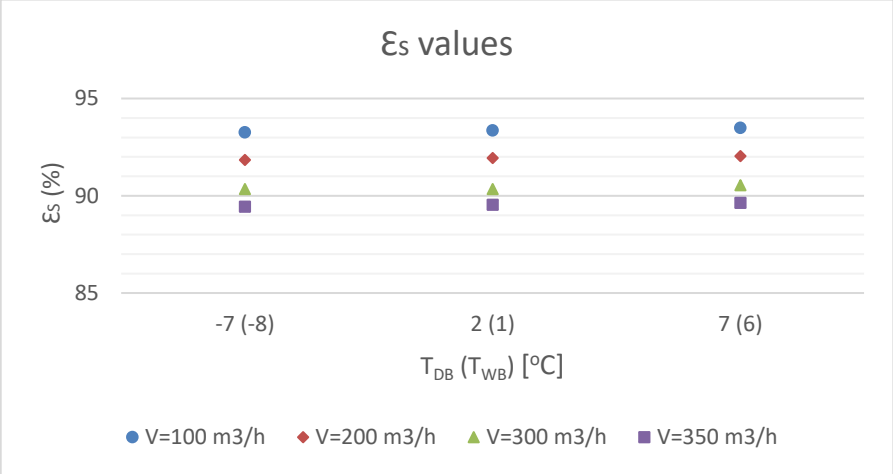

Figure 4.10. Sensible effectiveness (%) vs. dry-bulb (wet-bulb) temperature (°C) at different volume flow rates under EN standard test conditions.

Sensible Effectiveness Comparison between the PEE and PHE Exchangers

Figure 4.11 shows the comparison of sensible effectiveness of PEE and PHE exchangers under different dry-bulb temperatures and different volume flow rates for winter and summer conditions. The results show that the PHE overall has higher sensible effectiveness than the PEE, especially at higher air volume flow rates. Based on the results given by the tests, the average sensible effectiveness values for PHE in winter and summer conditions were 91% and 92%, respectively, while the average sensible effectiveness values for PEE were 87.2% in winter conditions and 87.8% in summer conditions. It can be noticed that the maximum values of sensible effectiveness were recorded in summer test conditions (with 40 °C ambient air as the supply air inlet temperature), at an air volume flow rate of 100 m^3/h, which were 94.2% for PHE and 94.1% for PEE.

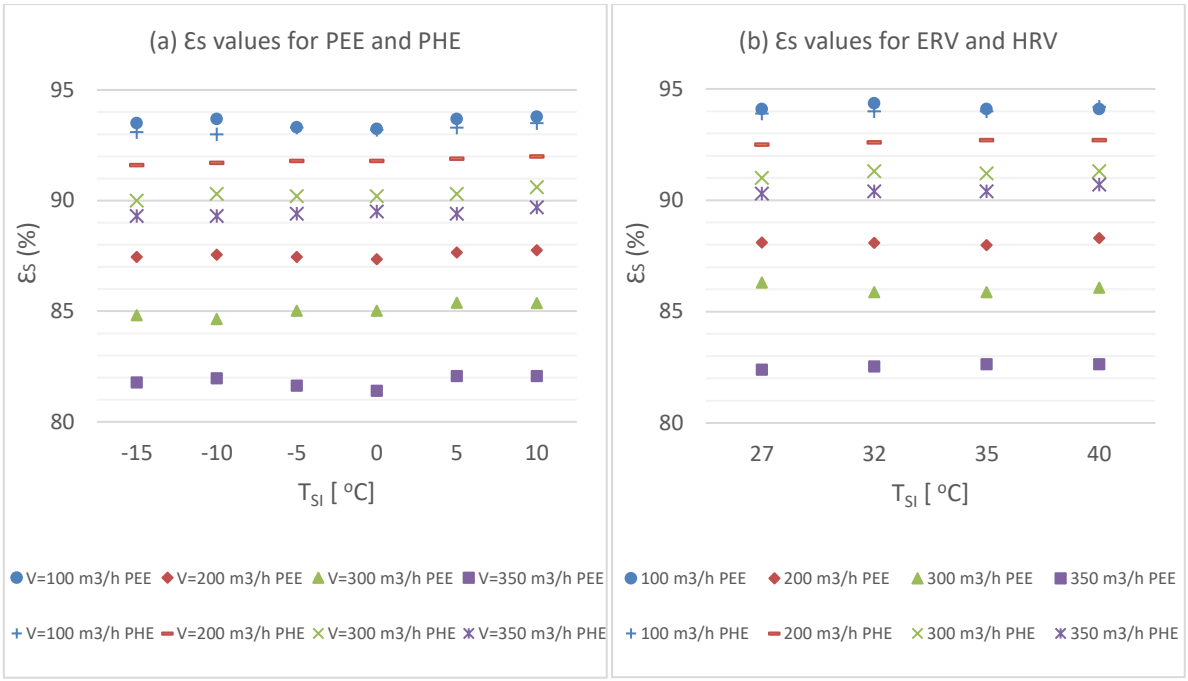

Figure 4.11. Sensible effectiveness (%) vs. dry-bulb temperature (°C) at different volume flow rates in (a) winter conditions and (b) summer conditions.

In the coming chapter, an experimental study of heat wheel operated in an AHU will be performed. Afterward, a simulation model will be built to see how this model can predict the effectiveness values comparing to the experimental values.

Chapter 5

TRNSYS Simulation Model for Heat Wheel Operated in Air Handling Unit

In this chapter, a complete system of an existing Air Handling Unit (AHU) with an air-to-air rotary heat wheel has been modeled for simulation using TRNSYS 18. The simulation results will be compared with the experimental results to see the agreements between the two outputs. The description of the investigated (AHU) and the developed TRNSYS simulation model will be described in the following sections. Furthermore, the output results will be discussed.

5.1 Description of the investigated AHU

Air Handling Unit (AHU), is a device used to regulate and circulate air as part of a heating, ventilating, and air-conditioning (HVAC) system. The main air handling components of the investigated system are an air-to-air rotary heat wheel that only recover the sensible heat, a mixing box which mix the supply and exhaust air stream with a different percentage, supply fan, exhaust fan, and direct expansion cooling/heating (DX) coil connected to a (VRV) variable refrigerant volume outdoor unit. **Figure 5.1** shows the elements of the investigated AHU and **Table 5.1** shows the list of the component description.

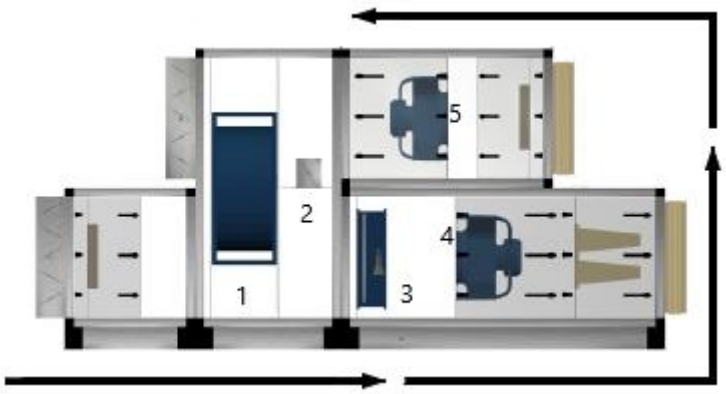

Figure 5.1. The schematic arrangement of components of AHU with the heat wheel.

Table 5.1. List of the description of the components.

1:	Air-to-air rotary heat wheel
2:	Mixing box
3:	Direct expansion cooling/heating (DX) coil
4:	Supply fan
5:	Exhaust fan

The detailed configuration for the AHU following the path of the arrow around **Figure 5.1** is as follows: the damper supply section, filter section, empty section, reciprocator heat wheel supply, mixing box supply, dx-coil, fan supply, filter supply, hole supply, hole return, filter return, and fan return.

The air damper was fully opened; the heat wheel rotation was operating at a constant speed throughout the experiment. The mixing box was fully closed so the supply air did not mix with the exhaust air.

The measurements were conducted from April 2019 to March 2020. The measurements were recorded on an hourly basis. The working hours of the retail shop were 7:00 a.m. to 8:00 p.m. throughout the year.

Figure 5.2 shows the air handling processes in the investigated AHU. The outside air passes through the air-to-air heat recovery wheel to recover the heat energy (state 1 to state 2) from the exhaust air inlet and it is further heated/cooled by a DX coil (state 2 to state 3) to the required supply air conditions at state 3. The air from the conditioned space enters the exhaust fan section and passes to the rotary heat wheel from the exhaust side, the supply air as upstream is passed through the rotary heat wheel, and it is cooled/heated from state 4 to state 5. On the regeneration side, the regeneration air is extracted (state 5 to state 6) into the ambient environment. The specification and the technical data of the AHU and the heat wheel, given by the producer, are provided in **Table 5.2.** The technical data for the supply and return fan are presented in **Table 5.3.** The technical specifications of the installed sensors and instrument are presented in **Table 5.4.**

Table 5.2. Specification and technical data for AHU and energy wheel

Parameter	Value	Unit
Length Overall	2897	mm
Insulation	Foam	-
Duct Supply (Width × Height)	1370 × 540	mm
Total heating capacity	12.3	kW
Total cooling capacity	10.9	kW
COP (Coefficient of Performance)	5.56	-
EER (Energy Efficiency Ratio)	3.99	-
Evaporating Temperature	6	°C
Heat Wheel Type	Sensible	%
Heat Wheel Effectiveness	74.9	%
Heat Wheel Pressure drop	80	Pa
Heat Wheel Power	12	kW

Table 5.3. Technical data for the supply and return fan

Device	Parameter	Value	Unit
Supply Fan	Type	Centrifugal Fan	-
	Total Static Pressure	619	Pa
	Flow Design	2250	m^3/h
	Rated Power	0.7	kW
Return Fan	Type	Centrifugal Fan	-
	Total Static Pressure	473	pa
	Flow Design	1850	m^3/h
	Rated Power	0.49	kW

Table 5.4 Specifications of the sensors and instruments.

Device	Working Range	Accuracy
Temperature Sensor	−40 to 150 °C	±0.4 °C
Humidity Sensor	10–90%	±3%
Air velocity Sensor	2–20 m/s	±0.2 m/s
Electricity energy meter	5–100 A	±1%

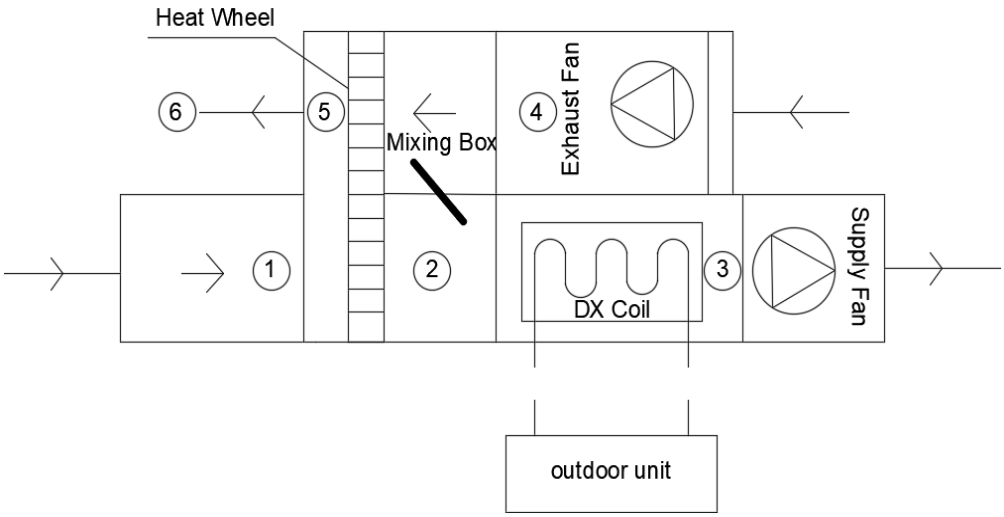

Figure 5.2. The schematic arrangement of components of AHU with the heat wheel.

Experimental tests were conducted by measuring the temperature, relative humidity, mass flow rate across the AHU, process, and regeneration air stream flow rate simultaneously using sensors. A digital sensor was used for precise measurement of the temperature and relative humidity at different states in AHU. The regeneration airflow rate at different sections in the AHU was also measured with the digital sensors. A digital temperature controller in a conditioned space controls the temperature depending on the changes in room temperature. The computer software by the manufacturer for monitoring and recording was used to observe and record all the data obtained by the sensors in the AHU. Since this research focused on the annual heat recovering by the heat wheel, the mixing box between the inlet and outlet sections of the AHU was set to be closed during the investigations. **Figure 5.3** shows a screenshot of the investigated AHU in the building management system (BMS) program. The recorded data were evaluated. Energetic investigations were performed on the performance of AHU using the measurements. To achieve this, the mathematical approaches described in Section 3 were implemented.

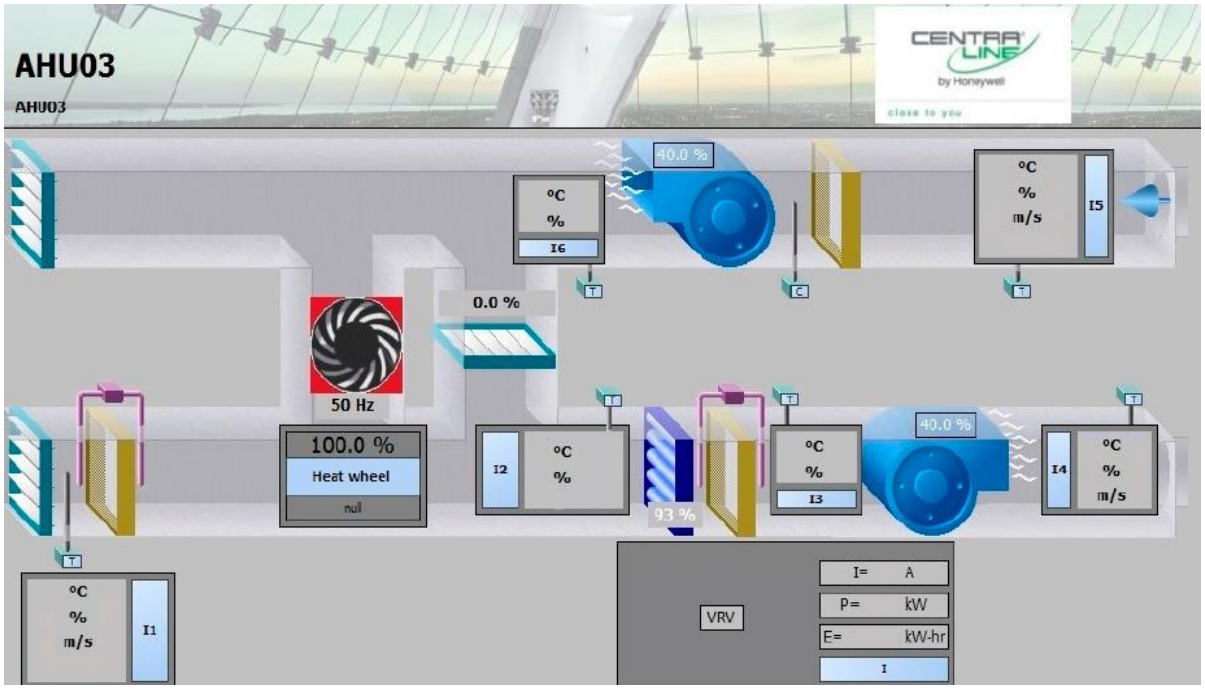

Figure 5.3. The AHU schematic in the building management system (BMS).

5.2 Description of the Mathematical Model

In this study, the performance of the air handling unit was investigated by calculating the cooling/heating capacity of the direct expansion coil, electrical power input of the VRV, coefficient of performance (COP), and the effectiveness of the heat recovery wheel. The cooling/heating capacity ($\dot{Q}_c$) of the system is expressed in **Equation (5.1)** [53]:

$$\dot{Q}_c = \dot{m}_a(h_3 - h_2) \tag{5.1}$$

where $\dot{m}_a$ is the mass flow rate of air leaving the coil (kg/s), which is calculated by the multiplication of the average measured velocity of the air (m/s) and the area of the cross-section of air duct (0.74 m^2), and the density of the air (ρ_{air}), which is around 1.2 kg/m^3. h_2 and h_3 are the enthalpies of the air in states 2 and 3, respectively **(Figure 5.2).**

The power consumption of the VRV system E_{comp} [54] is calculated using **Equation (5.2)**:

$$E_t = E_{comp} \tag{5.2}$$

Where E_{comp} is the power consumption of the compressor, which is measured by using an energy meter.

$\dot{Q}_r$ is the regeneration heat supplied by the energy wheel [53], which is calculated by:

$$\dot{Q}_r = \dot{m}_r(h_1 - h_2) \tag{5.3}$$

Where $\dot{m}_r$ is the mass flow rate of regeneration air and h_1 and h_2 are the enthalpies in states 1 and 2, respectively.

The coefficient of performance (COP) of the system is calculated [55] using the **Equation (5.4)**:

$$COP = \frac{\dot{Q}_c}{E_t} \tag{5.4}$$

The sensible effectiveness of heat recovery wheel (HRW) is determined by **Equation (5.5)** [56]:

$$\varepsilon = \frac{\dot{V}_s(T_1 - T_2)}{\dot{V}_{min}(T_1 - T_4)} \tag{5.5}$$

where T_1 is the outdoor air temperature at the supply inlet of the heat wheel, T_2 is the air temperature in the supply outlet of the heat wheel, and T_4 is the air temperature in the exhaust inlet of the heat wheel. $\dot{V}_s$ is the volume flow rate of the supply air (m^3/h) and $\dot{V}_{min}$ is the smaller volume flow rate (supply or exhaust air) (m^3/h).

The sensible heat transfer is determined by **Equation (5.6)** [57]:

$$\dot{Q}_s = \dot{V}_{min} \cdot \rho_{air} \cdot C_p \cdot (T_1 - T_4). \tag{5.6}$$

5.3 Description of the Developed TRNSYS Model

Figure 5.4 shows TRNSYS model of the AHU system. The components used in the model were selected from the TESS library. The system was modeled and simulated using TRNSYS to compare the performance of the simulated and the measured data throughout the year.

Type 9e (data reader) was used to read the ambient parameters for the measured outdoor dry bulb temperature and relative humidity. These parameters were read from an external file that contained the measured outdoor ambient parameters. The same type was used to read the return ambient parameters and the volume flow rate from the indoor space. The actual measurements from the outdoor and the return from the space were used to perform an accurate validation of the TRNSYS model.

The rotary heat wheel was modeled as type 760 as it represents sensible air-to-air heat recovery with controlled outlet conditions, DX coil was modeled as type 136, type 65c, and type 46a used as an output plotter and printer. Type 111b represented the supply and return air fans. The cooling and heating process signals were monitored using type 165 from the TESS library. Type 14 (time-dependent function) was used as a schedule for the running system to work during the working hours (7:00 a.m. to 8:00 p.m.).

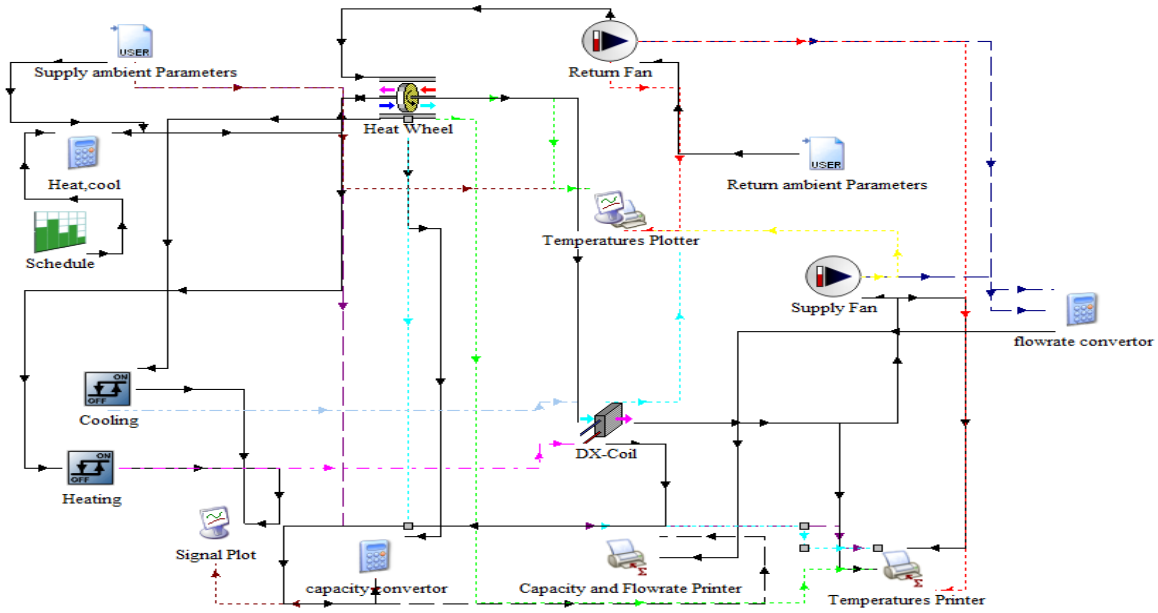

Figure 5.4. TRNSYS simulation model.

5.4 Results and Discussion

The measured and simulated ambient temperature from the TRNSYS model during winter and summer are presented in this section. The functioning hours of the AHU were between 7:00 a.m. and 8:00 p.m., which means the unit, was turned off after 8:00 p.m.

Figure 5.5 shows a graph representing the fresh outlet from the heat wheel and exhaust inlet between the simulated and measured temperature the summer period (cooling). **Figure 5.6** represents the fresh outlet from the heat wheel and exhaust inlet between the simulated and measured temperature in the winter period (heating).

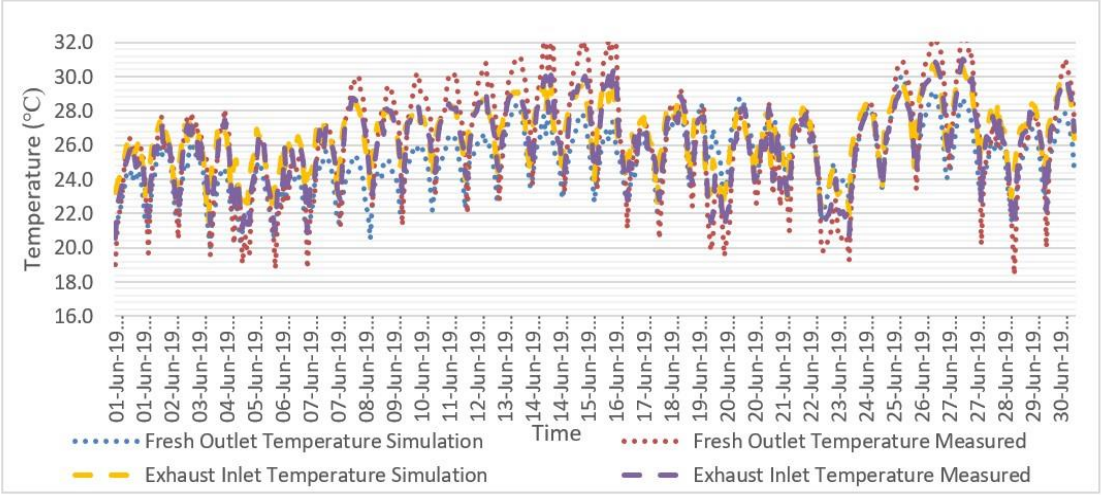

Figure 5.5 The fresh outlet and exhaust inlet around the heat wheel during summer.

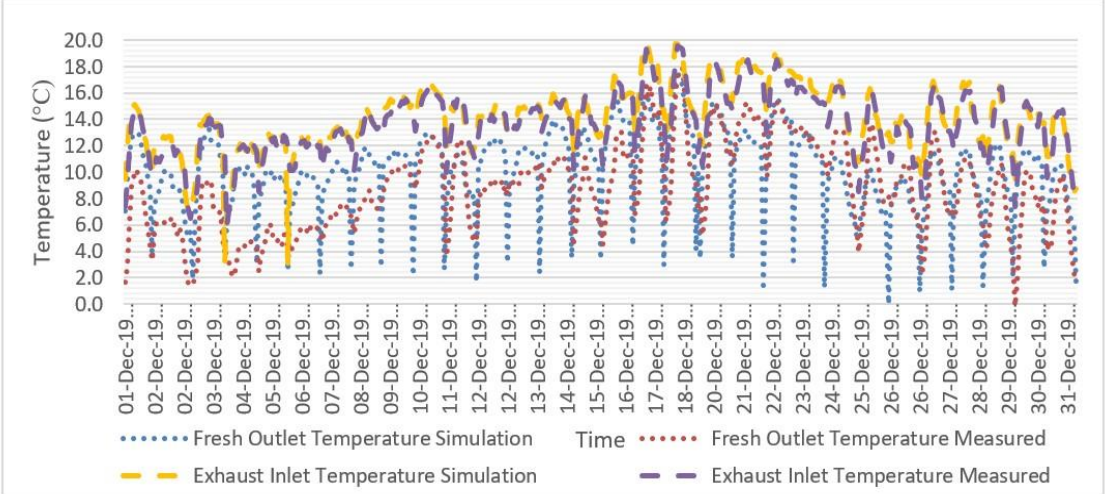

Figure 5.6 The fresh outlet and exhaust inlet around the heat wheel during winter.

On the heat wheel recovery sides, the monitored fresh air outlet from the heat wheel during summer was slightly higher than the simulation results, which would lead to higher energy consumption in the DX coil. During winter, it had lower values, which would lead to more energy from the VRF outdoor unit being consumed.

In the exhaust inlet section of the heat wheel, temperatures with a slight difference in the measured values temperature were observed during both winter and summer months.

In the following equations, the supply and exhaust air volume flow rate (during summer and winter) will be calculated.

For summer, the fresh air volume flow supply was measured by a sensor located at state 1. The mathematical approach to calculate the air volume flow rate is:

$$\dot{V}_s = \mathrm{A} \cdot \omega_{avg} \cdot 3600 \tag{5.7}$$

where $\dot{V}_s$ is the volume flow rate of the supply air (m^3/h), A is the area of cross-section of air duct (0.74 m^2), and ω_{avg} is the average velocity of the supply fresh air in summer (0.411 m/s).

$$\dot{V}_{ss} = 1095\ (\mathrm{m}^3/\mathrm{h})$$

The exhaust fresh air volume flow was measured by a sensor located at state 5. The average velocity of the exhaust fresh air in summer was 0.339 m/s.

$$\dot{V}_{es} = 901.5\ (\mathrm{m}^3/\mathrm{h})$$

For winter, the average velocity of the supply fresh air was 0.362 m/s.

$$\dot{V}_{sw} = 963\ (\mathrm{m}^3/\mathrm{h})$$

The average velocity of the exhaust fresh air in winter was 0.268 m/s.

$$\dot{V}_{ew} = 714.3\ (\mathrm{m}^3/\mathrm{h})$$

The reason for some differences in the higher supply airflow is that exhaust airflow is only an operational set since there are many doors and windows in the building that have leakages, so some of the supply air leaves the conditioned spaces as it is injected by the diffusers. The simulation volume flow rate values were taken from the monitored values as these values were inputs in the TRNSYS simulation.

Figure 5.7 and **Figure 5.8** represent the VRV power (in kW) for summer and winter, respectively.

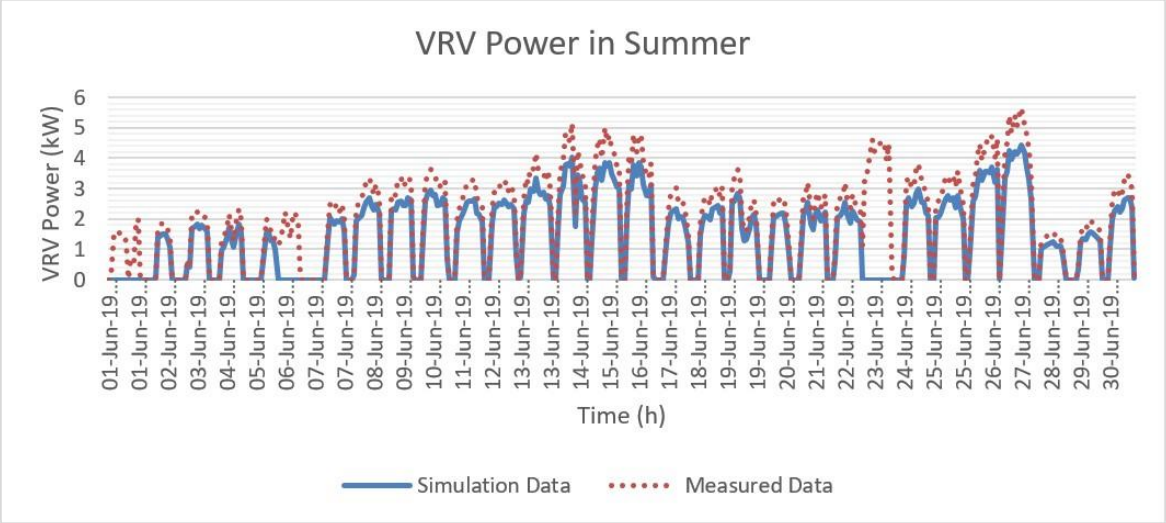

Figure 5.7. The measured and simulated power consumption in summer.

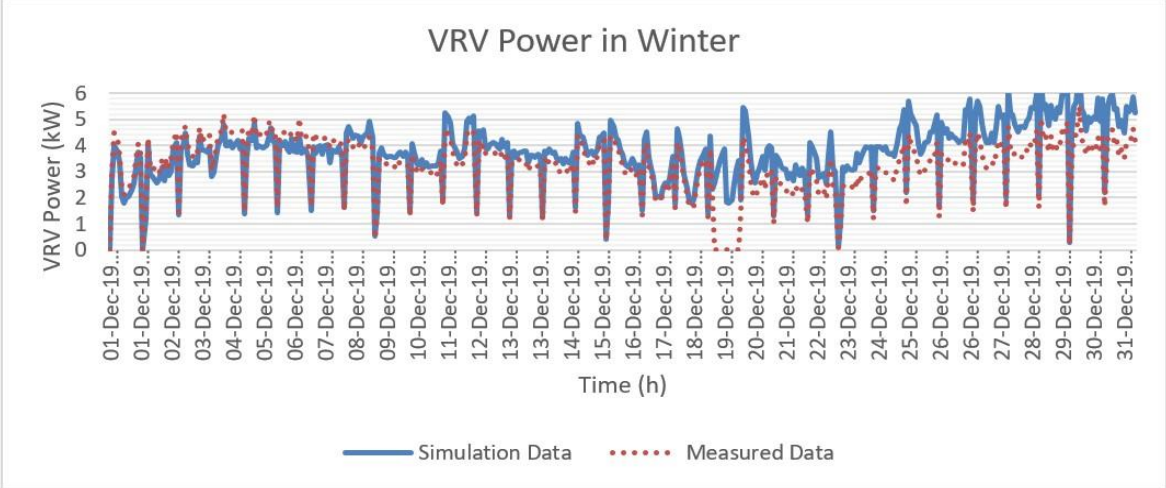

Figure 5.8. The measured and simulated power consumption in winter.

Figures 5.7 and **5.8** show that the monitored VRV power in summer was higher than the simulated results. This could be due to the high monitored ambient temperatures during June. The results of the VRV power in winter showed values between the measured and simulated results.

Figures 5.9 and **5.10** show the sensible effectiveness values (ε_s) of the heat wheel as a function of fresh air inlet temperature in winter (heating) and summer (cooling), respectively

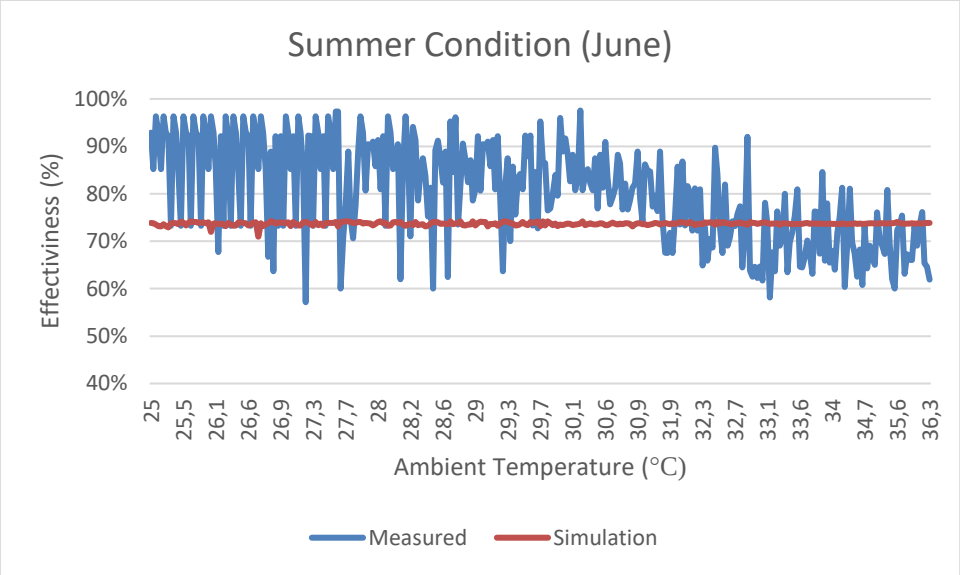

Figure 5.9. The measured and simulated sensible effectiveness values in summer.

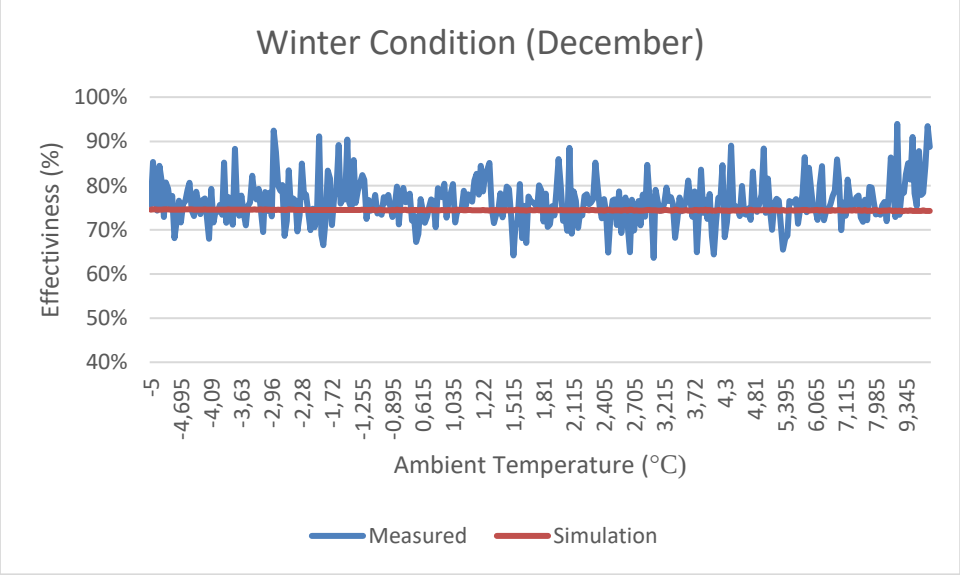

Figure 5.10. The measured and simulated sensible effectiveness values in winter.

Figure 5.10 shows that the measured effectiveness in winter varied with an average of 74.1%. The simulation had an almost constant trend throughout the month, with an average value of around 73.9%. **Figure 5.9** shows that the measured effectiveness of the HWR in summer had relatively higher values than the simulated results. The maximum value reported was around 97.6%, with an average effectiveness of around 80.2%. The simulation results showed more stable values of effectiveness than the measured values as a function of outdoor air temperature.

The difference in effectiveness between the measured and simulated values occurred due to the heat wheel in the simulation that takes the value of effectiveness as an input value. That is why it showed almost constant value throughout the month. The effectiveness value for the heat wheel was calculated according to **Equation (5.5)** depending on the measured temperatures recorded.

Figure 5.11 shows the sensible heat transfer (kWh) by the heat wheel. It represents the heat transfer rate for the whole year by heat wheel

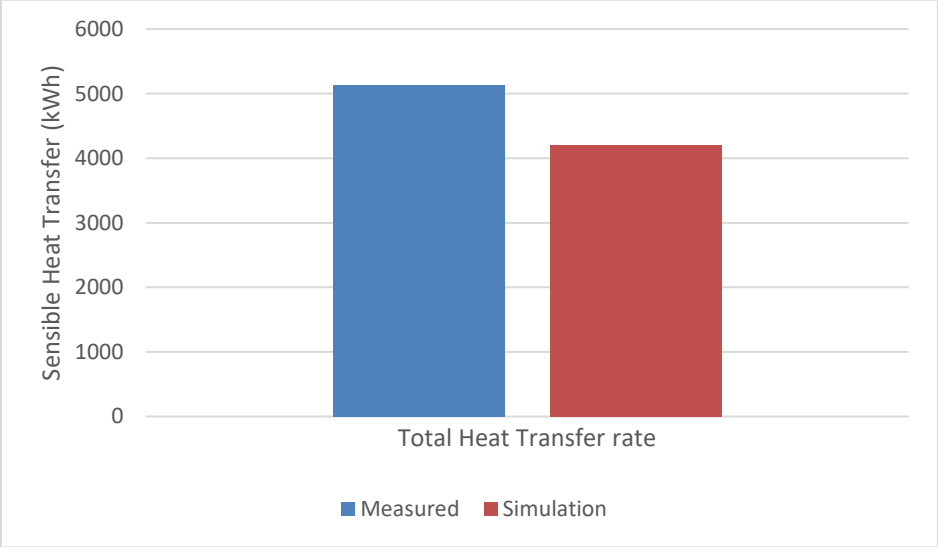

Figure 5.11. The measured and simulated sensible heat transfer (kWh).

The calculated sensible heat transfer by the measured parameters of the heat wheel was relatively higher than the simulation results for many reasons, such as the higher calculated

effectiveness from the measured ambient parameters and the higher difference between the supply inlet and the exhaust inlet temperature in the measured values. The calculated sensible heat transfer was more confident.

In chapter 6, an experimental study on an operated VRF system in an existing building will be performed to be compared with a simulation model results, afterwards, using an ERV to the simulation model to analyses the energy saving that could be saved.

Chapter 6

Simulation of Variable Refrigerant Flow Air-Conditioning System combined with Energy Recovery Ventilation

The energy performance of an existing variable refrigerant flow system in a building will be measured in this chapter. a TRNSYS model was built to be used as a reference when a VRF system will be introduced. Afterwards, A heat recovery unit will be added to the generated model for the purpose to achieve lower energy consumption.

6.1 Building Description and VRF System Model

Building energy simulation tool (TRNSYS 18) is used in this stage of the study. The simulation programs linked with Google SketchUp [58] that divides the building into different thermal zones to be easily imported to both simulation programs. The VRF system that was modeled is an existing running system at the Department of Building Service Engineering and Process Engineering, located on the first floor in one of the campus buildings at Budapest University of Technology and Economics. The building summary information is shown in **Table 6.1.**

Table 6.1 Building information

Item	**Parameter**
Location	Budapest, Hungary
Building Type	Offices building
Gross floor area	26 m (L) 13.7 m (W) 4.1 m (H)
HVAC system	VRF heat pump system

The building is composed of twelve outer zones and one inner zone. The Building model from SketchUp can be seen in **Figure 6.1**.

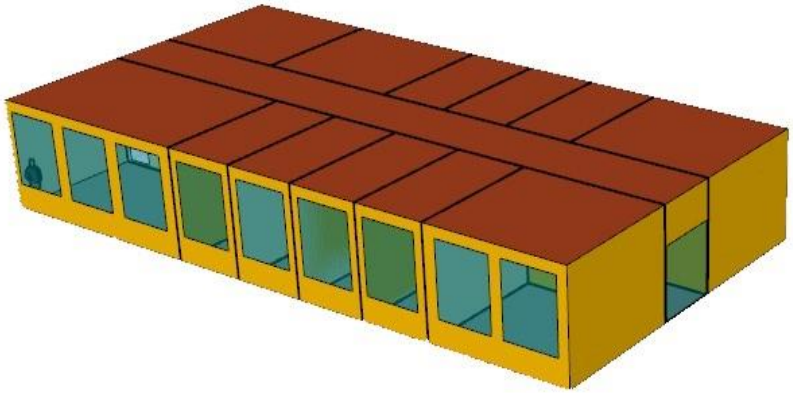

Figure 6.1. Simulation Building Image from SketchUp.

Lighting, Equipment, and Occupancy schedules were presented in **Figure 6.2** through the survey in order to calculate the heat gain from these parameters for the VRF system. The basis of this survey was by walkthrough the offices and monitoring the Equipment used in these offices and the number of people occupied these offices. The lighting was fully utilized during the working hours.

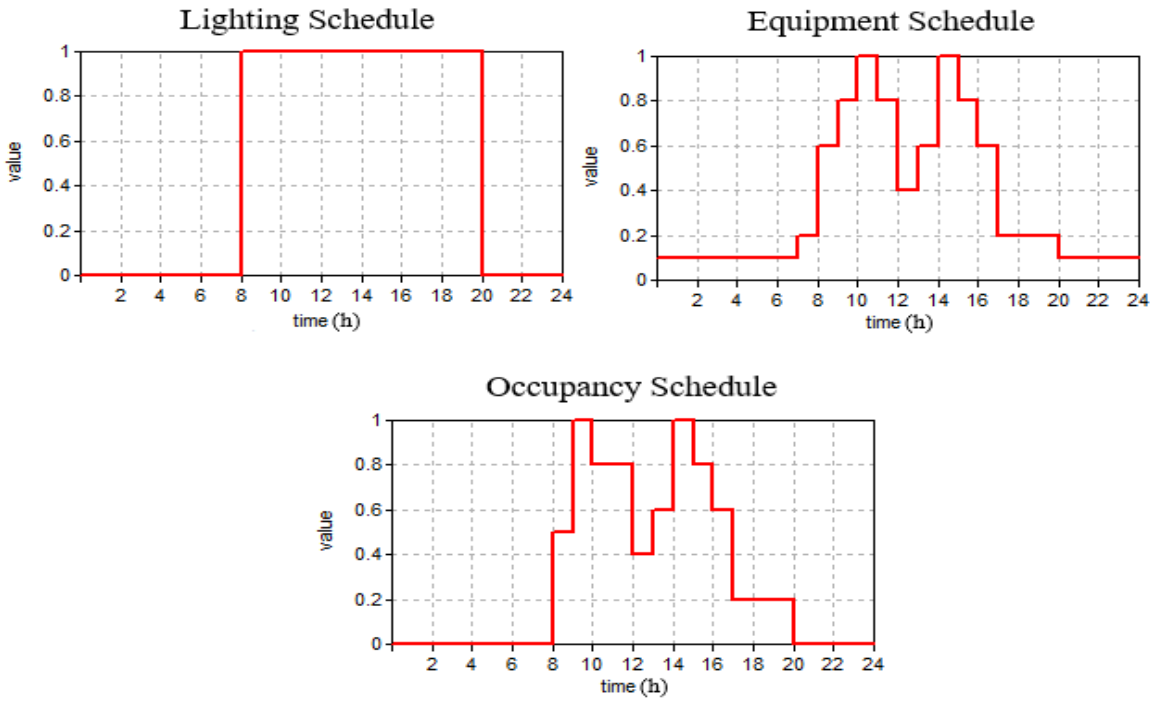

. **Figure 6.2.** Lighting, Equipment and Occupancy schedules.

According to the main features of buildings, the thermal properties of the building envelope, heat gains, and internal loads for HVAC system is shown in **Table 6.2.** which was collected from the building specs from the technical department in the university.

Table 6.2. Heat gains and internal loads

Item	**U-value**
Exterior Walls	0.40 W/ m^2.K
Roof	0.36 W/ m^2.K
Floor	0.36 W/ m^2.K
Exterior Windows	2.70 W/m^2.K SHGC = 0.3
Item	**Parameter**
Equipment	16 W/m^2
Number of occupant	2 persons for Small offices 3 persons for Big offices 20 person for Lecture Room
Lighting	30 W/m^2

The department floor depends on an individual VRF system that does not require a service room or ductwork, with the advantages of reduced noise since the duct system is neglected.

The properties VRF system with the capacity and the number of indoor units connected to the outdoor unit and its specifications is shown in **Table 6.3**.

Table 6.3. Properties of Existing VRF system

VRF System	Cooling Capacity	50.40 kW
	Heating Capacity	56.70 kW
	Cooling Power Input for OU	13.88 kW
	Heating Power Input for OU	13.57 kW
	HP (Equivalent horsepower)	18 Hp
	Combined Unit	ARUN180LT2
	Independent Unit	ARUN120LT2+ARUN60LT2
	Compressor Type	DC Scroll
	Motor Output	(5,356+5,300)+5,356 W
	Refrigerant name	R410A
	Refrigerant Charge	11.7 kg
	Refrigerant Control	Electronic Expansion Valve
	Condenser Type	Wide Louver
	Condenser Fan Type	DC Inverter
	Number of Indoor Units	18
Indoor Units Specifications*	Cooling Capacity	2800 W
	Heating Capacity	3200 W
	Air Volume Flow rate (H, M, L)	(8, 7.5, 7.1) m^3/min
	Power Input	30 W
	Set Temperature (H, C)	22ºC, 24ºC

- All the 18 indoor units in the target system have the same capacity with a different number of indoor units in each room, depending on room size. Two types of indoor units were installed in the building. 4-Way cassette unit and wall-mounted indoor unit.
- The indoor ambient conditions were selected as per recommended inside design values in ASHRAE Standard 62[59]

6.2 Measurement and instruments

Experimental performance tests were conducted by measuring energy consumption, air temperature, and relative humidity. The energy consumption in [kWh] is monitored by a power distributor indicator developed by the VRF manufacturer [60]. The set temperatures [°C], was monitored with the help of a central controller. These devices are shown in **Figure 6.3.** Room Temperatures [°C] and relative humidity [%] values were measured with the help of TESTO Smart Probe type metering instruments. These probes were placed inside the room. The calibration for TESTO instruments were discussed in the Chapter 7.

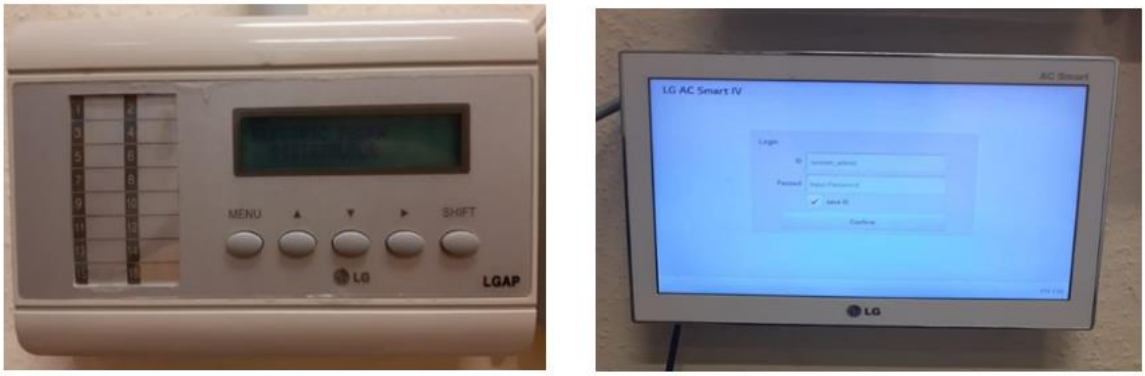

Figure 6.3. Power Distributor Indicator (Left) Advanced Control Smart (Right)

6.3 Test Plan

The measurement plan was made to test the real performance of the VRF system and compare it with the simulation model for both programs. The measured performance data is then used as a reference for the validation of modeling algorithms. The VRF detailed, measured data has been collected as follow:

- The measurement plan was tested in Heating and Cooling mode.
- The boundary condition for this experiment is

  (-15 ~ 40 ^{o}C) Supply Air Temperature, (10 ~ 100 %) Supply Relative Humidity

  480 m^3/h Supply Volume Flow rate, 50 kW VRF Power
- The test was conducted for one month in heating mode (December 2019) and one month in cooling (July 2019) during the working hours (8:00 am – 8:00 pm) from Monday to Friday.
- The experimental measurements were made for two offices (office 4 and office 5) in the department to observe and monitor the performance of the system easily.
- The measurements took place inside these two offices at the top of the desk in each office.
- All measurements were taken under continuous monitoring of the temperature, relative humidity, and energy consumption of the VRF system on an hourly basis.
- All target value pairs T [°C] – RH [%] were measured under constant parameter for volume flow rate

6.4 Description of the Developed TRNSYS Model

Figure 6.4 shows TRNSYS model of the system. The following **Table 6.4** lists standard TRNSYS types used to perform simulation in TRNSYS simulation studio. The weather data used here is the data collected from the measured parameters by using data reader type in TRNSYS. Other ambient temperatures such as (wind velocity, solar zenith angle, solar azimuth angle, and the rest of the solar radiation parameters were obtained from the data weather TMY from TRNSYS weather data file. The simulated results were validated with the experimental data. The necessary macros in the TRNSYS model were included in **Figure 6.4** representing the model.

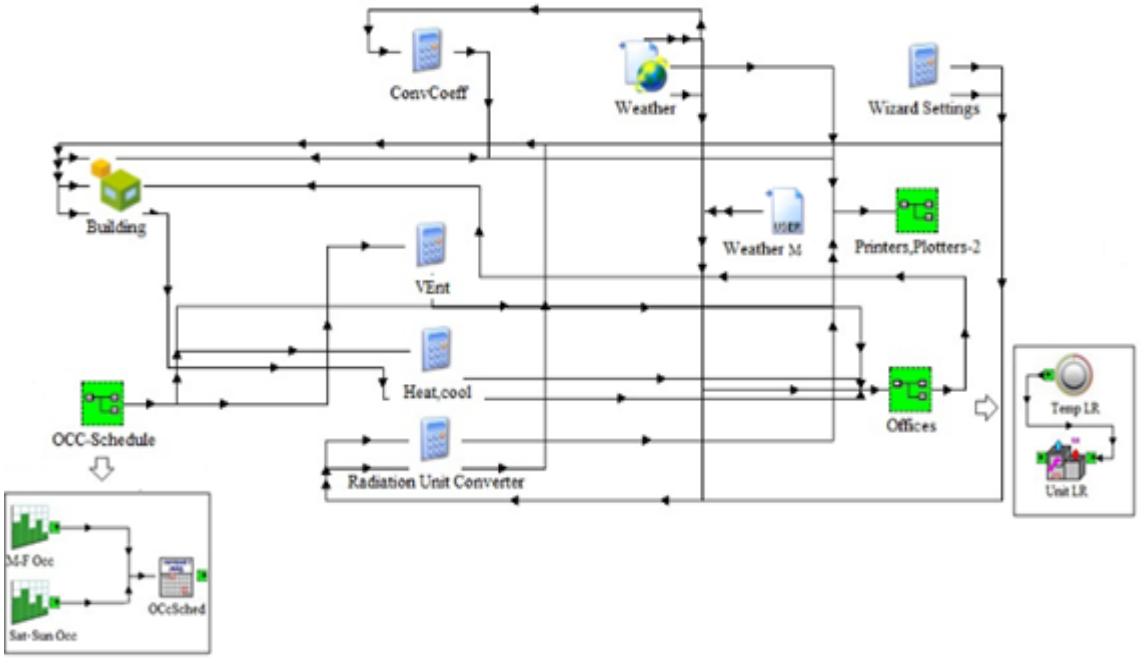

Figure 6.4. TRNSYS model of the system

Table 6.4 List of components used in TRNSYS simulation

Number	TRNSYS Type	Component Name
1	Type9	Data Reader from an external file
2	Type954a	Air Source Heat Pump Model
3	Type166	Simple Room Thermostat
4	Type56	Multi-Zone Building
5	Type14h	Time-Dependent Forcing Function
6	Type41c	Load Profile Sequencer
7	Type65d	Graphic plotter
8	Type25	Printer
9	Equa	Equation

6.5 VRF System Results and Discussion

At first, the measured and simulated temperature of the VRF system in July (summer condition) will be presented.

Figure 6.5 shows the graph representing the analysis of the measured and simulated temperature from TRNSYS simulation of the VRF system during summer conditions

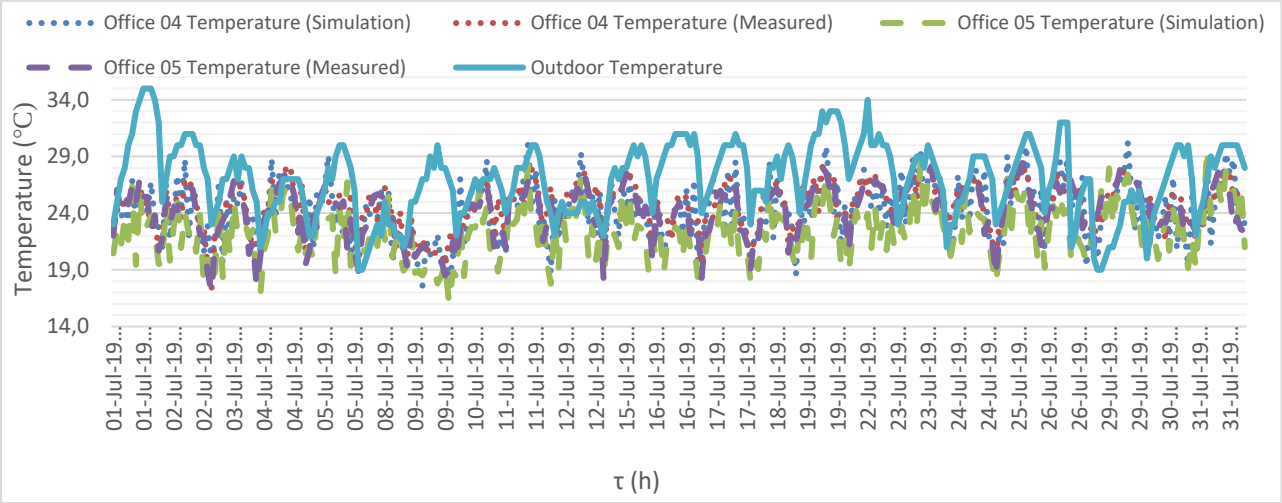

Figure 6.5 The measured & simulated indoor temperature in the two office spaces in summer

The measured and simulated temperature of the VRF system in December (winter condition) is shown in **Figure 6.6**, representing the analysis of the measured and simulated temperature from TRNSYS simulation of the VRF system during winter condition.

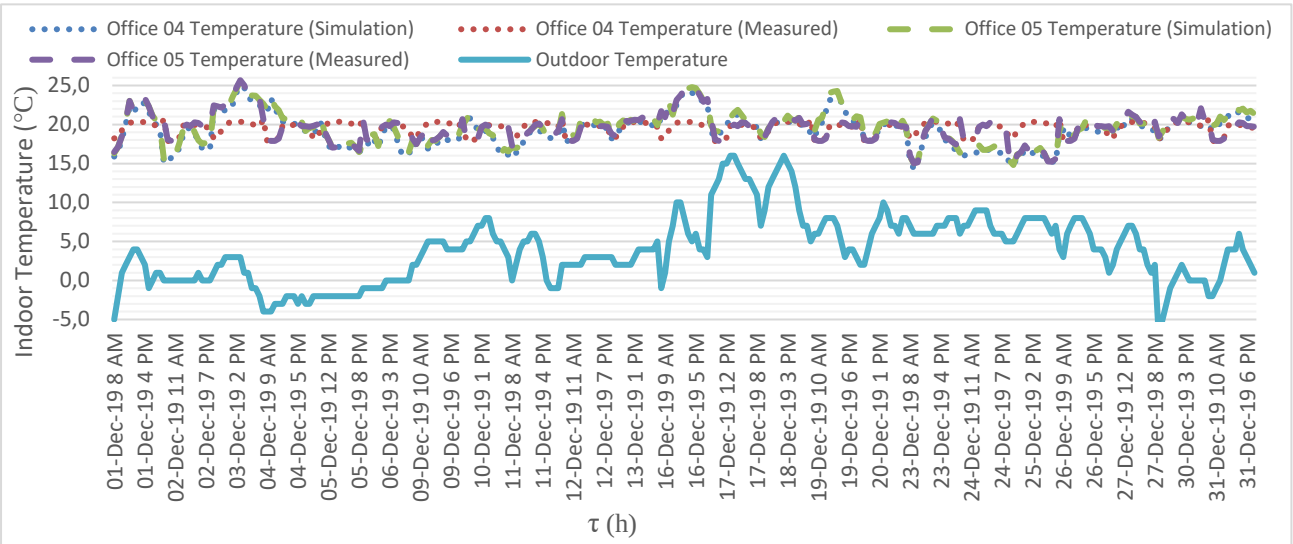

Figure 6.6 The measured & simulated indoor temperature in the two office spaces in Winter

From the above graphs, it can be noticed that the tendency of measured indoor temperature varying around the specific set point temperature (22°C Winter, 24°C summer). TRNSYS results show a close approximate to the measured temperature. However, it can show a slight difference in certain days.

The measured and simulated Relative Humidity of the VRF system in July (summer condition) will be presented. **Figure 6.7** shows the graph representing the analysis of the measured and simulated Relative Humidity from TRNSYS simulation of the VRF system during summer condition.

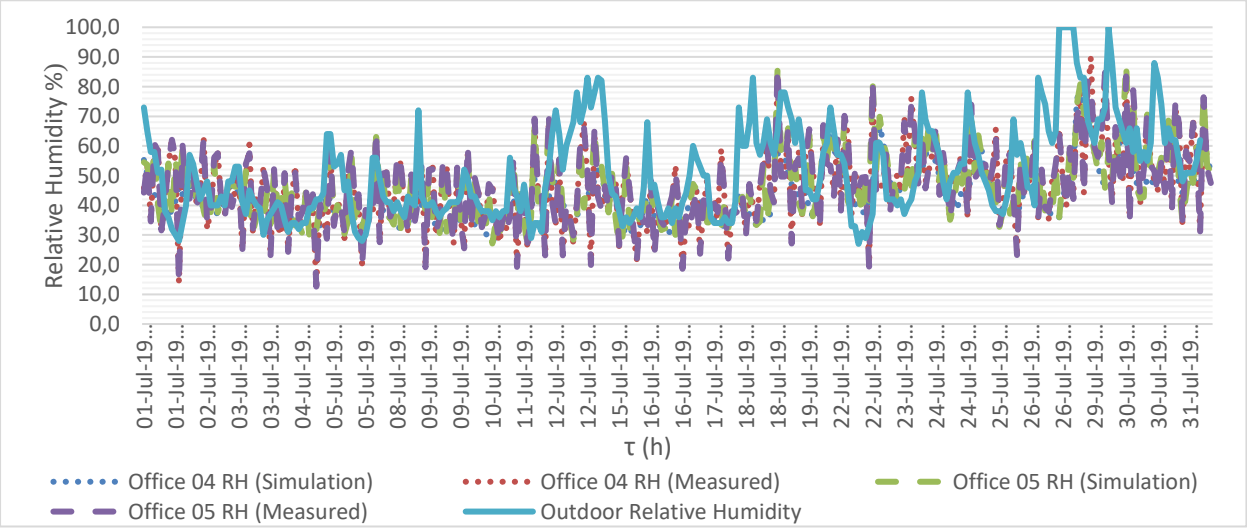

Figure 6.7 The measured & simulated indoor RH in the two office spaces in summer

The measured and simulated Relative Humidity of the VRF system in December (winter condition) is presented. **Figure 6.8** that shows the analysis of the measured and

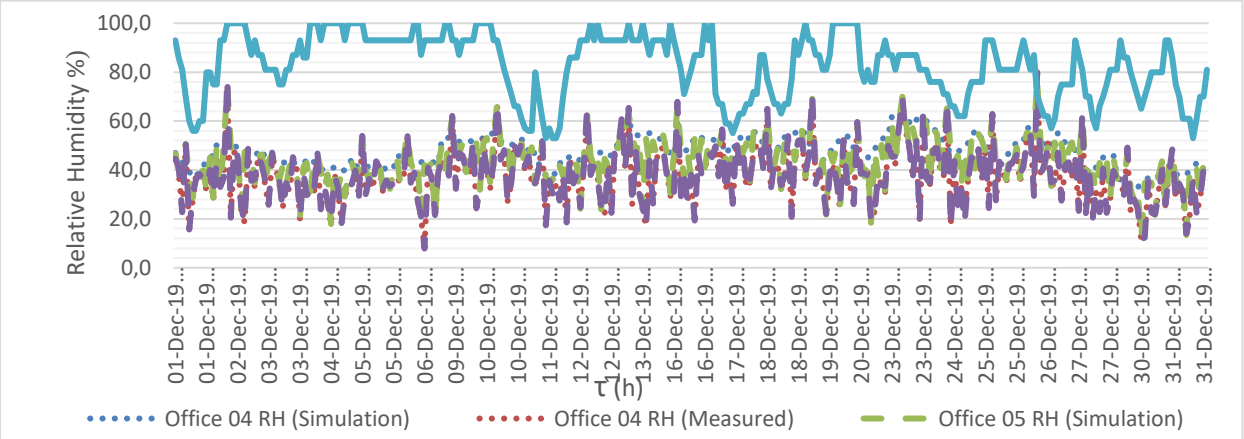

Figure 6.8 The measured & simulated indoor RH in the two office spaces in winter

simulated Relative Humidity from TRNSYS simulation of the VRF system during winter condition

From the above figures, it can be observed that the range of measured relative Humidity in summer falls within 50% to 75% and within 40% to 60% in Winter. The measured relative Humidity shows a more constant trend than the simulation one. The actual RH in winter was relatively high in winter.

The measured and simulated Accumulated Power Input in (kWh) of the VRF system in (summer and winter condition) will be presented.

Figure 6.9 represents the accumulated measured and simulated power from TRNSYS simulation program of the VRF system for the two target offices combined in summer conditions. While **Figure 6.10** represents the accumulated measured and simulated power from TRNSYS simulation program of the VRF system for the two target offices combined in winter conditions.

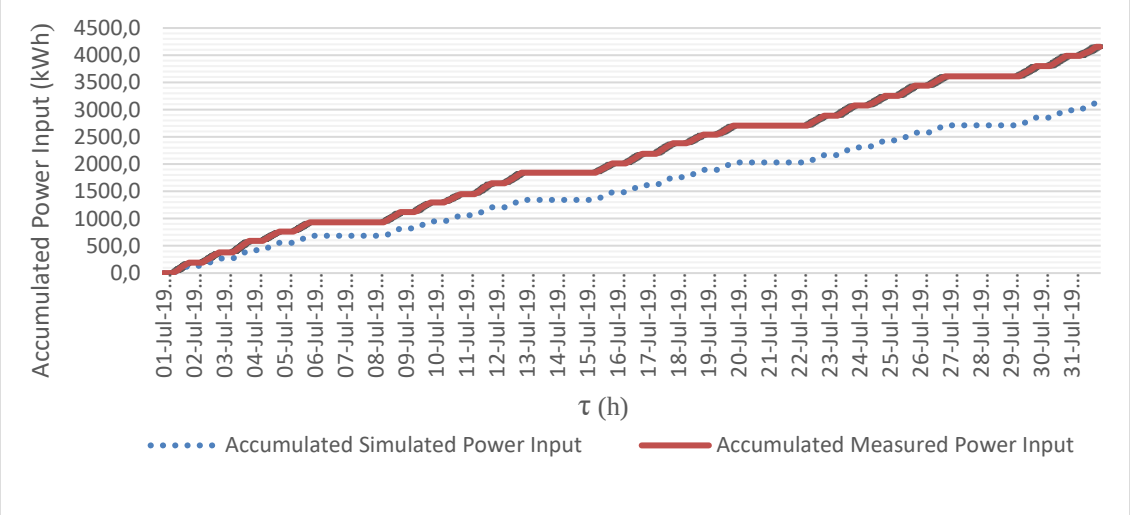

Figure 6.9 The hourly power use in (kWh) of VRF system in the two offices in summer

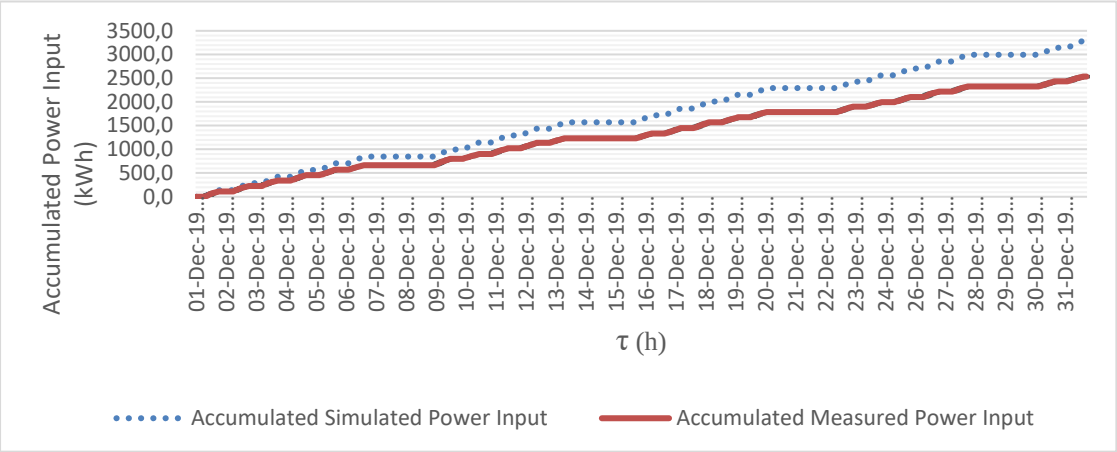

Figure 6.10 The hourly power use in (kWh) of VRF system in the two offices in winter

The accumulated power here represents the power input for both units in the selected offices (office 04, office 05) for the whole month.

The actual accumulated power in kWh was measured by the electric power distributor, while the simulated power input was calculated by multiplying the total energy input (compressor + outdoor unit fan + indoor unit fan) of the air source heat pump by the number of operating hours. The count method for electric power distribution [59]:

- Power Consumption of each Indoor Unit = Power Consumption of Outdoor Unit × [Weighting Power of each Indoor Unit / Weighting Power of total Indoor Units]

Weighting Power of each Indoor Unit = Operation (On/Off) × [Capacity of Indoor Unit × LEV open rate × Fan step of Indoor Unit]

The operation hours of the system were between 8:00 am to 8:00 pm during the working days (Monday-Friday), during the off-hours of the days and the weekends, the TRNSYS model was set up to be off to simulate as the actual model works.

From the accumulated power input figures, it can be noticed that the measured power input was higher than the simulation results in summer. Unlike the winter condition, the measured power input was lower than the simulation results. This can be attributed to different factors, like the difference in temperatures and other ambient conditions which affect directly on the accumulated power input.

6.6 Simulation of the system combined with ERV unit

Energy recovery ventilation (ERV) is an energy recovery process unit used to handle the outdoor ventilation air by preheating or precool the outgoing air [61]. The ERV system consists of a supply fan, exhaust fan, and an air-to-air heat exchanger.

The energy recovery ventilation (ERV) system will be studied and simulated to be connected to the existing VRF system of the department to compare the actual energy use of the VRF system with the energy simulation data and to calculate the energy savings. Type 667 from TRNSYS HVAC library was used, and it was connected to the building (Type 56) and the weather file

Design ventilation requirements

According to ASHRAE Standard 62 [59], the minimum ventilation rates for an office and lecture room is 3.8 L/s-Person. Depending on this rate, two ERV units with the same size will be considered here to cover the ventilation requirements for this study. The main properties of the ERV system are shown in **Table 6.5** as per the manufacturer engineering manual [61].

Table 6.5 Properties of ERV system

ERV System	Rated power	250 W
	Airflow rate	450 m^3/h (both hot and cold sides)
	Sensible Effectiveness	87 %
	Latent Effectiveness	69 %

6.7 ERV Results and Discussion

In this section, the results will be presented after simulating the VRF system equipped with ERV unit, and then a comparison will be made with the existing system with no ERV installed.

Figure 6.11 and **Figure 6.12** show the comparisons between the simulated temperature and relative Humidity in the office space between ERV and non-ERV cases for both Winter (December) and summer (July) conditions. Indoor temperature variations in Winter were maintained at approximately 20–23◦C. The average outdoor temperature fell to around -6◦C on the coldest day in December. Relative Humidity ranged in Winter from 30% to 40% for both cases (with and without the ERV system). But with slightly lower values in case 1 (with the ERV system). The average air temperature in summer ranged from about 15◦C to 28◦C during the month. The indoor temperature during the summer was maintained at approximately 26–28.5◦C while the relative Humidity for ERV and non-ERV cases fall between 45% to 65% with noticeable higher values in case 2 (without ERV system).

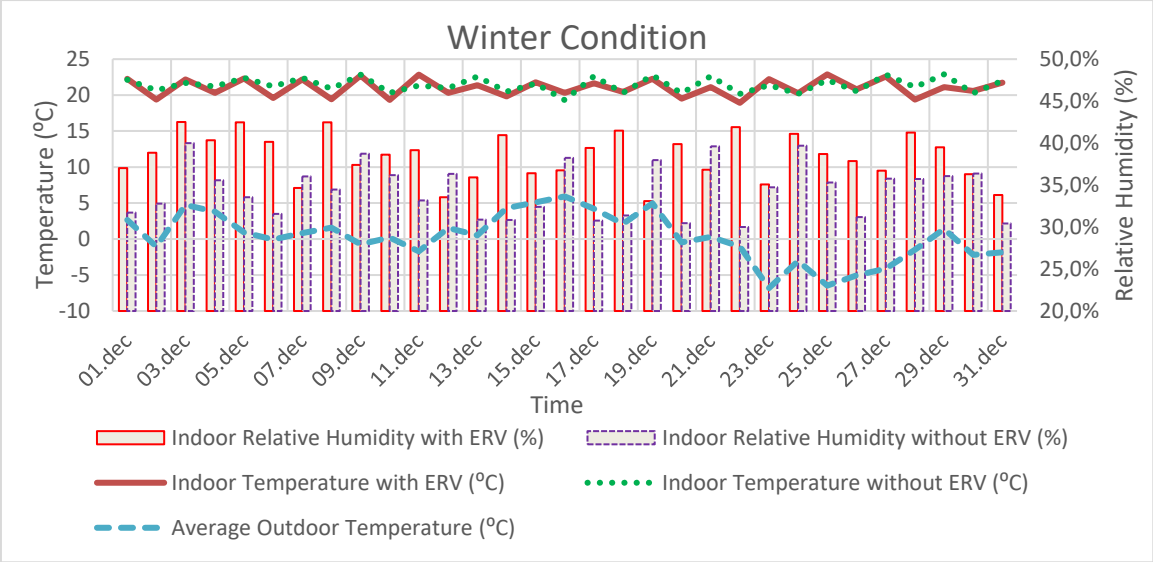

Figure 6.11 Comparisons of indoor air temperature and relative Humidity between ERV and non-ERV in December (Winter)

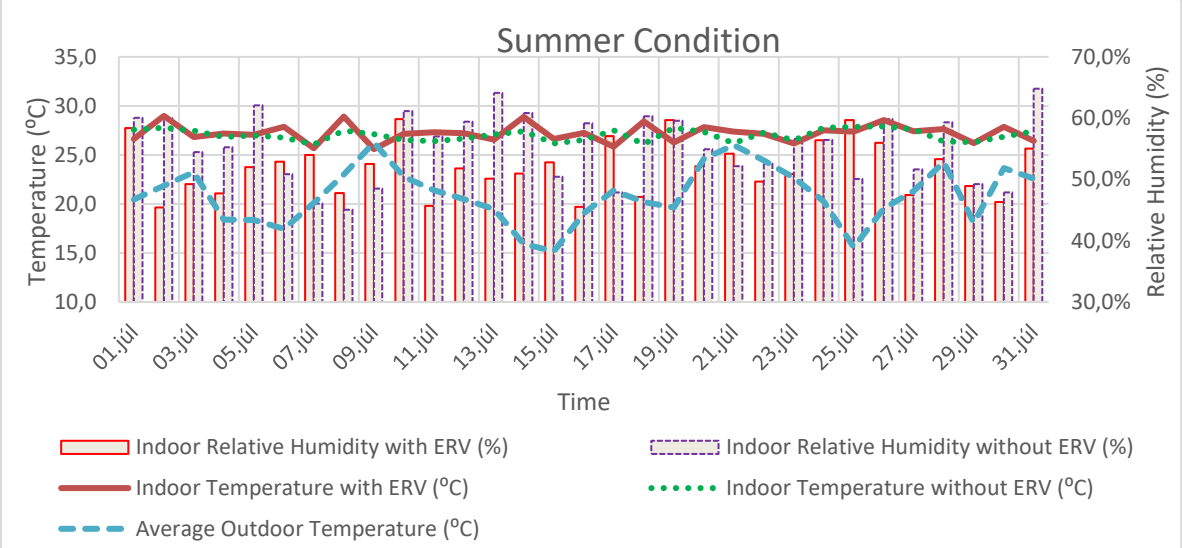

Figure 6.12 Comparisons of indoor air temperature and relative Humidity between ERV and non-ERV in July (Summer)

Figure 6.13 and **Figure 6.14** summarizes the total energy consumption of the total air conditioning units installed in the department. According to the running-operating schedule from 8:00 am to 08:00 pm, one Winter and one summer day of data were obtained when the ERV was operating. Energy consumption in Winter rose rapidly from 8:00 am (when the working period started), and then it declines until it begins to stabilize after 3:00 pm until 8:00 pm (when the working period ended). On the other hand, the energy consumption in summer rose slowly from 8:00 am at it keeps rising till 3:00 pm (peak hour), then it begins to decline slowly until8 p.m.(when the working period ended)

Energy consumption was relatively large in Winter due to the high-temperature difference between indoor and outdoor air. In addition, the results indicated that energy consumption was reduced by 20–30% when using the ERV system.

In the summer condition, unlike the winter condition, the energy consumption was not that high. Therefore, compared to energy recovery in the cold season, the ERV system had less impact when employed in the hot season.

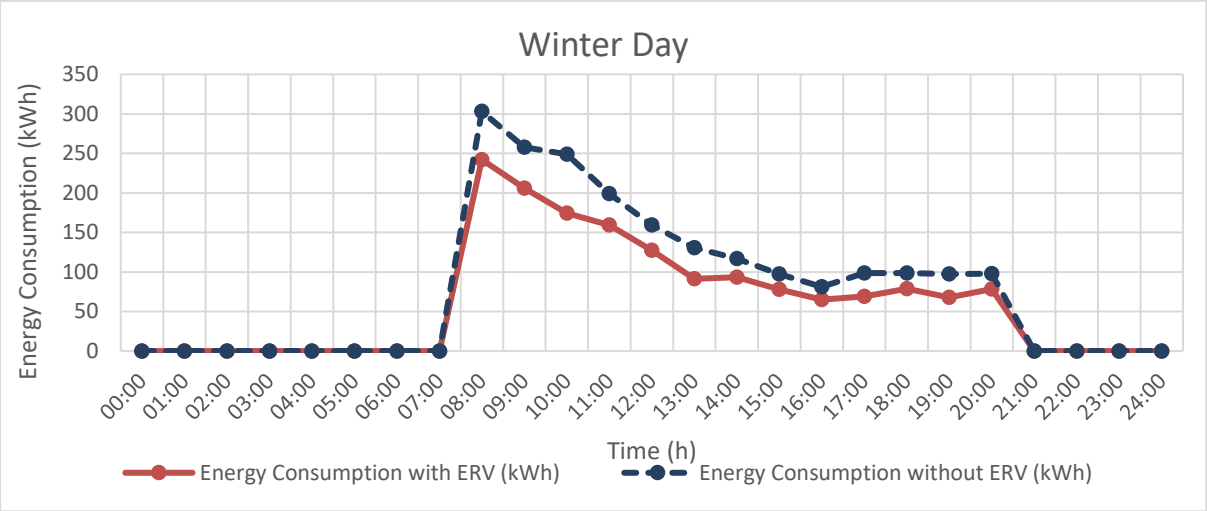

Figure 6.13. Comparisons of energy consumption between the ERV and non-ERV on a winter day

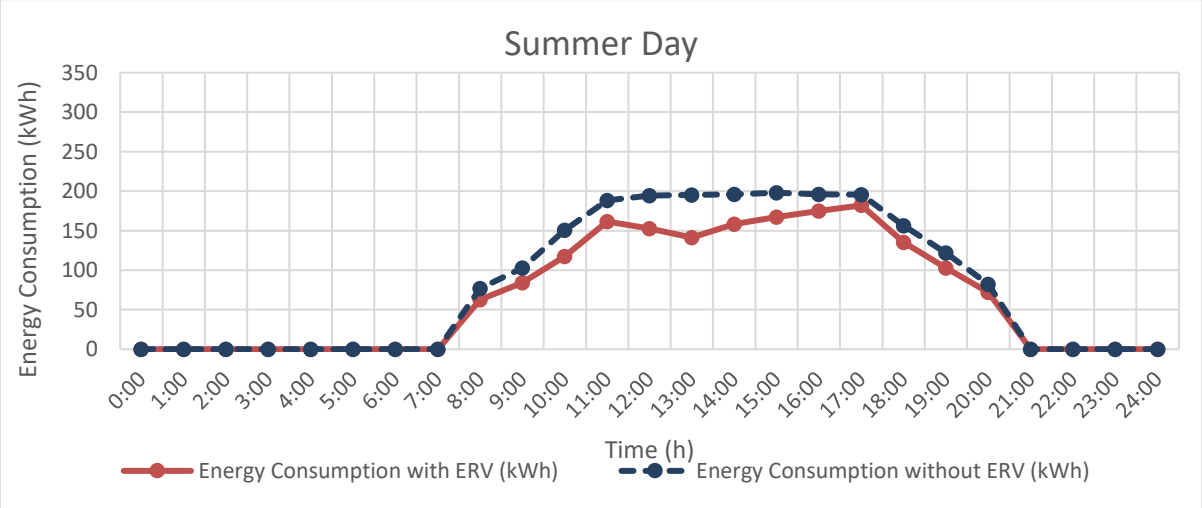

Figure 6.14 Comparisons of energy consumption between the ERV and non-ERV on a summer day

Chapter 7

Uncertainty Calculations and Model Validation

In this chapter, the uncertainty calculation will be applied for the investigated Sorption Wheel and the Polymer Membrane Material-Based Counter-Flow Energy Exchanger. Afterwards, a validation will be applied from the developed model that was used for the AHU and for the VRF system that was discussed earlier.

7.1 Uncertainty Calculations

The uncertainties in calculations are discussed in this section in order to determine the percentage error while measuring. As in the most relevant research studies carried out in the field, following experimental tests, instead of statistical calculations [62]

Kline and Mc Clintock [63] have presented the method used for estimating uncertainty in experimental results as shown in the equation below **Equation (7.1).** The method is constructive on precise specifications of uncertainties in the many primary experimental measurements [64]. It is more clear to define the experimental uncertainties **Equation (7.1)** rather than to experimental errors in the experiments. The analysis combine all the errors in the results.

$$\omega_R = \pm\sqrt{\left(\frac{\partial R}{\partial x_1}\times\omega_{x_1}\right)^2+\left(\frac{\partial R}{\partial x_2}\times\omega_{x_2}\right)^2+\cdots+\left(\frac{\partial R}{\partial x_n}\times\omega_{x_n}\right)^2} \tag{7.1}$$

The calibration result for the humidity and temperature metering instrument and the hot-wire anemometer can be shown in **Table 7.1**

Table 7.1 Calibration result of the multifunction instrument

Nominal value	Normal value	Measured value	Deviation	Uncertainly
40 %RH	39.9%RH	40.5 %RH	0.6 %RH	0.5 %RH
0 °C	0.09 °C	0.3 °C	0.21 °C	0.08 °C
1 m/s	0.98 m/s	1.00 m/s	0.02 m/s	0.05 m/s

7.1.1 Uncertainty Calculations in Desiccant Coated Total Energy Recovery Wheel

The temperature and relative humidity sensors were placed in the mid-section in the test facility before and after the energy wheel. Sample of the calculations presented below to shows how the uncertainty in the effectiveness were calculated during the research.

Data Observed and measured

1- Volumetric flow rate = 400 m^3/h

2- Temperature of the supply inlet = -15 ^oC

3- Relative Humidity of the supply inlet = 100%

4- Temperature of the exhaust inlet = 22 ^oC

5- Relative Humidity of the exhaust inlet = 35%

The **Equations (7.2-7.4)** show the calculations of uncertainty in sensible, latent and total effectiveness's:

$$\omega_{\varepsilon_s} = \pm\sqrt{\left(\frac{\partial \varepsilon_s}{\partial m_{si}} \times \omega_{m_{si}}\right)^2 + \left(\frac{\partial \varepsilon_s}{\partial T_{si}} \times \omega_{T_{si}}\right)^2 + \left(\frac{\partial \varepsilon_s}{\partial T_{so}} \times \omega_{T_{so}}\right)^2 + \left(\frac{\partial \varepsilon_s}{\partial T_{ei}} \times \omega_{T_{ei}}\right)^2} = \pm 3.72\% \quad (7.2)$$

$$\omega_{\varepsilon_L} = \pm\sqrt{\left(\frac{\partial \varepsilon_L}{\partial m_{si}} \times \omega_{m_{si}}\right)^2 + \left(\frac{\partial \varepsilon_L}{\partial x_{si}} \times \omega_{x_{si}}\right)^2 + \left(\frac{\partial \varepsilon_L}{\partial x_{so}} \times \omega_{x_{so}}\right)^2 + \left(\frac{\partial \varepsilon_L}{\partial x_{ei}} \times \omega_{x_{ei}}\right)^2} = \pm 5.93\% \quad (7.3)$$

$$\omega_{\varepsilon_T} = \pm\sqrt{\left(\frac{\partial \varepsilon_T}{\partial m_{si}} \times \omega_{m_{si}}\right)^2 + \left(\frac{\partial \varepsilon_T}{\partial h_{si}} \times \omega_{h_{si}}\right)^2 + \left(\frac{\partial \varepsilon_T}{\partial h_{so}} \times \omega_{h_{so}}\right)^2 + \left(\frac{\partial \varepsilon_T}{\partial h_{ei}} \times \omega_{h_{ei}}\right)^2} = \pm 6.77\% \quad (7.4)$$

Figure 7.1 shows the uncertainties for all the effectiveness values in the function of dry bulb ambient temperature for summer and winter condition at lowest volume flow rate ($\dot{V}$ = 400 m^3/s) and maximum wheel rotation speed (ω = 20 rpm).

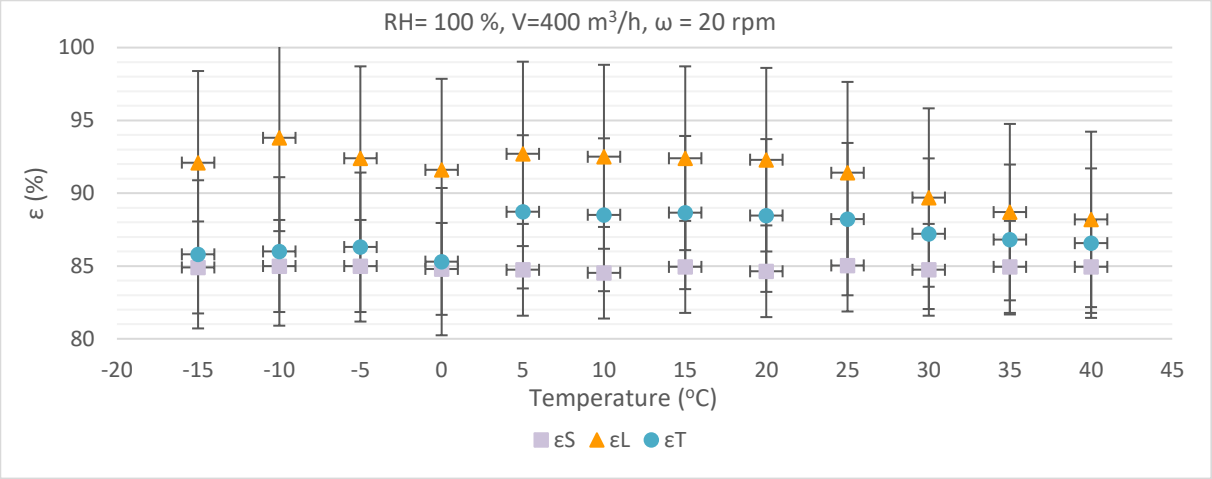

Figure 7.1 Uncertainty in effectiveness (%) vs. Dry Bulb Temperature (°C) for effectiveness at ω = 20 rpm and at V = 400 m^3/h

7.1.2 Uncertainty Calculations in Material-Based Counter-Flow Energy Exchanger

In this Sub-Section, uncertainty in effectiveness for a polymer membrane (polyethylene–polyether copolymer) material-based counter-flow energy exchanger (PEE), and a polystyrene material-based counter-flow heat exchanger (PHE) will be applied

Below, one sample was taken to evaluate the following parameters in order to calculate the uncertainty in the effectiveness:

1. Volumetric flow rate = 300 m^3/h;
2. Temperature of the supply air inlet = −7 °C;
3. Relative humidity of the supply air inlet = 75%;
4. Temperature of the exhaust air inlet = 20 °C;
5. Relative humidity of the exhaust air inlet = 38%.

Uncertainty in sensible effectiveness was calculated as follows:

$$\omega_{\varepsilon_s} = \pm\sqrt{\left(\frac{\partial \varepsilon_s}{\partial m_{si}} \cdot \omega_{m_{si}}\right)^2 + \left(\frac{\partial \varepsilon_s}{\partial T_{si}} \cdot \omega_{T_{si}}\right)^2 + \left(\frac{\partial \varepsilon_s}{\partial T_{so}} \cdot \omega_{T_{so}}\right)^2 + \left(\frac{\partial \varepsilon_s}{\partial T_{ei}} \cdot \omega_{T_{ei}}\right)^2} \quad ($$

$$\omega_{\varepsilon_S} = \pm 2.92\%.$$

Uncertainty in latent effectiveness was calculated as follows:

$$\omega_{\varepsilon_L} = \pm \sqrt{\left(\frac{\partial \varepsilon_L}{\partial m_{si}} \cdot \omega_{m_{si}}\right)^2 + \left(\frac{\partial \varepsilon_L}{\partial x_{si}} \cdot \omega_{x_{si}}\right)^2 + \left(\frac{\partial \varepsilon_L}{\partial x_{so}} \cdot \omega_{x_{so}}\right)^2 + \left(\frac{\partial \varepsilon_L}{\partial x_{ei}} \cdot \omega_{x_{ei}}\right)^2} \quad ($$

$$\omega_{\varepsilon_L} = \pm 5.04\%.$$

Uncertainty in total effectiveness was calculated as follows:

$$\omega_{\varepsilon_T} = \pm \sqrt{\left(\frac{\partial \varepsilon_T}{\partial m_{si}} \cdot \omega_{m_{si}}\right)^2 + \left(\frac{\partial \varepsilon_T}{\partial h_{si}} \cdot \omega_{h_{si}}\right)^2 + \left(\frac{\partial \varepsilon_T}{\partial h_{so}} \cdot \omega_{h_{so}}\right)^2 + \left(\frac{\partial \varepsilon_T}{\partial h_{ei}} \cdot \omega_{h_{ei}}\right)^2} \quad ($$

$$\omega_{\varepsilon_T} = \pm 6.12\%.$$

Figure 7.2 demonstrates the uncertainties for all values of effectiveness as a function of dry-bulb ambient temperature for PEE and PHE at an air volume flow rate of 300 m^3/h for heating performance tests based on EN standards.

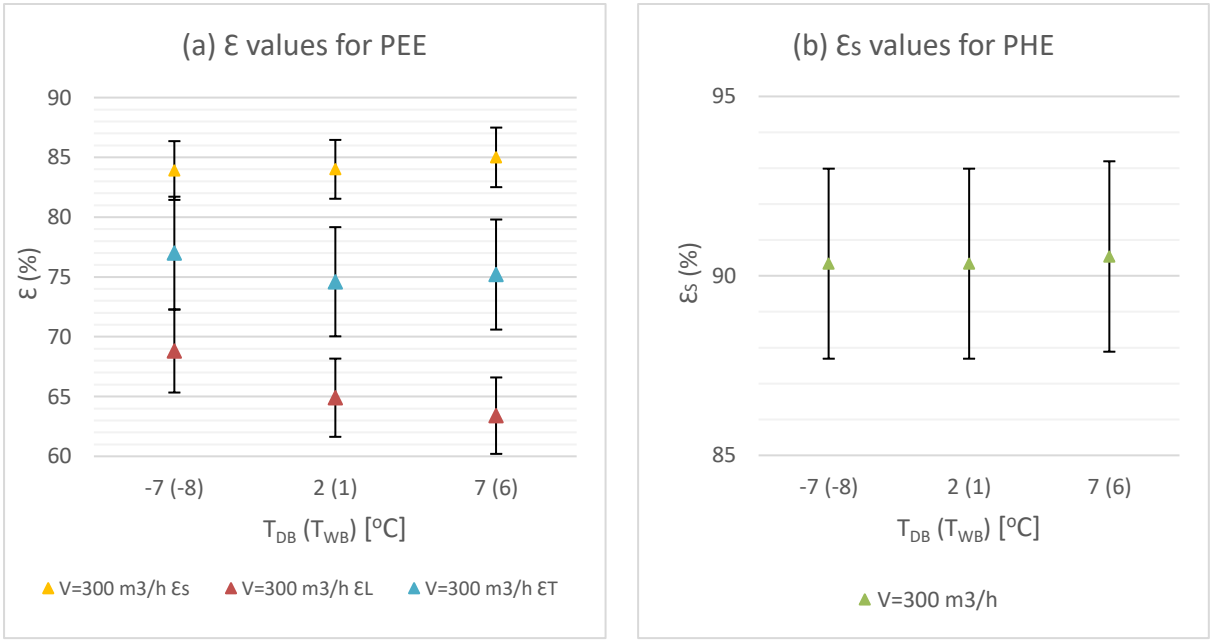

Figure 7.2 Uncertainty in effectiveness (%) vs. dry-bulb (wet-bulb) temperature (°C) at a volume flow rate of 300 m^3/h for (a) (PEE) and (b) (PHE).

7.2 Model Validation

In this Section, Validation of the developed TRNSYS simulation models that was developed in the previous chapter is performed by comparing these models with the actual data. Model validation has a key role in determining the quality of the model. [65]

ASHRAE Guideline 14-2014 [66] is used as the standard of VRF model validation. As the hourly data analysis is used, the baseline model of NMBE (Normalized Mean Bias Error) and CVRMSE (Coefficient of Variation of the Root Mean Square Error) shall not exceed 10% and 30%, respectively to be considered validated as shown in **Table 7.2**

Table 7.2 The calibration criteria of ASHRAE Guideline 14-2014

Data Type	Index	ASHRAE Guideline Calibration
Monthly Criteria %	NMBE	±5
	CV (RMSE)	15
Hourly Criteria %	NMBE	±10
	CV (RMSE)	30

NMBE is a normalization of the MBE index that is used to scale the results of MBE, making them comparable. It quantifies the MBE index by dividing it by the mean of measured values, giving the global difference between the real values and the predicted ones. As in the case of MBE, positive and negative values mean the under- or over-prediction of this normalization. ASHRAE Guidelines subtract measured values from simulated ones.

CV(RMSE) (Coefficient of Variation of the Root Mean Square Error) measures the variability of the errors between measured and simulated values. It “gives an indication of the model’s ability to predict the overall load shape that is reflected in the data [67]. It is not subject

to cancellation errors, and hence, AHSRAE Guidelines use it with NMBE to verify the accuracy of the models.

NMBE and CVRMSE calculated by **Equations (7.5)** and **(7.6)**, where y_i is the actual metered value, $\hat{y}$ is the predicted value, $\bar{y}$ is the average of the y_i , and N is the total number of data points. [67]

$$NMBE = \frac{\frac{1}{N}\sum_i^N (y_i - \hat{y}_i)}{\bar{y}} \times 100 \quad (7.5)$$

$$CV(RMSE) = \frac{\sqrt{\frac{1}{N}\sum_i^N (y_i - \hat{y}_i)^2}}{\bar{y}} \times 100 \quad (7.6)$$

In conclusion, NMBE gives an indication of the total difference between the actual model and predicted (simulation) model. While CV (RMSE) provides a reference for the model's ability to predict the overall results reflected in the data [68]. These two deviations provide a comprehensive visualization for the model performance

7.2.1 Model Validation for the developed AHU TRNSYS Model

The new AHU TRNSYS model was validated by comparing this model with the actual data. Measured weather parameters were used as input data for the simulation models. Then a comparison was conducted between the simulated and measured values to determine the accuracy of the developed TRNSYS model.

The simulated energy use in heating and cooling mode are all within the range of ±10% (**Table 7.3**). This is within the acceptable criteria range, with the model considered calibrated if the absolute value of NMBE was less than 10%. Besides, it shows that the CVRMSE for

heating and cooling mode is 19% and 24%, respectively, which is considered acceptable as the criteria for CVRMSE is less than 30%.

Table 7.3 Calibration results of the simulation model.

	Total Energy Consumption	NMBE (%)	CVRMSE (%)
Heating Measured Total (kWh)	6342	5.5%	19%
Heating Simulation Total (kWh)	6753		
Cooling Measured Total (kWh)	2034	7%	24%
Cooling Simulation Total (kWh)	1864		

7.2.2 Model Validation for the developed VRF System TRNSYS Model

In this Sub-Section. The VRF System TRNSYS model will be validated by comparing this model with the actual data.

Table 7.4 shows the Calibration results of the VRF algorithms for the accumulated power input in heating and cooling mode

Table 7.4. Calibration results of the VRF algorithms in heating and cooling operations

	Criteria	Total Energy Consumption
Total Measured Total (kWh)		6596.3
TRNSYS Simulated Total (kWh)		6185.6
NMBE (%)	±10%	7.8 %
CVRMSE (%)	30%	26.8 %

The simulated energy use in heating mode is all within the range of ±10%. Therefore, it is considered within the acceptable criteria range, as shown in the table above. Thus, the TRNSYS VRF model could be considered validated by the field test data.

Chapter 8

Conclusion and Summary

In this chapter, the conclusions from all the studies that was made during the PhD work will be presented. Likewise, the summary which will contain all the new scientific results that was obtained during the research work will be listed. Finally, the recommendations and further development will be provided for future work.

8.1 Conclusion

The first part of the presented study was performed experimentally to study the performance of a Desiccant Coated Total Energy Recovery Wheel, Heat Wheel and a Polymer Membrane Material-Based Counter-Flow Energy Exchange with two different types of recovery system units used, Energy recovery and Heat Recovery units. These energy recovery unit were tested under different ambient and operation conditions. The instruments used in the experiment was calibrated. The economic effect of using energy recovery units on ventilation system was exposed. The second part used TRNSYS Simulation program to build a model to verify the agreement between the experimental and simulation results.

Based on the studies performed during the PhD work, the following conclusions can be derived:

8.1.1 Sorption energy wheel

- The sensible effectiveness obtained from the experiments showed an increasing trend by decreasing the air volume flow rate under winter and summer ambient air conditions. However, the results show almost the same sensible effectiveness values under different dry bulb air temperatures and same wheel rotation speeds.

- It could be obtained that the values of the sensible effectiveness start to reduce when wheel speed reaches a value of 10 rpm and lower.
- The latent and total effectivenesses showed an increasing trend by decreasing the air volume flow rate and increasing the wheel rotation speed.
- The latent and total effectiveness values have a maximum value under wheel speed 20 rpm, and constantly decrease as a function of rpm.
- It can be obtained from all the test data that the peak value of the latent effectiveness reached almost 94 %.
- The maximum latent and total effectiveness values were found at the lowest ambient air dry bulb temperatures.
- The latent and total effectiveness values increased by decreasing the relative humidity of the ambient air under different temperature levels.

8.1.2 Polymer Membrane Material-Based Counter-Flow Energy Exchanger

- The results showed that the values of the sensible effectiveness under different outdoor air temperature and relative humidity values are almost the same values for the PEE and PHE, and only the air volume flow rate, as an operation parameter, has an effect on the sensible effectiveness.
- The maximum value of sensible effectiveness was found at the lowest air volume flow rate(100 m^3/h), which was 94.2% for the PHE and 94.1% for the PEE in summer conditions. The reason for this much lower sensible effectiveness at higher air volume flow rates for the PEE is due to the transfer of additional moisture to the supply air stream from the exhaust air stream.
- The PEE is likely to be used when there is a need to maintain the indoor air relative humidity level during the winter heating period or to reduce the moisture of the outdoor air (as supply inlet air) during the summer cooling period.

- The values of the latent and total effectiveness decrease when the relative humidity of the outdoor air increases.
- The maximum values of the latent and total effectiveness could be obtained for the lowest outdoor air dry-bulb temperature values.

8.1.3 Heat Wheel Operated in Air Handling Unit

- The analysis of the supply air condition (fresh air inlet) of the heat wheel showed that the system can save energy in different weather conditions and it is more useful than the conventional air conditioning systems.
- The sensible effectiveness values of the heat wheel measured were higher than the simulated data in summer, whereas it was lower in winter.
- The simulation value of sensible effectiveness showed a constant trend that was close to the given effectiveness values in the technical data sheet of the producer (74.9%).
- The NMBE and CVRMSE used to validate the model showed that the TRNSYS model has an acceptable range as the criteria for NMBE and CVRMSE are less than 10% and 30%, respectively. The developed TRNSYS model can be useful for predicting the performance of such extreme conditions.

8.1.4 VRF System combined with Energy Recovery Ventilation

- The mean temperature and humidity difference between simulation and measured data in the selected testing period was 4.3%and 7.6%.
- The simulated power input was lower than the measured results in summer. Unlike the winter condition, the measured power input was lower than the simulation results
- It turns to be that the TRNSYS model for VRF system shows a good approximate when comparing its simulation results with the actual measured results, and it could be used when estimating the cooling and heating load for a VRF system.

- Estimating the results of ERV system based on short-time measurement (one day in summer and Winter) is not very accurate to take it for granted. Still, it gives useful information that contributes to future development for calculating the capacity and consumption when using an ERV system in simulation modeling.

8.2 New Scientific Results

Thesis 1 [68] [69]

The sorption wheel's performance was evaluated under a vast range of ambient air condition parameters to get the sorption wheel's effectiveness values for steady-state conditions under different ambient air (as supply air inlet) conditions. It was found that increasing the wheel rotation speed would increase the latent effectiveness values. As it shows at the maximum wheel speed (20 rpm), the maximum value was for the latent effectiveness, which reached almost 94%, as shown in **Figure 8.1.** Whereas at low wheel rotation speeds, the latent effectiveness will be very low as it goes down to 50%. Sensible effectiveness values under low rotation speeds have much fewer effects under the investigated states of operation. It drops to a value close to 65%, as shown in **Figure 8.2.**

Similarly, the values of the sensible effectiveness for the sorption wheel begin to reduce from wheel speed 10 rpm and lower. In contrast, the latent effectiveness positively correlates with the rotation speed as the values decrease the latent effectiveness when the wheel speed rotation begins to decrease.

Boundary Conditions.

(-15 ~ 40 °C) Supply Air Temperature, (30 ~ 100 %) Supply Relative Humidity

(2 ~ 20 rpm) Wheel Rotation Speed, (400 ~ 1200 m^3/h) Supply Volume Flow rate

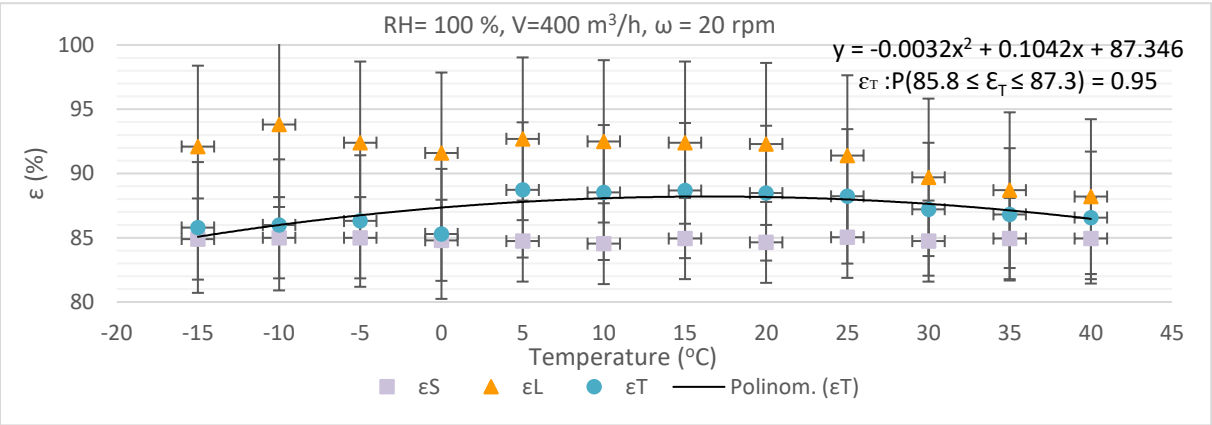

Figure 8.1. Maximum effectiveness (%) vs. Dry Bulb Temperature (°C) for effectiveness at ω = 20 rpm and at $\dot{V}$ = 400 m^3/h.

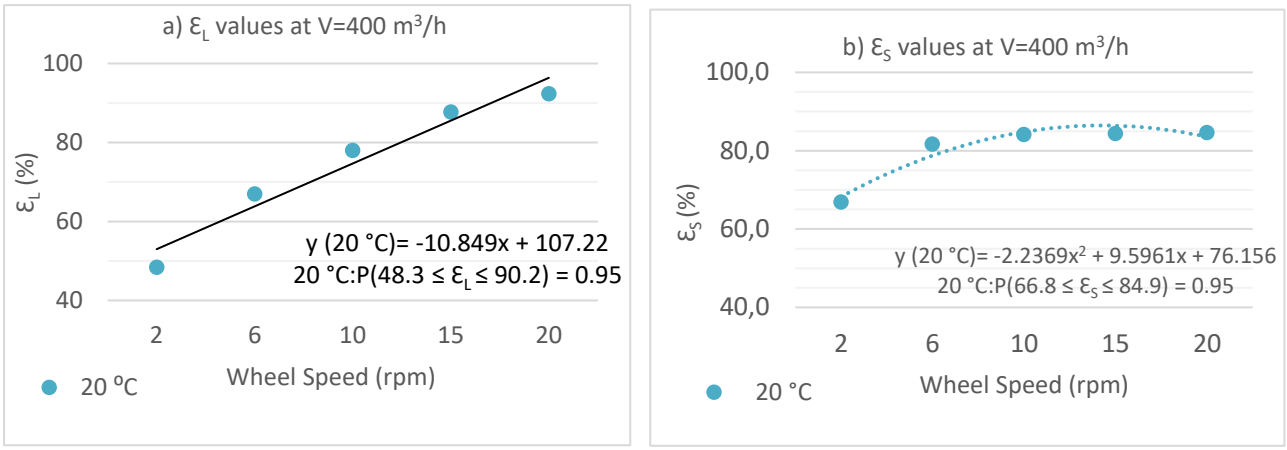

Figure 8.2. (a) Latent Effectiveness and (b) Sensible effectiveness (%) vs. Wheel speed rotation (rpm) for (20 °C) dry bulb temperature at $\dot{V}$ = 400 m^3/h

It can be summarized that the maximum effectiveness value for the sorption wheel occurred in the latent effectiveness. The dry bulb temperature has no effects on sensible effectiveness. In contrast, it affects the latent and total effectiveness by decreasing the value while the dry bulb temperature increases. The maximum sensible and latent effectiveness could be obtained at the highest wheel speed rotation.

Thesis 2 [68] [69]

It was found that the sensible effectiveness values obtained from the investigated sorption energy wheel experimental test show a decreasing trend when increasing the volume flow rate of the air. However, it shows almost the same values under different dry bulb temperatures the same wheel speed, as shown in **Figure 8.3**.

Boundary Conditions
(-15 ~ 40 °C) Supply Air Temperature, (30 ~ 100 %) Supply Relative Humidity
(2 ~ 20 rpm) Wheel Rotation Speed, (400 ~ 1200 m^3/h) Supply Volume Flow rate

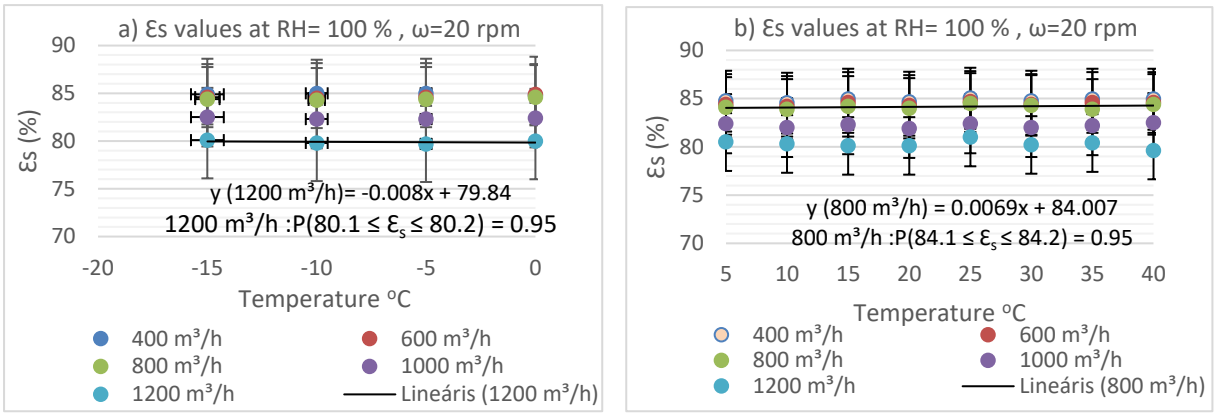

Figure 8.3. Sensible effectiveness (%) vs. Dry Bulb Temperature (°C) at different air volume flow rate and at ω = 20 rpm; (a) Winter Condition, (b) Summer Condition

In conclusion, the obtained sensible effectiveness values from the sorption wheel experiment show that the effectiveness values increase by decreasing the supply air volume flow rate. Besides, the dry bulb temperature (outside air temperature) has no effect on the performance of the sorption wheel.

Thesis 3 [68] [69] [70]

The sorption wheel's maximum effectiveness values are obtained at lower relative humidity values and lower airflow rate values. In addition, the highest effectiveness values occurred mostly at lower values of dry bulb temperatures.

As per the experimental results in **Figure 8.4**, the maximum effectiveness values (latent, total) occurred at the lowest relative humidity and the lowest airflow rate executed in this experiment. (400 m^3/h). In general, the effectiveness values almost increase while the dry bulb temperature decreases, and the maximum effectiveness value occurred at T= 5 °C.

Boundary Conditions

(-15 ~ 40 °C) Supply Air Temperature, (30 ~ 100 %) Supply Relative Humidity

(2 ~ 20 rpm) Wheel Rotation Speed, (400 ~ 1200 m^3/h) Supply Volume Flow rate

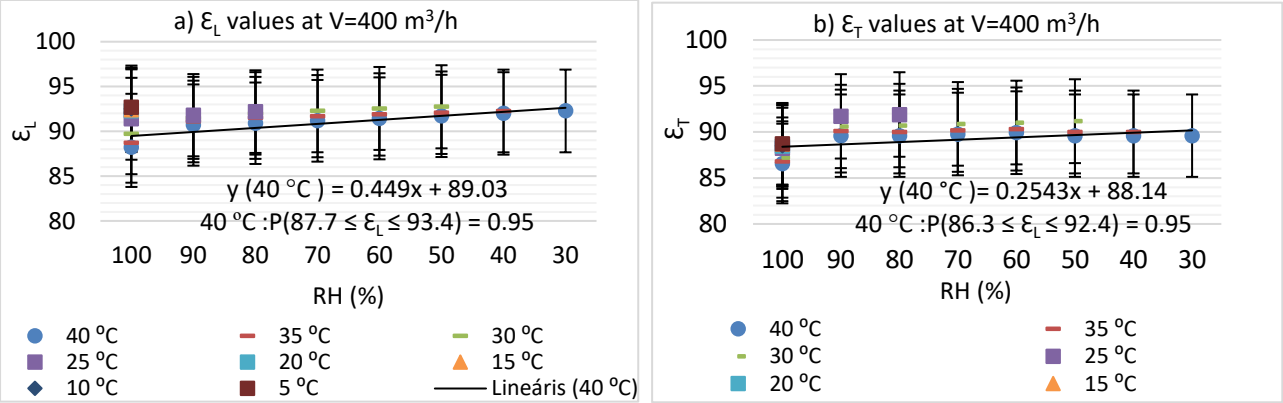

Figure 8.4. Latent (a) and Total (b) effectiveness (%) vs. Relative Humidity (%) at different dry bulb temperature (°C) and at $\dot{V}$ = 400 m^3/h

In General, the obtained latent and total effectiveness values from the sorption wheel experiment show that the effectiveness values increase by decreasing the supply air's relative humidity. In addition, the effectiveness values increase while the dry bulb temperature decreases.

Thesis 4 [70]

The experimental results showed that if the indoor air quality requirements are lower, then using a polystyrene sensible air-to-air counter-flow heat exchanger (PHE) is suitable for heat recovery. The investment cost is lower. If the total energy exchange (heat and moisture exchange for better indoor air quality) is essential, then the polymer membrane air-to-air counter-flow energy exchanger (PEE) is required. Even though the investment cost of PEE is higher, the amount of energy saved on the pre-heater can be 87.1% higher than when operating the ventilation unit with the PHE exchanger, based on this study

Figure 8.5. Shows the comparison of PEE and PHE exchangers' sensible effectiveness under different dry-bulb temperatures and different volume flow rates for winter and summer conditions. The results show that the PHE overall has higher sensible effectiveness than the

PEE, especially at higher air volume flow rates. Based on the tests' results, the average sensible effectiveness values for PHE in winter and summer conditions were 91% and 92%, respectively, while the average sensible effectiveness values for PEE were 87.2% in winter conditions and 87.8% in summer conditions.

The maximum values of sensible effectiveness were recorded in summer test conditions (with 40 °C ambient air as the supply air inlet temperature), at an air volume flow rate of 100 m3/h, 94.2% PHE and 94.1% for PEE.

Boundary Conditions

(-15 ~ 40 °C) Supply Air Temperature, (30 ~ 100 %) Supply Relative Humidity

(100 ~ 350 m^3/h) Supply Volume Flow rate

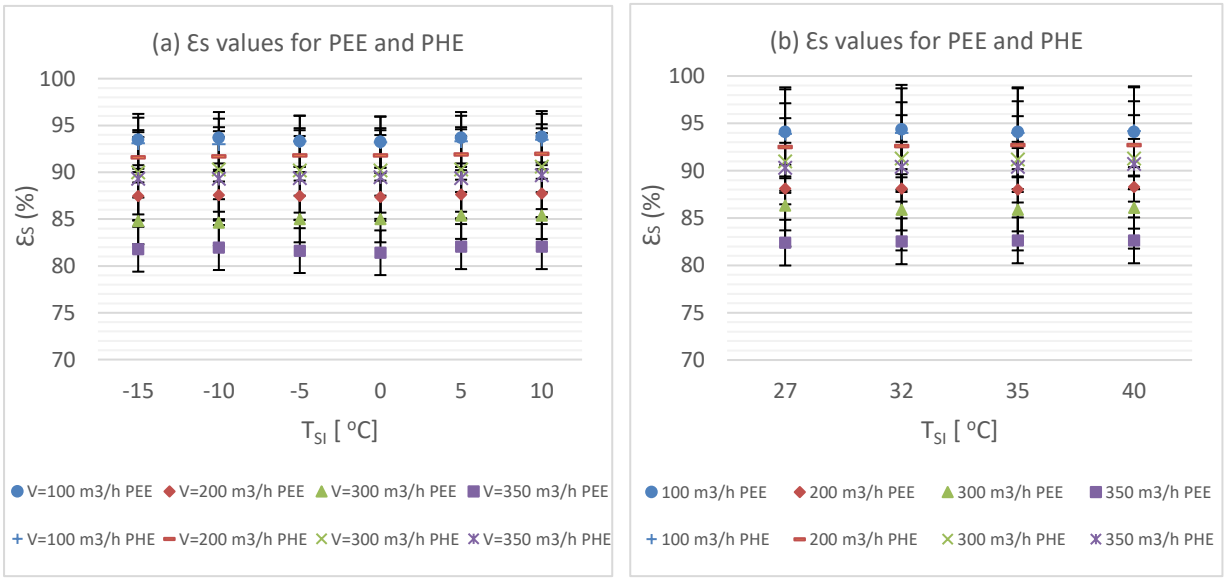

Figure 8.5. Sensible effectiveness (%) vs. dry-bulb temperature (°C) at different volume flow rates in (a) winter conditions and (b) summer conditions.

In General, the obtained effectiveness from the experiment on PHE and PEE show that the highest effectiveness occurred at lower volume flow rates; in general, the same rule goes with other different volume flow rates. The dry-bulb temperature (outside air temperature) has no effect on the performance of PHE and PEE. The sensible effectiveness values for PHE are higher than for PEE under the same ambient conditions.

Thesis 5 [71]

The developed TRNSYS model for a heat wheel operated in air handling unit AHU can help to predict the performance for such extreme conditions. The validation of the model shows a good agreement between the simulation and measured values. The values of Normalized Mean Bias Error (NMBE) and Coefficient of Variation of the Root Mean Square Error CV (RMSE) were 5.5% and 19%, respectively, for heating conditions. Therefore, it is suitable for determining ventilation systems' energy consumption and detailed investigation of the heat wheel's annual energy performance with high accuracy. The absolute value of NMBE and CV (RMSE) was less than 10% and 30%, respectively as per ASHRAE Guideline 14-2014 [50]. **Table 8.1.** show the calibration results of the simulation model.

Boundary Conditions

(-15 ~ 40 ^{o}C) Supply Air Temperature, (10 ~ 90 %) Supply Relative Humidity

(500 ~ 2000 m^{3}/h) Supply Volume Flow rate, 10.9 kW VRV Power

Table 8.1. Calibration results of the simulation model.

	Total Energy Consumption	NMBE (%)	CVRMSE (%)
Heating Measured Total (kWh)	6342	5.5%	19%
Heating Simulation Total (kWh)	6753		
Cooling Measured Total (kWh)	2034	7%	24%
Cooling Simulation Total (kWh)	1864		

It can be summarized that the newly developed TRNSYS simulation model is valid to be used in similar cases. Therefore, it is considered a new scientific result as it was not listed or discussed before.

Thesis 6 [71]

The AHU air-conditioning system's performance can be further enhanced by equipping a sorption wheel for the supply of regeneration energy to maximize the energy savings by transferring the air's humidity from the extract air. It can save almost 20% annually in the heating season comparing to the heat wheel.

Test conditions statement.

(-15 ~ 40 ^{o}C) Supply Air Temperature, (10 ~ 90 %) Supply Relative Humidity

(500 ~ 2000 m^3/h) Supply Volume Flow rate, 10.9 kW VRV Power

In conclusion, the heat wheel was found to be reliable in performance, environmentally friendly, and has a significant energy-saving impact on electrical consumption. Based on the developed TRNSYS model can be used to simulate the performance heat wheel under different operating conditions with high accuracy.

Thesis 7 [72]

The developed TRNSYS VRF model is considered validated by the field test data. Therefore, it could be used when estimating the cooling and heating load for a VRF system. The NMBE (Normalized Mean Bias Error) of the T (temperature), RH (relative humidity) values obtained are calculated using the following equations

$$(NMBE)_T = \frac{\frac{1}{N}\sum_{i=1}^{N}(T_{sim} - T_{Act})}{\bar{T}_{Act}} \times 100 \, , (NMBE)_{RH} = \frac{\frac{1}{N}\sum_{i=1}^{N}(RH_{sim} - RH_{Act})}{\overline{RH}_{Act}} \times 100$$

where T_{Act} , $RH_{Act}$is the actual metered temperature , relative humidity value, T_{sim} , $RH_{sim}$is the simulated temperature / relative humidity value, $\bar{T}_{Act}$, $\overline{RH}_{Act}$ is the average of the actual metered temperatures / relative Humidity, N is the total number of data points.
Substituting in the equations above, the obtained $(NMBE)_T$ and $(NMBE)_{RH}$ is 4.3% and 7.6%, respectively.

Boundary Conditions

(-15 ~ 40 ^{o}C) Supply Air Temperature, (10 ~ 100 %) Supply Relative Humidity

480 m^3/h Supply Volume Flow rate, 50 kW VRF Power

Statistical comparisons were used to estimate the validity of the model. The statistics parameters Coefficient of Determination (R^2), Root Mean Squared Error (RMSE), and Normalized Root Mean Square Error (NRMSE) [52] are used to check the quality of the

simulation model for the indoor temperature and relative humidity. The results of the regression method are presented in **Figure. 8.6.** It is realized that the obtained model can predict the results accurately.

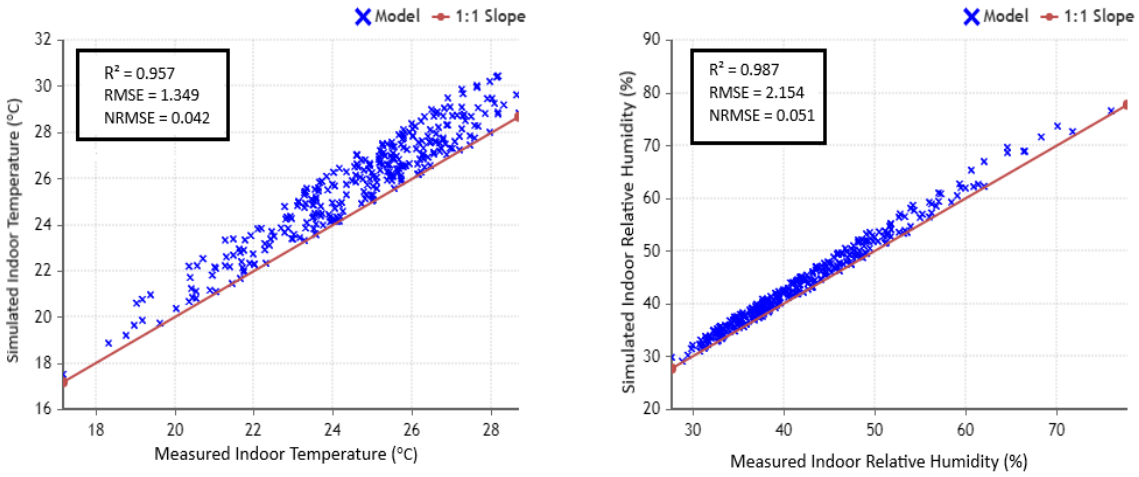

Figure 8.6 Regression methods used for statistical comparison

It can be summarized that the newly developed VRF TRNSYS simulation model is valid to be used to estimate the performance of a VRF system. Therefore, it is considered a new scientific result because modeling a VRF system is not available directly in any building energy simulation tool.

Thesis 8 [72]

The Energy Recovery Ventilation (ERV) system reduced air conditioning energy consumption. **Figures 8.7** and **8.8** summarize the total Energy consumption of the total air conditioning units installed into the offices of the department. According to the running-operating schedule from 8:00 am to 08:00 pm, one winter and one summer day of data were obtained when the ERV was operating.

Energy consumption was relatively large in winter due to the high-temperature difference between indoor and outdoor air. In addition, the results indicated that energy consumption was reduced by 30% when using the ERV system.

In the summer condition, unlike the winter ones, the energy consumption was not so high. Therefore, compared to energy recovery in the cold season, the ERV system had less impact when employed in the hot season. Moreover, the results show that it is possible to reduce the estimated heating load related to ventilation more likely than the cooling load.

Boundary Conditions

(-15 ~ 40 °C) Supply Air Temperature, (10 ~ 100 %) Supply Relative Humidity

480 m^3/h Supply Volume Flow rate, 50 kW VRF Power

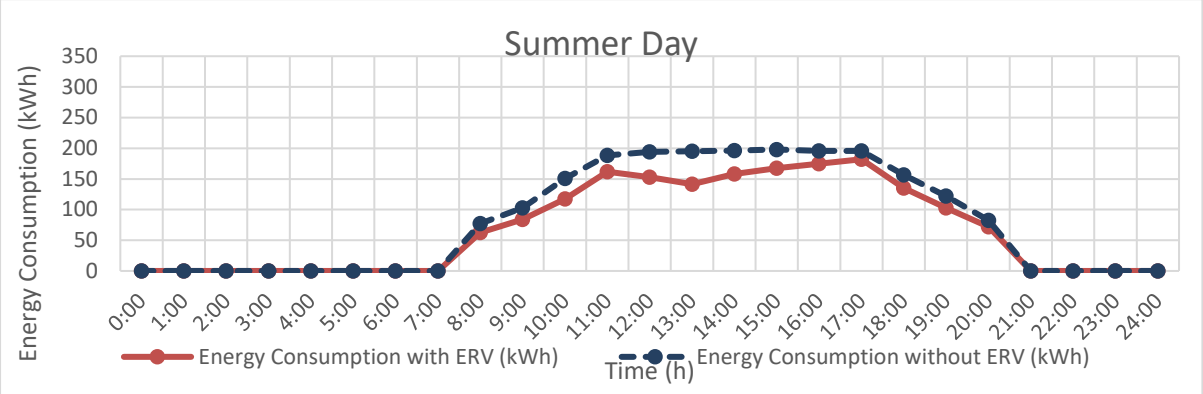

Figure 8.7. Comparisons of energy consumption between the ERV and non-ERV on a winter day

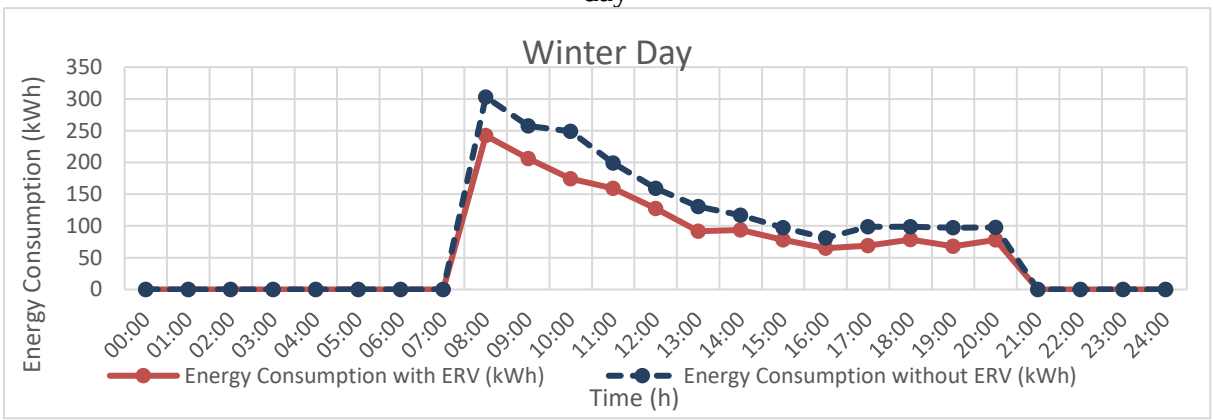

Figure 8.8. Comparisons of energy consumption between the ERV and non-ERV on a summer day

In conclusion, using an Energy Recovery Ventilator (ERV) under an existing VRF HVAC system operation will reduce the system's energy consumption by almost 30% in the heating season and about 20% in the cooling season.

Since the developed TRNSYS simulation model was validated and the simulation results show good agreement with the measured data, the results have novel scientific impacts using the validated model to predict the amount of energy saving from using ERV unit incorporated with VRF system.

8.3 Practical Application of Scientific Results

Using energy recovery systems in HVAC application has its own advantages. It influences not only on the scientific community but also in the investment companies. The economic side is very attractive for companies and end-users. Besides, the environmental problems and CO_2 reduction are very incorrigible for using energy recovery systems. Hence, the benefits of using energy recovery systems in HVAC can be summarized as:

1- Reduce the energy consumption of ventilation system

2- Reduce the CO_2 emission

3- Decrees the running cost

4- Enhance the cooling and heating process when using moisture transfer energy wheel as it maintain the indoor air quality

8.4 Recommendations

The following recommendation topics are considered to be done for more sufficient and attractive investments in the field

1- More types for different energy recovery units should be studied in order to find more energy recovery unit to save more energy in the practical form

2- Wider ambient air condition could be more helpful for the building service engineers and experts who works in the practice.

3- More numerical work shall be done to predict the performance of different types of energy recovery systems to help understanding the behavior of these systems.

4- Comprehensive study on the energy recovery system shall be made taking into consideration more factors affecting on the performance of the energy recovery systems.

References

[1] Tariq, R., Sheikh, N. A., Xamán, J., & Bassam, A. (2019). Recovering waste energy in an indirect evaporative cooler–A case for combined space air conditioning for human occupants and produce commodities. Building and Environment, 152, 105-121.

[2]- Lechner, N. (2014). *Heating, cooling, lighting: Sustainable design methods for architects*. John wiley & sons.

[3] Tsirigoti, D., & Tsikaloudaki, K. (2018). The effect of climate conditions on the relation between energy efficiency and urban form. Energies, 11(3), 582.

[4] Wan, K. K., Li, D. H., Liu, D., & Lam, J. C. (2011). Future trends of building heating and cooling loads and energy consumption in different climates. Building and Environment, 46(1), 223-234.

[5] Lam, J. C., Tang, H. L., & Li, D. H. (2008). Seasonal variations in residential and commercial sector electricity consumption in Hong Kong. Energy, 33(3), 513-523.

[6] Ahmed, K., Carlier, M., Feldmann, C., & Kurnitski, J. (2018). A new method for contrasting energy performance and near-zero energy building requirements in different climates and countries. Energies, 11(6), 1334.

[7] Dieckmann, J. (2008). Improving humidity control with energy recovery ventilation. ASHRAE Journal, 50(8), 38.

[8] Ghazanfari, S. A., & Wahid, M. A. (2018). Heat transfer enhancement and pressure drop for fin-and-tube compact heat exchangers with delta winglet-type vortex generators. Facta Universitatis, Series: Mechanical Engineering, 16(2), 233-247.

[9] Sahdev, R. K., Kumar, M., & Dhingra, A. K. (2017). Forced convection drying of Indian groundnut: an experimental study. Facta Universitatis, Series: Mechanical Engineering, 15(3), 467-477.

[10] Papakostas, K. T., Tiganitis, I., & Papadopoulos, A. M. (2018). Energy and economic analysis of an auditorium's air conditioning system with heat recovery in various climatic zones. Thermal Science, 22(Suppl. 3), 933-943.

[11] Al-Badi, A. H., & Al-Saadi, S. N. (2020). Toward energy-efficient buildings in Oman. International Journal of Sustainable Energy, 39(5), 412-433.

[12]- Sachs, H. M., Lin, W., & Lowenberger, A. K. (2009). *Emerging energy saving-HVAC technologies and practices for the buildings sector (2009)*. American Council for an Energy-Efficient Economy.

[13] Simonson, C., *et al.,* Heat and Moisture Transfer in Energy Wheels during Sorption, Condensation, and Frosting Conditions, *Journal of heat transfer-transactions of ASME, 120* (1997), pp. 699

[14] Sparrow, E., *et al.*, Heat and mass transfer characteristics of a rotating regenerative total energy wheel, *International Journal of Heat and Mass Transfer, 50* (2007), pp. 1631–1636

[15] Jeong, J., *et al.*, Practical thermal performance correlations for molecular sieve and silica gel loaded enthalpy wheels, *Applied Thermal Engineering, 25* (2005), pp.719–740

[16] Harmati, N., *et al.,* Energy Performance Modelling and Heat Recovery Unit Efficiency Assessment of an Office Building, *Thermal Science, 19* (2015) pp. 865-880

[17] Angrisani, G., *et al.,* Experimental analysis on the dehumidification and thermal performance of a desiccant wheel, *Applied Energy*, *92* (2012), pp. 563–572

[18] Chung, H. J., Lee, J. S., Baek, C., Kang, H., & Kim, Y. (2016). Numerical analysis of the performance characteristics and optimal design of a plastic rotary regenerator considering leakage and adsorption. *Applied thermal engineering*, *109*, 227-237.

[19] Smith, K. M., & Svendsen, S. (2016). The effect of a rotary heat exchanger in room-based ventilation on indoor humidity in existing apartments in temperate climates. *Energy and Buildings*, *116*, 349-361.

[20] Goodarzia, G., Thirukonda, N., Heidari, S., Akbarzadeh, A., & Date, A. (2017). Performance evaluation of solid desiccant wheel regenerated by waste heat or renewable energy. *Energy Procedia*, *110*, 434-439.

[21] Goldanlou, A. S., Kalbasi, R., & Afrand, M. (2020). Energy usage reduction in an air handling unit by incorporating two heat recovery units. Journal of Building Engineering, 32, 101545.

[22] Calautit, J. K., O'Connor, D., Tien, P. W., Wei, S., Pantua, C. A. J., & Hughes, B. (2020). Development of a natural ventilation windcatcher with passive heat recovery wheel for mild-cold climates: CFD and experimental analysis. Renewable Energy, 160, 465-482.

[23] Lam, J. C., Tang, H. L., & Li, D. H. (2008). Seasonal variations in residential and commercial sector electricity consumption in Hong Kong. *Energy*, *33*(3), 513-523.

[24] Giannakopoulos, C., Hadjinicolaou, P., Zerefos, C., & Demosthenous, G. (2009). Changing energy requirements in the Mediterranean under changing climatic conditions. *Energies*, *2*(4), 805-815.

[25] Karlsson, J., Roos, A., & Karlsson, B. (2003). Building and climate influence on the balance temperature of buildings. *Building and environment*, *38*(1), 75-81.

[26] Calise, F., D'Accadia, M. D., Barletta, C., Battaglia, V., Pfeifer, A., & Duic, N. (2017). Detailed modelling of the deep decarbonisation scenarios with demand response technologies in the heating and cooling sector: A case study for Italy. *Energies*, *10*(10), 1535.

[27] Giuseppe, E. M. M. I., Marco, M. A. R. I. O. T. T. I., Angelo, Z. A. R. E. L. L. A., & Michele, D. C. (2017). The use of air handling units in residential near zero-energy buildings. *WIT Trans. Ecol. Environ*, *224*, 147-158.

[28] Al-Zubaydi, A. Y. T., & Hong, G. (2018). Experimental investigation of counter flow heat exchangers for energy recovery ventilation in cooling mode. *International Journal of Refrigeration*, *93*, 132-143.

[29] Guillén-Lambea, S., Rodríguez-Soria, B., & Marín, J. M. (2017). Control strategies for energy recovery ventilators in the South of Europe for residential nZEB—Quantitative analysis of the air conditioning demand. *Energy and Buildings*, *146*, 271-282.

[30] Davidsson, H., Bernardo, R., & Hellström, B. (2013). Hybrid ventilation with innovative heat recovery—a system analysis. Buildings, 3(1), 245-257.

[31] Jani, D. B., Mishra, M., & Sahoo, P. K. (2015). Performance studies of hybrid solid desiccant–vapor compression air-conditioning system for hot and humid climates. *Energy and Buildings*, *102*, 284-292.

[32] Wallin, J., & Claesson, J. (2014). Improving heat recovery using retrofitted heat pump in air handling unit with energy wheel. *Applied thermal engineering*, *62*(2), 823-829.

[33] Zendehboudi, A., Zendehboudi, A., & Hashemi, R. (2014). A Study on the Performance of a Solar Desiccant Cooling System by TRNSYS in Warm and Humid Climatic Zone of IRAN.

[34] Rasouli, M., Akbari, S., Simonson, C. J., & Besant, R. W. (2014). Energetic, economic and environmental analysis of a health-care facility HVAC system equipped with a run-around membrane energy exchanger. *Energy and buildings*, *69*, 112-121.

[35] Jokisalo, J., Kurnitski, J., Vuolle, M., & Torkki, A. (2003). Performance of balanced ventilation with heat recovery in residential buildings in a cold climate. International Journal of Ventilation, 2(3), 223-236.

[36] Bogatu, D. I., Carutasiu, M. B., Ionescu, C., & Necula, H. (2019). Validation of a TRNSYS model for a complex HVAC system installed in a low-energy building. *Upb Scientific Bulletin, Series C: Electrical Engineering and Computer Science*, *81*(1), 245-260.

[37] Fan, Y., Kameishi, K., Onishi, S., & Ito, K. (2014). Field-based study on the energy-saving effects of CO2 demand controlled ventilation in an office with application of energy recovery ventilators. *Energy and buildings*, *68*, 412-422.

[38] Park, D. Y., Yun, G., & Kim, K. S. (2017). Experimental evaluation and simulation of a variable refrigerant-flow (VRF) air-conditioning system with outdoor air processing unit. *Energy and Buildings*, *146*, 122-140.

[39] Torregrosa-Jaime, B., Martínez, P. J., González, B., & Payá-Ballester, G. (2019). Modelling of a variable refrigerant flow system in EnergyPlus for building energy simulation in an Open Building Information modelling environment. *Energies*, *12*(1), 22.

[40] Zhu, Y., Jin, X., Du, Z., Fang, X., & Fan, B. (2014). Control and energy simulation of variable refrigerant flow air conditioning system combined with outdoor air processing unit. *Applied thermal engineering*, *64*(1-2), 385-395.

[41] Kani-Sanchez, C., & Richman, R. (2017). Incorporating variable refrigerant flow (VRF) heat pump systems in whole building energy simulation–Detailed case study using measured data. Journal of Building Engineering, 12, 314-324.

[42] Li, Y. M., & Wu, J. Y. (2010). Energy simulation and analysis of the heat recovery variable refrigerant flow system in winter. *Energy and Buildings*, *42*(7), 1093-1099.

[43] Zhai, Z. J., & Rivas, J. (2018). Promoting variable refrigerant flow system with a simple design and analysis tool. *Journal of Building Engineering*, *15*, 218-228.

[44] Yau, Y. H., & Amir, M. (2020). Energy use analysis of the variable refrigerant flow (VRF) system versus the multi-split unit using TRNSYS. *Heat and Mass Transfer*, *56*(2), 671-690.

[45] Zhang, R., Sun, K., Hong, T., Yura, Y., & Hinokuma, R. (2018). A novel Variable Refrigerant Flow (VRF) heat recovery system model: Development and validation. Energy and Buildings, 168, 399-412.

[46] Kalaimani, R., Jain, M., Keshav, S., & Rosenberg, C. (2020). On the interaction between personal comfort systems and centralized hvac systems in office buildings. *Advances in Building Energy Research*, *14*(1), 129-157.

[47] Hoval Enventus (2018), *Rotary heat exchangers for Heat Recovery in Ventilation Systems*.

[48] Testo, TESTO Smart Probs Manual, https://www.testo.com/en/products/smartprobes

[49] ASHRAE, (2011) *HVAC Applications*, Inc. Atlanta, GA, USA.

[50] ASHARE. (2016) ASHARE Handbook: HVAC Systems and Equipment, Inc. Atlanta, GA, USA, 2016

[51] PN-EN-13141-7: (2010). Ventilation for buildings – Performance testing of components/products for residential ventilation – Part 7: Performance testing of mechanical supply and exhaust ventilation units (including heat recovery) for mechanical ventilation systems intended for single family dwellings.

[52] Understanding Heat Exchangers-Cross-Flow, Counter-Flow (Rotary/Wheel) and Cross-Counter-Flow Heat Exchangers. 2012 Zehnder Group AG report. Available online: www.zehnderamerica.com (accessed on 29 October 2020).

[53] Speerforck, A., & Schmitz, G. (2016). Experimental investigation of a ground-coupled desiccant assisted air conditioning system. *Applied energy*, *181*, 575-585..

[54] Jani, D. B., Mishra, M., & Sahoo, P. K. (2018). Performance analysis of a solid desiccant assisted hybrid space cooling system using TRNSYS. *Journal of Building Engineering*, *19*, 26-35.

[55] De Antonellis, S., Intini, M., Joppolo, C. M., & Leone, C. (2014). Design optimization of heat wheels for energy recovery in HVAC systems. *Energies*, *7*(11), 7348-7367..

[56] Kassai, M. (2019). Energy Performance Investigation of a Direct Expansion Ventilation Cooling System with a Heat Wheel. *Energies*, *12*(22), 4267.

[57] Standard AS. Standard 84-1991, Method of testing air-to-air heat exchangers. *American Society of Heating, Refrigerating and Air Conditioning, Engineers Inc.*, Atlanta. 1991.

[58] Google SketchUp, (2016). SketchUp Make, *Trimble Inc.*

[59] ASHRAE, ANSI/ASHRAE Standard 62. 1–2014, Ventilation for Acceptable Indoor Air Quality, *American Society of Heating, Refrigerating and Air-Conditioning Engineers, Inc., Atlanta, GA, 2010.*

[60] LG. LG Power Distribution Indicator Models: PQNUD1S00, *OWNER'S & INSTALLATION MANUAL*. http://www.lgservice.com/

[61] Zehnder Group Deutschland (2016). GmbH, Service Manual, Lahr · Germany.

[62] González-Briones, A., Chamoso, P., Yoe, H., & Corchado, J. M. (2018). GreenVMAS: virtual organization based platform for heating greenhouses using waste energy from power plants. *Sensors*, *18*(3), 861.

[63] Kline, S. J. (1953). Describing uncertainty in single sample experiments. *Mech. Engineering*, *75*, 3-8.

[64] Holman, J. P. (2001). *Experimental methods for engineers*.

[65] Tariq, R., Hussain, Y., Sheikh, N. A., Afaq, K., & Ali, H. M. (2020). Regression-based empirical modeling of thermal conductivity of CuO-water nanofluid using data-driven techniques. *International Journal of Thermophysics*, *41*(4), 1-28.

[66] Granderson, J., Touzani, S., Custodio, C., Sohn, M., Fernandes, S. (2015). Assessment of Automated Measurement and Verification (M&V) Methods, *Building Technology and Urban Systems Division Lawrence Berkeley National Laboratory*, LBNL-187225

[67] Monetti, V., Davin, E., Fabrizio, E., André, P., & Filippi, M. (2015). Calibration of building energy simulation models based on optimization: a case study. *Energy Procedia*, *78*, 2971-2976.

[68] Kassai M, Al-Hyari L. Experimental Investigation on Operation Parameters of 3Å Molecular Sieve Desiccant Coated Total Energy Recovery Wheel for Maximum Effectiveness, **Thermal Science**, Volume 24, Issue 3 Part B, pp. 2113-2124, DOI: 10.2298/TSCI181106014X (**IF=1.541**) (**WoS: Q3; SJR:Q3**) (2020)

[69] Kassai M, Al-Hyari L. Investigation of Ventilation Energy Recovery with Polymer Membrane Material based Counter-flow Energy Exchanger for Nearly Zero-Energy Buildings. **Energies**, Vol. 12(9), 1727, pp. 1-21, DOI: 10.3390/en12091727 (2019) (**IF=2.707**) (**WoS: Q2; Scopus; SJR: Q1**).

[70] Faisal Abdelrazzaq Alhyari L, Kassai M. Experimental Investigation on Sensible Effectiveness of Desiccant Rotary Energy Recovery Unit. EXPRES 2019, 11th International Symposium on Exploitation of Renewable Energy Sources, effectiveness, security and PhD Student Meeting, Subotica, Serbia, 11-13. April, 2019, Subotica, Serbia, pp. 11-15., (ISBN 978-86-919769-4-1) (2019).

[71] Al-Hyari, L.; Kassai, M. Development and Experimental Validation of TRNSYS Simulation Model for Heat Wheel Operated in Air Handling Unit. **Energies**, 13(18), 4957; DOI: 10.3390/en13184957 (**IF=2.702**) (**WoS: Q3; Scopus; SJR: Q2**). (2020)

[72] Al-Hyari, L., & Kassai, M. (2021). Development of TRNSYS Model for Energy Performance Simulation of Variable Refrigerant Flow Air-Conditioning System combined with Energy Recovery Ventilation. **International Journal of Green Energy**, 1-12. (**IF=1.338**) (**WoS: Q4; Scopus, SJR: Q3**),

[73] Al-Hyari L, Kassai M. Energetic Investigation of Energy Recovery Technologies in Air Handling Units. **International Review of Applied Sciences and Engineering**, Vol. 9., Issue 1, pp. 49-57 Print ISSN 2062-0810, Online ISSN 2063-4269, DOI: 10.1556/1848.2018.9.1.7, (**Scopus; SJR: Q3**) (2018)

Appendix A

Kline and McClintock established a method to calculate the uncertainty. They defined the uncertainty as a range where the true value lies in the mean ± uncertainty interval (b to 1).

For example, if a temperature measurement was as follows (Equation (A1)):

$$T = 25\ °C \pm 1\ °C, \tag{A1}$$

then the ± sign in Equation (A1) means that the experimenter is not sure about the results, and it defines the range where the true value lies. In the example above, the experimenter implies that the true value lies between 24 °C and 26 °C.

As an explanation of how these uncertainties propagate into the results, let the result R be a function of an independent number (*n*) of variables $v_1, v_2, \ldots, v_n$.

For a small variation in the variables, this relationship can be expressed in linear form as follows (Equation (A2)):

$$\partial R = \frac{\partial R}{\partial v_1} + \frac{\partial R}{\partial v_2} + \ldots + \frac{\partial R}{\partial v_n}. \tag{A2}$$

Based on the first theorem defined by Kline and McClintock, if R is a linear function of *n* independent variables, and if the maximum deviation of the *i*th variable from its mean is $(\pm \partial v_i)_{max}$, then the maximum deviation of R from its mean value is given by Equation (A3).

$$\partial R_{max} = \left|\frac{\partial R}{\partial v_1}\partial v_{1_{max}}\right| + \left|\frac{\partial R}{\partial v_2}\partial v_{2_{max}}\right| + \ldots + \left|\frac{\partial R}{\partial v_n}\partial v_{n_{max}}\right|. \tag{A3}$$

Equation (A3) might be used as an approximation for calculating the uncertainty interval in the result by simply substituting ω_i for v_i as follows:

$$\omega_R = \left|\frac{\partial R}{\partial v_1}\omega_1\right| + \left|\frac{\partial R}{\partial v_2}\omega_2\right| + \ldots + \left|\frac{\partial R}{\partial v_n}\omega_n\right|. \tag{A4}$$

Equation (A4) can be referred to as the linear equation. Based on the second theorem defined by Kline and McClintock, if R is a linear function of *n* independent variables, each of

which is distributed with a standard deviation σ_i, then the standard deviation of R is given by Equation (A5).

$$\sigma_R = \left[\left(\frac{\partial R}{\partial v_1}\right)^2 {\sigma_1}^2 + \left(\frac{\partial R}{\partial v_2}\right)^2 {\sigma_2}^2 + \ldots + \left(\frac{\partial R}{\partial v_n}\right)^2 {\sigma_n}^2\right]^{\frac{1}{2}}. \quad \text{(A5)}$$

The best measure of uncertainty is neither the maximum value nor the standard deviation, but some interval based on certain odds. For the special case in which the variables are distributed normally, the distribution of the results will also be normal, and the third theorem described below applies. Based on the third theorem defined by Kline and McClintock, if R is a linear function of *n* independent variables, each of which is normally distributed, then the relationship between the interval for the variables ω_i and the interval for the results ω_R, which gives the same odds for each of the variables and for the results, is given by Equation (A6).

$$\omega_R = \left[\left(\frac{\partial R}{\partial v_1}\omega_1\right)^2 + \left(\frac{\partial R}{\partial v_2}\omega_2\right)^2 + \ldots + \left(\frac{\partial R}{\partial v_n}\omega_n\right)^2\right]^{\frac{1}{2}}. \quad \text{(A6)}$$

Equation (A6) is used directly as an approximation for calculating the uncertainty interval in the result. It is referred to as the second-power equation.